SYNTHETIC LOADING OF INDUCTION MOTORS USING A SINUSOIDAL MODULATION TECHNIQUE

SYNTHETIC LOADING OF INDUCTION MOTORS USING A SINUSOIDAL MODULATION TECHNIQUE

By

ANDREI B. IANOS, B. ENG & MGMT.

A Thesis

Submitted to the School of Graduate Studies

in Partial Fulfillment of the Requirements

for the Degree

Master of Applied Science

McMASTER UNIVERSITY

MASTER OF APPLIED SCIENCE (2010) McMaster University

(Electrical and Computer Engineering) Hamilton, Ontario

TITLE: Synthetic Loading of Induction Motors using a Sinusoidal Modulation Technique

AUTHOR: Andrei B. Ianos (McMaster University)

SUPERVISOR: Professor Barna Szabados

NUMBER OF PAGES: x, 86

ABSTRACT

A Sinusoidal Modulation technique is proposed for the synthetic loading of induction machines at full load based on power electronics control. The sinusoidal modulations are based on the two axis method and reference-frame theory. The method applies specifically to induction machines for which physical load testing is unadvisable or unattainable. This allows motor manufactures to fully test their products while utilizing current motor production as the basic setup of their test system decreasing costs.

Previous modulation technique methods are either too costly or incur high oscillation currents rendering the systems impractical. The Sinusoidal Modulation technique computer simulations show the ability of the method to suppress power fluctuations on the driver motor of the system. Experimental and simulation results are analyzed and compared to prove simulation accuracy and system viability. Experimental data gathered at half rated load show maximum fluctuations on the driver motor in the range of 2%.

ACKNOWLEDGEMENTS

First and foremost, I would like to thank my supervisor, Dr. Szabados for his guidance, patience and long lasting support throughout the course of the thesis. Your vast knowledge and guidance has given me the ability to gain unprecedented knowledge both theoretically and experimentally and for that I thank you.

To Cheryl Gies, thank you for always looking out for me whenever I walked by your door. Whether it be a form I needed to fill out or a simple smile and a how are you, you always had time for me which meant more than you can image. Thank you.

To Adam Marianski and Steve Spencer, your advice, experience and your willingness to help contributed enormously to this project. Your countless hours spent in the lab with me are greatly appreciated. Thank you.

Lastly, and most importantly, I would like to thank my family. Your support, patience and constant drive has helped me achieve my goals and shaped me into the person I am today. Thank you.

TABLE OF CONTENTS

CHAPTER 1: INTRODUCTION **1**

1-1 Background **1**

1-2 Objectives **3**

1-3 Thesis Structure **4**

CHAPTER 2: LITERATURE REVIEW **5**

2-1 Proposed Synthetic Loading Methods **5**
2-1-1 Synthetic Loading Principles 5
2-1-2 Proposed Phase Modulation Methods 6
2-1-2-1 Use of Wound Rotor Induction Machine 7
2-1-2-1-1 Bang-Bang Control 7
2-1-2-1-2 Sinusoidal Modulation 11
2-1-2-2 Modulation Parameters 12

CHAPTER 3: MATHEMATICAL MODEL **15**

3-1 Reference Frame Theory **15**
3-1-1 Background 15
3-1-2 Equations of Transformation 15

3-2 Squirrel Cage Induction Motors **17**

3-3 Synchronous Generators **20**

3-4 Complete Mathematical Model **23**

3-5 State Space Representation and Mathematical Simulation **24**
3-5-1 Control Algorithm 26

CHAPTER 4: EXPERIMENTAL SETUP **27**

4-1 Printed Circuit Board Design **27**
4-1-1 Building Blocks 27
4-1-1-1 Operational Amplifiers 27

4-1-1-1-1 Impedance Buffer 28
4-1-1-1-2 Level Shifter 28
4-1-1-1-3 Integrator 30
4-1-1-1-4 Digital Comparator 31
4-1-1-2 Monostables 32
4-1-1-3 Set-Reset Flip Flops 33
4-1-1-4 IGBT IC 34
4-1-1-5 Voltage and Current Measurement Components 37
4-1-2 Carrier Wave Creation 39
4-1-3 Pulse Width Modulation Signal Creation 41
4-1-4 Board Designs 43
4-1-4-1 Measurement Board 43
4-1-4-2 Control Board 47

4-2 Software Implementation with LabView 51
4-2-1 Software Objectives 51
4-2-2 Implementation and Design 51
4-2-2-1 Control Signal Algorithm 52
4-2-2-2 Data Acquisition 54
4-2-2-2-1 Characteristics 54
4-2-2-2-2 Synchronization of Two Cards 54
4-2-2-2-3 Data Recording 54
4-2-2-3 Automated Control 55
4-2-2-4 User Interface 55

4-3 Equipment Setup 56
4-3-1 Power Supplies 57
4-3-2 Physical Machine Connections 58
4-3-3 Start Up Procedures 59
4-3-4 Control and Measurement Connections 61

4-4 Rotating Machine Setup 62
4-4-1 Machine Parameters 63
4-4-1-1 DC Resistance Test 64
4-4-1-2 Blocked Rotor Test 64
4-4-1-3 No Load Test 65
4-4-1-4 Motor/Generator Characteristics 65

CHAPTER 5: COMPARISON OF THEORETICAL AND EXPERIMENTAL RESULTS 66

5-1 No Load Conditions on D0 66

5-2 One Motor Load on D0 68

5-3 Two Motor Load on D0 70
5-3-1 Balanced Loads 70
5-3-2 Unbalanced Loads 71
5-3-2-1 Magnitude Adjustment 73
5-3-2-2 Magnitude and Phase Adjustment 76
5-3-2-2-1 Manual Phase Adjustment 78
5-3-2-2-2 Automatic Phase Adjustment 80

CHAPTER 6: CONCLUSIONS AND RECOMMENDATIONS 82

6-1 Conclusions 82

6-2 Recommendations for Future Work 83

REFERENCES 85

LIST OF FIGURES

FIGURE 2-1- PRINCIPLE OF SYNTHETIC LOADING ADAPTED FROM [6] 6
FIGURE 2-2 - TWO FREQUENCY METHOD ADAPTED FROM [3] 6
FIGURE 2-3 - DUAL FIELD WINDING CONTROL ADAPTED FROM [6] 8
FIGURE 2-4 - NEW PHASE MODULATION TECHNIQUE ADAPTED FROM [3] 8
FIGURE 2-5 - CONVERSION OF A WOUND ROTOR INDUCTION MACHINE ADAPTED FROM [3] 9
FIGURE 2-6 - SINGLE SYSTEM PHYSICAL IMPLEMENTATION ADAPTED FROM [3] 10
FIGURE 2-7 - PARALLEL SYSTEM PHYSICAL IMPLEMENTATION ADAPTED FROM [3] 11
FIGURE 2-8 - MODULATION DEPTH AND FREQUENCY ADAPTED FROM [5] ..13
FIGURE 3-1 - TRANSFORMATION FOR STATIONARY CIRCUITS USING TRIGONOMETRIC RELATIONSHIPS 16
FIGURE 3-2 - SYMMETRICAL 3-PHASE INDUCTION MACHINE CIRCUIT 18
FIGURE 3-3 - EQUIVALENT 3-PHASE SYMMETRICAL INDUCTION MACHINE CIRCUIT IN THE ARBITRARY REFERENCE FRAME 19
FIGURE 3-4 - EQUIVALENT 2-PHASE SYNCHRONOUS GENERATOR CIRCUIT 21
FIGURE 3-5 - EQUIVALENT SYNCHRONOUS MACHINE CIRCUIT IN THE ROTOR REFERENCE FRAME 22
FIGURE 3-6 - EQUIVALENT SINGLE SYSTEM CIRCUIT 24
FIGURE 3-7 - MATLAB SIMULATION SYSTEM FLOW CHART FROM [3] 26
FIGURE 4-1 - IDEAL OPERATIONAL AMPLIFIER 28
FIGURE 4-2 - IMPEDANCE BUFFER 28
FIGURE 4-3 - LEVEL SHIFTER 29
FIGURE 4-4 - NON INVERTING CLOSED LOOP GAIN CIRCUIT 30
FIGURE 4-5 - OP-AMP INTEGRATOR 30
FIGURE 4-6 - DIGITAL COMPARATOR 32
FIGURE 4-7 - MONOSTABLE 33
FIGURE 4-8 – SET-RESET FLIP FLOP 33
FIGURE 4-9 - IRAMX20UP60A IC EXTERNAL PACKAGE [18] 34
FIGURE 4-10 - H-BRIDGE CIRCUIT 35
FIGURE 4-11 - IRAMX20UP60A PIN CONFIGURATION[18] 36
FIGURE 4-12 - IR IC HEAT SINK AND FAN 37
FIGURE 4-13 - POWER TRANSFORMER 38
FIGURE 4-14 - CURRENT TRANSFORMER 38
FIGURE 4-15 - CARRIER WAVE CREATION BLOCK DIAGRAM 39

FIGURE 4-16 - CARRIER WAVE CREATION BLOCK DIAGRAM 40
FIGURE 4-17 - PWM SIGNAL CREATIONS THROUGH COMPARISON 41
FIGURE 4-18 - PWM SIGNAL CREATION BLOCK DIAGRAM 42
FIGURE 4-19 - PWM CREATION CIRCUIT 43
FIGURE 4-20 - MEASURING BOARD SCHEMATIC 44
FIGURE 4-21 - MEASUREMENT BOARD LAYOUT 45
FIGURE 4-22 - MEASUREMENT BOARD TOP VIEW 46
FIGURE 4-23 - MEASUREMENT BOARD INTERIOR VIEW 46
FIGURE 4-24 - CONTROL BOARD BREADBOARD DESIGN 47
FIGURE 4-25 - CONTROL BOARD SCHEMATIC 48
FIGURE 4-26 - CONTROL BOARD LAYOUT 49
FIGURE 4-27 - CONTROL BOARD TOP VIEW 50
FIGURE 4-28 - INTERIOR VIEW 50
FIGURE 4-29 - LABVIEW SOFTWARE INTEGRATION IN HIGH LEVEL FORM .. 52
FIGURE 4-30 - SINUSOIDAL AND COSINUSOIDAL MODULATION SIGNALS ... 53
FIGURE 4-31 - LABVIEW CHART FOR ON SCREEN DISPLAY 55
FIGURE 4-32 - LABVIEW USER INTERFACE 56
FIGURE 4-33 - DRIVER MOTOR CONNECTIONS 57
FIGURE 4-34 - RECTIFIED AND ISOLATED DC SIGNAL 58
FIGURE 4-35 - SYNCHRONOUS GENERATOR AND INDUCTION MOTOR CONNECTIONS 59
FIGURE 4-36 - COMPLETE FIVE MACHINE SYSTEM 60
FIGURE 4-37 - PT AND CT PLACEMENT FOR THE FIVE MACHINE SYSTEM 61
FIGURE 4-38 - IN-LAB EXPERIMENT SETUP 62
FIGURE 4-39 - EQUIVALENT INDUCTION MACHINE DIAGRAM 64
FIGURE 5-1 - SIMULATED AND EXPERIMENTAL RESULTS FOR UNLOAD POWER ON D0 67
FIGURE 5-2 - SIMULATED AND EXPERIMENTAL RESULTS FOR LOAD POWER ON D0 67
FIGURE 5-3 - SIMULATED RESULTS FOR ONE MODULATED LOAD 68
FIGURE 5-4 - EXPERIMENTAL RESULTS FOR ONE MODULATED LOAD 69
FIGURE 5-5 - SIMULATION RESULTS FOR PERFECTLY BALANCED LOADS ... 71
FIGURE 5-6 - SIMULATION RESULTS FOR UNBALANCED LOADS WITHOUT MAGNITUDE ADJUSTMENT 72
FIGURE 5-7 - SIMULATED RESULTS FOR MAGNITUDE ADJUSTMENT OF UNBALANCED LOADS 74
FIGURE 5-8 - EXPERIMENTAL RESULTS FOR MAGNITUDE ADJUSTMENT OF UNBALANCED LOADS 76

FIGURE 5-9 - MODULATED SIGNALS WITHOUT PHASE CORRECTION 77
FIGURE 5-10 - MODULATED SIGNALS WITH PHASE CORRECTION....................77
FIGURE 5-11 - SIMULATED RESULTS FOR MAGNITUDE AND PHASE ADJUSTMENT OF UNBALANCED LOADS 78
FIGURE 5-12 - EXPERIMENTAL RESULTS FOR MAGNITUDE AND PHASE ADJUSTMENT OF UNBALANCED LOADS 79
FIGURE 5-13 - EXPERIMENTAL RESULTS FOR THE AVERAGE POWER OF AUTOMATIC PHASE SHIFT CORRECTION OF UNBALANCED LOADS 81
FIGURE 5-14 - EXPERIMENTAL RESULTS FOR THE INSTANTANEOUS POWER FLUCTUATIONS FOR THE AUTOMATIC PHASE SHIFT CORRECTION OF UNBALANCED LOADS...81

Chapter 1: Introduction

1-1 Background

Proper motor selection is largely dependent on the operating characteristics of the load. The selection process is often times complex and involves taking into account the power, torque and speed characteristics of the machine, the operating conditions, environmental surroundings and the temperature the machine will reach while operating.[1] This information is valuable to both manufacturer and consumer and product standards have been developed by regulatory bodies such as the National Electrical Manufactures Association (NEMA) and the Institute of Electrical and Electronics Engineers (IEEE).[2] These standards are put in place to ensure uniformity and uphold safety standards.

One of the most important selection properties of an electric motor is its temperature rise under full load operation. This has major impacts on the reliability of the machine and its operation lifetime, the machines performance, or efficiency, and the insulation material's lifetime.[3] An empirical rule approximation states that for each additional eight to ten degree rise in temperature, the organic insulation material's life is decreased by 50%.[4] As many machine windings have organic insulation temperature is quite a concern. If the operating temperature is continuously exceeded, the material will lose its dielectric properties and durability and the machine's performance will at first suffer, and then break down.[3] This causes safety concerns for the machine itself as well as workers and nearby equipment.

Therefore, there is a clear need for machine testing under full load conditions. The conventional method of testing is to physically attach a load to the shaft. Two electric machines can be mechanically connected to work as a motor-generator pairing. The machines are then run for six to eight hours, or until all temperatures have stabilized, and the winding temperature is measured along with all other name plate required data and recorded.[5] There are however, numerous pitfalls to utilizing this method of testing. Firstly, there is a high amount of energy dissipated in the form of heat over the abovementioned test period. This energy dissipation may seem trivial for small machines, but large machines, in the range of MW, draw a lot of power and produce a lot of heat. Secondly, the process of mechanically mounting and aligning of shafts can be difficult, expensive and time consuming. For large machines, the equipment, instrumentation and sensors are costly. Furthermore, the load itself is costly to produce and its cost of production cannot be justified when only a few machines will be tested, therefore there is a lack of availability of a large enough load for full load testing. It has been shown that the number of electric machines produced decreases as the power rating of the machine increases.[3] For vertical, or upright, electric machines, mechanical shaft mounting is not even an option.[6]

As such, there is a clear need for alternative techniques to run large electric machines at full load to determine rated conditions. Synthetic loading techniques have been proposed to achieve the aforementioned objectives without mechanically connecting electric machines shaft to shaft. The Two-Frequency method was first proposed by Ytteberg in 1921 [7] and then later revisited by Romeira in 1948, Fong in 1972 and 1976, Kron in 1973, Radic and Strupp in 1976, Schwenk in 1977 and Gaintsev in 1985.[5] Ytteberg's original method was applicable to both squirrel cage and wound rotor machines. Romeira's proposed two frequency method worked only for wound rotor motors. Fong's method required that all six motor leads be accessible, thus, increasing manufacturing cost.[5] Further assessment showed that the Two Frequency method incurred unstable stator voltage fluctuation which provided inaccurate results.[5]

A "Constant Speed of Rotating Magnetic Field" (CSORMF) method was introduced by [8] in 1994 which produces a rotating magnetic field with constant speed and sinusoidally varying magnitude.[8] The method provides comparable results with the two frequency method while producing a smaller torque. The smaller torque is beneficial as it comes with a reduction in power fluctuations. However, for large machines, any fluctuations on the grid are significant fluctuations.

A "New Phase Modulation" technique proposed by Soltani and Szabados in 2001 which utilized up to date power electronics equipment to create a more accurate power inverter to run a system of five machines instead of a three machine system. The increase in the number of machines was justified by the assumption that "motor manufactures prefer to build rotating machines rather than buying special purpose large transformers" [6] for full load testing. The New Phase Modulation technique implemented a driver motor, two synchronous generators and two squirrel cage induction machines. The driver motor was used to bring the generators to full speed. The modulation technique produced a variable frequency voltage from each of the two generators, which in turn were used as sources for the two squirrel cage machines. Each generator/motor created a pair or system which was controlled in opposition of phase from the other pair. One of the two pairs contained the unit under test and the other pair a recovery unit designed to limit power fluctuations.[9] However, under further assessment [3] it was found that although simulation results showed no fluctuations on the driver motor, experimental results did not agree, fluctuating by 10%.

A "Sinusoidal Phase Modulation" technique proposed by Szabados alters the control signal from square waves and fixed DC sources to sinusoidal signals. The optimized new phase modulation technique utilizes advances in power electronics and decrease in cost to manufacture a new, more accurate and flexible control circuit for modulation. The sinusoidal signals provide the optimal form of synthetic modulation for the electric machine under test but require very precise control. The physical setup is kept constant with the New Phase Modulation technique. Simulation results show as before, that if the power exchange through each of the two systems is in exact opposition, the driver motor exhibits no power fluctuations. Experimental results show a fluctuation in the driver motor of less than 2%.

1-2 Objectives

The objectives in this thesis are to eliminate the power fluctuations observed in [3] by designing a more accurate control system, designing a measurement circuit to safely step down high motor voltages and currents to acceptable data acquisition levels and to alter the modulation signals to ideal values.

Two components are involved in the designing of the control circuit for the sinusoidal modulation scheme; hardware and software. The first objective is to design a control printed circuit board (PCB) accurate and fast enough to receive and send real time commands and measurements. The PCB safely steps down high voltages and currents through the use of power transformers (PTs) and current transformers (CTs). These low voltage conditioned signals are then used as inputs for data acquisition cards. These values are recorded and stored for analysis. Furthermore, the control PCB components must be able to sustain the high voltages and currents required to drive the experiments and ensure that the high side is completely isolated from the low side control voltages. The second objective is to design a software interface which is able to mimic the ideal sinusoidal modulation parameters as closely as possible and with the most degrees of freedom as possible. An important design variable to take into account is the ability to finely tune the phase shift between machines as this was identified as a problem in [3]. The software must also allow for real time control, automated control and have the ability to store and display the data.

The third objective of this thesis is to simulate and experiment with the Sinusoidal Modulation technique which utilizes sinusoidal modulations as opposed to the square wave modulations utilized in [3]. This is the ideal modulation method as described in [9] but requires precisely controlled DC sources which require accurate equipment to implement. [9]

1-3 Thesis Structure

This thesis contains six chapters. Chapter two summarizes and explains past synthetic loading techniques as well as the Sinusoidal Modulation technique to be examined in this thesis along with the optimum modulation parameters. Chapter three summarizes the mathematical model implemented in [3] and its modifications along with the machines used for simulations and experiments. Chapter four explains the hardware and software design features of this experiment. The two control and two measurement printed circuit boards design steps are explained here in detail. The LabView designed virtual environment utilized for control and measurement is also described along with the rotating machine setup, instrumentation and physical arrangements. Chapter five compares simulated and experimental results achieved for attempting to negate power fluctuations using the optimized new phase modulation technique. Chapter six lists the arrived at conclusions and gives insight into future work.

Chapter 2: Literature Review

2-1 Proposed Synthetic Loading Methods

There have been a number of different proposals developed [10],[11], [9] and [3] which aim at achieving rated heat run tests without mechanically loading an electric machine by supplying a variable frequency. Before these proposals are reviewed, it is beneficial to their understanding that we quickly review the basic operation of induction motors.[3]

2-1-1 Synthetic Loading Principles

A balanced three phase induction machine supplied by a fixed frequency power supply connected to the stator will produce a rotating electric field at a constant speed, or synchronous speed. The rotor in the induction machine has a tendency to follow this speed. Since the synchronous speed is proportional to the supply frequency expressed by Equation 2-1, where $f_s$is the supply frequency, P is the number of poles and $n_s$is the synchronous speed, any changes in supply frequency will affect the speed of the rotor. As the supply frequency is increased, the rotating electric field created in the stator speeds up causing a speed increase in the rotor. For the rotor to accelerate, the induction machine must draw heavier line currents from the supply. Conversely, if the supply frequency is decreased, the rotating electric field created by the stator is rotating slower than the rotor causing the rotor to slow down. This is accompanied by heavier currents been drawn from the rotor, effectively turning the motor into a generator. A continuous change in frequency is accompanied by continues energy transfers which show themselves in the form of heat dissipation causing temperature increases in the electric machine. Thus appropriate changes in frequency should be able to increase the temperature of the electric machine under test to rated values.[4], [1], [3]

$$n_s = \frac{2 \times f_s}{P} \quad in\, r/s$$

Equation 2-1

The principle of equivalent loading is illustrated in Figure 2-1.[9] The air gap voltage, E, of an induction machine which is not loaded is nearly equivalent to the applied armature voltage, V, in both magnitude and phase. Since the machine is not loaded, we also expect to see a small no load current I_0, as illustrated in Figure 2-1a. Figure 2-1b illustrates the increase in the no-load current, calculated by taking the difference between the air gap voltage and armature voltage, of an induction machine that is loaded. Figure

2-1b also shows the increase in the angle β. The objective of synthetic loading is to increase the angle, β, without having a mechanical load connected to the shaft.

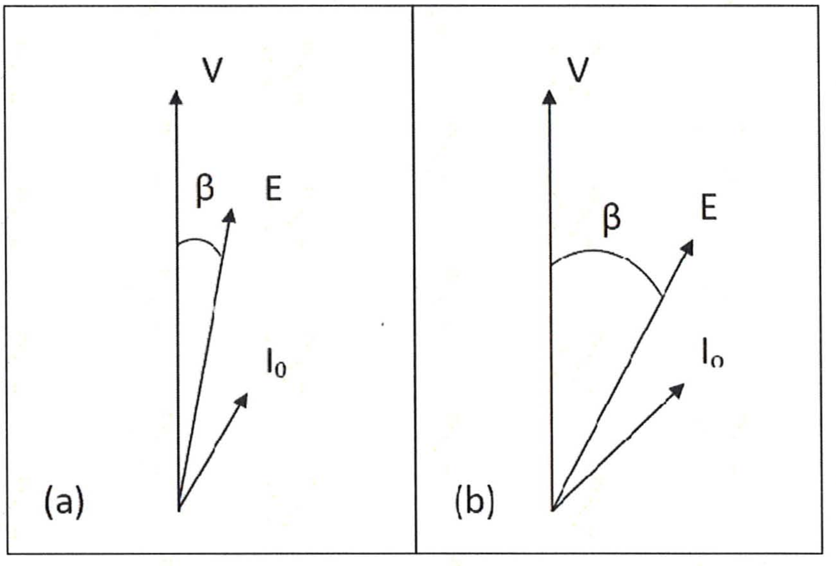

Figure 2-1- Principle of Synthetic Loading adapted from [6]

2-1-2 Proposed Phase Modulation Methods

The "Two-Frequency Modulation" method proposed by [12] utilized two three phase generators connected in series to produce a variable frequency for a third test machine. In [12], all three machines were induction machines. Figure 2-2 illustrates the two-frequency method graphically using phasor diagrams.

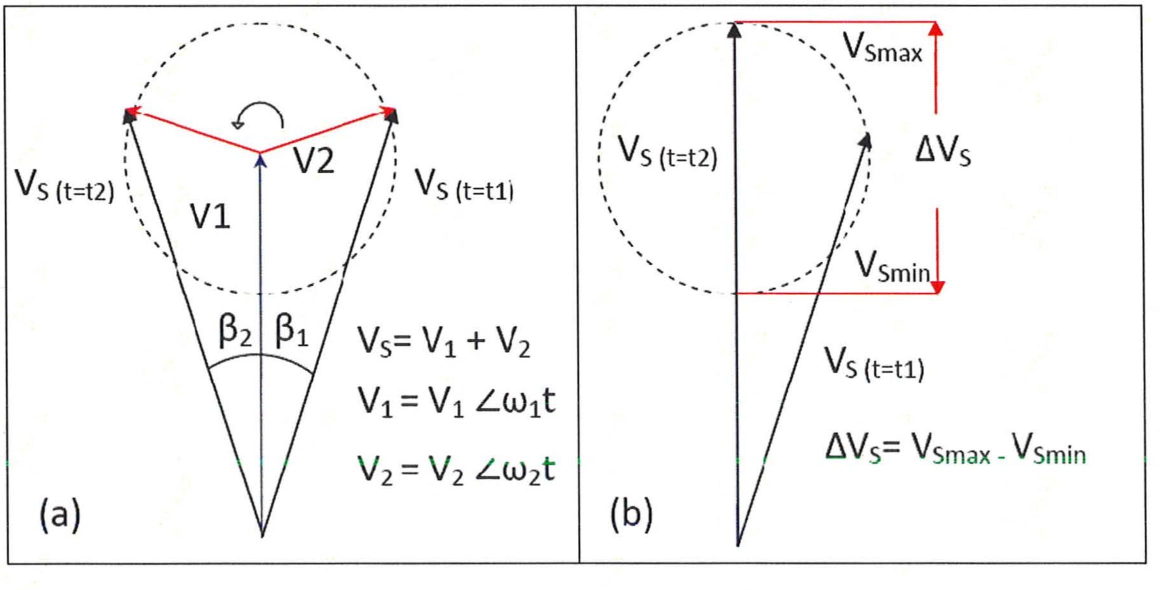

Figure 2-2 - Two Frequency Method adapted from [3]

Figure 2-2a shows two phasors, V_1 in blue and V_2 in red, each rotating at different frequencies, ω_1 and ω_2. The resultant vector V_S, the sum of V_1 and V_2, rotates along the dashed circle at a rate of ω_1 - ω_2, while increasing and decreasing in magnitude at a rate between ω_1 and ω_2. This causes the rotor of the machine under test to vary its speed, storing energy in the rotor when accelerating and returning the stored energy when decelerating, thus emulating a loaded machine. To ensure rated conditions are met during the heat run, angles β_1 and β_2 must be sufficiently large. This is achieved by increasing the magnitude of voltage V_2.[3]

However, it was pointed out in [5] that the two frequency modulation method experienced terminal voltage fluctuations of 80% of the rated value. These fluctuations are illustrated in Figure 2-2b. To achieve rated heat run conditions, the magnitude of V_2 has to be around 40% of the magnitude of V_1. This causes the voltage ΔV_S to fluctuate between 60% and 140% of the rated values driving the machine to undervoltage or saturation.[5] This can cause measurement inaccuracies as well as large power swings at the modulation frequency.[5] If the test machine is large enough, these fluctuations between the grid and test machine can cause short term power outages and long term damage to the grid. As such, a new modulation method is needed to suppress the power fluctuations between the test machine and the grid.

2-1-2-1 Use of Wound Rotor Induction Machine

A "New Phase Modulation" technique was proposed in [9] in efforts to alleviate power fluctuations between the test motor and the grid. The "New Phase Modulation" Method incorporates the use of wound rotor machines and power electronics to control the modulation frequency.

2-1-2-1-1 Bang-Bang Control

The new phase modulation technique requires a wound rotor synchronous machine with spatially aligned rotor windings 90 degrees out of phase as shown in Figure 2-3a.[6] By supplying a controlled DC pulse to the direct axis and a fixed DC pulse to the quadrature axis one can create a flux that fluctuates between β_1 and β_2 as shown in Figure 2-3b.[6] The direct axis excitation current I_1 at $t = t_1$ along with the quadrature axis excitation current I_2 produce a flux Φ_1 at phase angle β_1. At a later time $t = t_2$, a flux Φ_2 is created producing an oscillating flux with a phase angle between β_1 and β_2.

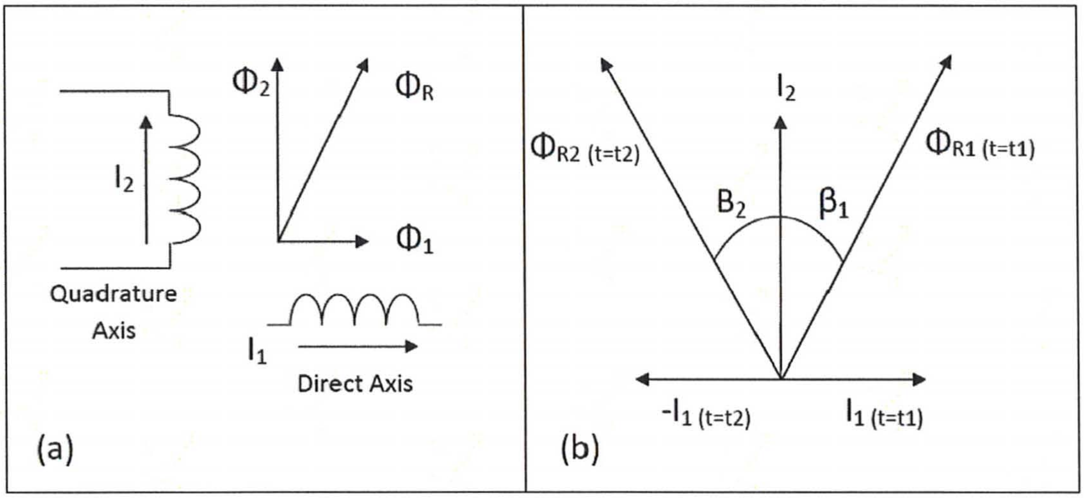

Figure 2-3 - Dual Field Winding Control Adapted from [6]

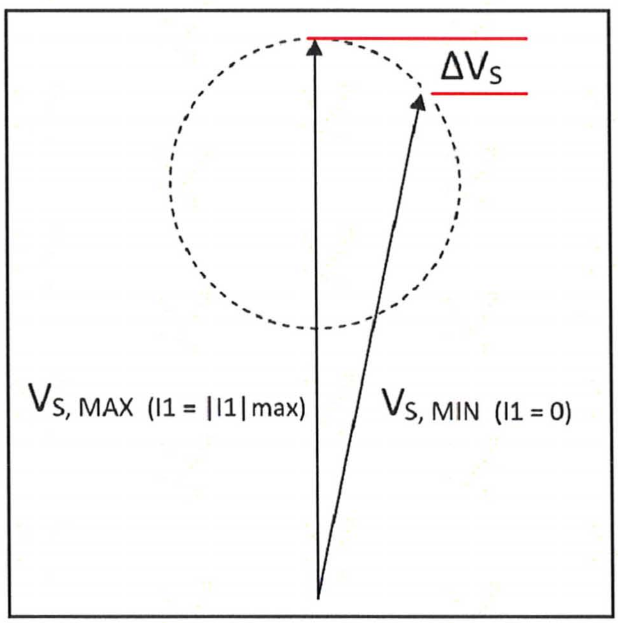

Figure 2-4 - New Phase Modulation Technique Adapted from [3]

The advantage of the bang-bang control is the resultant voltage V_S, which varies as the derivative of the phase angles β_1 and β_2 and the synchronous frequency created by the generator. The voltage magnitude is shown in Figure 2-4 and its angular velocity is described by Equation 2-2. This is beneficial because the voltage V_S has much smaller fluctuation when compared to the two-frequency method in Figure 2-2b.

$$\omega_0 - \frac{d\beta_2}{dt} \leq \omega_S \leq \omega_0 + \frac{d\beta_1}{dt} \qquad \textbf{Equation 2-2}$$

The rotor windings of the wound rotor machine are physically arranged 120 degrees apart. By connecting two of the three windings in series and leaving the third untouched, we can create the required 90 degree spatial difference necessary for modulation. Figure 2-5 shows the conversion of the wound rotor induction machine to a synchronous generator.[3] The summation of the induced flux in phase A and phase B are 90 degrees out of phase with the flux induced in phase C.

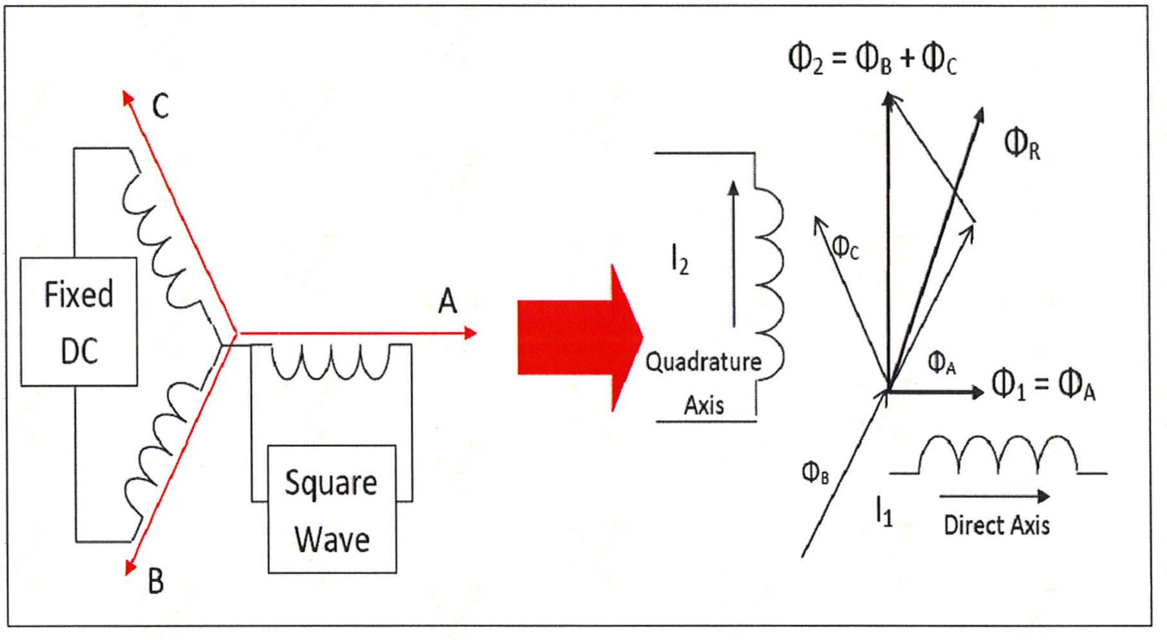

Figure 2-5 - Conversion of a Wound Rotor Induction Machine Adapted from [3]

By switching the controlled DC pulse in a bang-bang mode one effectively varies the current between positive and negative values in the direct axis. The approach used in [6] is to use a controlled inverter to produce a square wave. This will induce a flux along the direct axis which will vary between positive and negative values. The flux induced along the quadrature axis by I_2will always point in one direction since it is controlled by a fixed DC source. By appropriately choosing modulation values of the two currents it is possible to increase and decrease the phase angle as required.[3]

The physical implementation proposed in [5] is seen in Figure 2-6. A squirrel cage induction machine is used as the driver motor D0, which drives the synchronous generator G, created above. These two machines are connected mechanically.[3] The modulated voltage Vs produced by the synchronous generator is used to drive the motor under test, M. The drawback to this method is that the full swing power fluctuations will be felt by the driver motor and the grid making the setup unattractive, especially for large machines. Figure 2-7 shows the setup proposed by [6] and [3], which utilizes a second pair of synchronous generator and motor which is used to absorb these power swings.

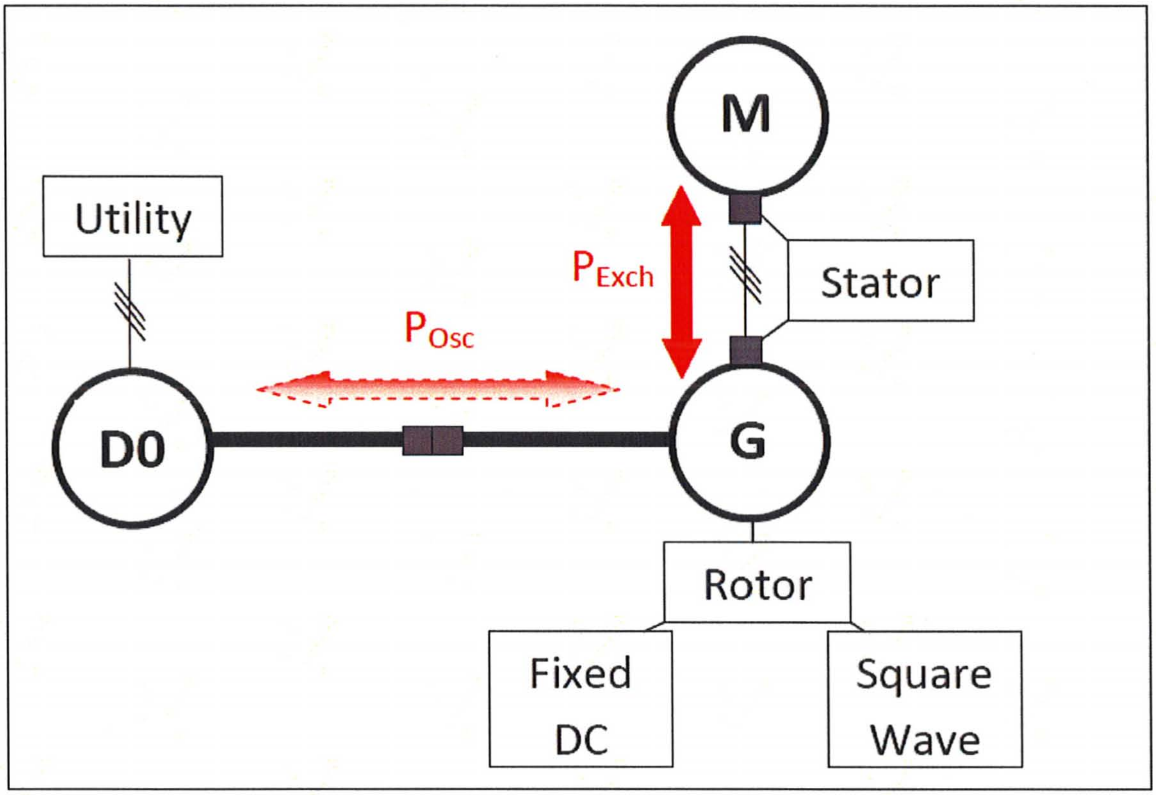

Figure 2-6 - Single System Physical Implementation adapted from [3]

The two generators G1 and G2 are mechanically coupled to the driver motor D0. The two generators are also coupled electrically to the test motor M1, and the recovery unit M2.[6] This creates two generator-motor pairings or systems. The power fluctuation can be negated by modulating each pair 180 degrees out of phase. Thus when one motor is accelerating, the other motor is decelerating effectively containing the power fluctuations between the two systems while leaving the driver motor to account for the losses of the five machine setup.[3]

The proposed modulation method can test both squirrel cage induction machines as well as wound rotor machines and since each generator can be controlled individually, the machine under test and the recovery machine do not have to be identical. This is an important feature in controlling power fluctuations since no two machines are ever created exactly the same. Individual control allows for machine customized control signals to counteract machine imbalance. A drawback of the new phase modulation method is the use of the square wave modulating pulse. The square wave voltage effectively creates an exponential current rise and fall in the field windings due to the inductive properties of the machines.[3] The exponential modulations along with the inability to finely control the phase angle of modulation precisely between the two systems caused the lowest power fluctuation felt by the driver motor to be in the range of 10% or 100W for a maximum loading of 1KW.[3] This power fluctuation must be further negated before the method can become a viable test method for industry.

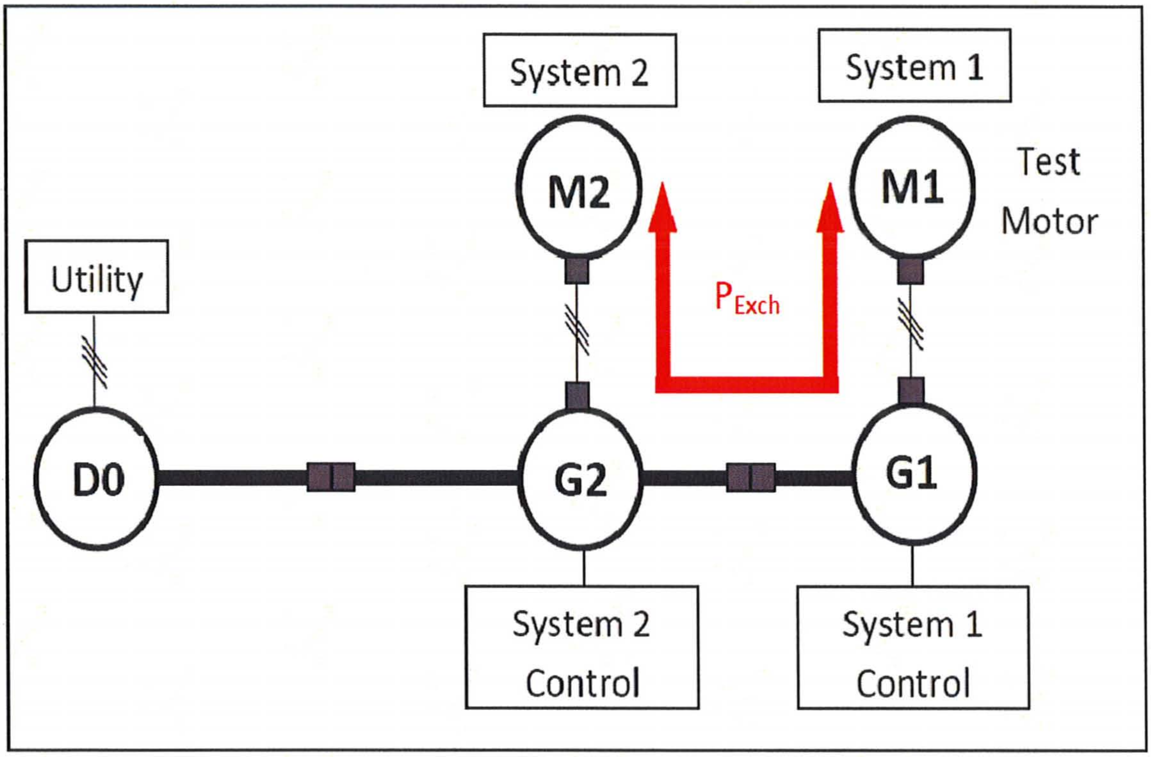

Figure 2-7 - Parallel System Physical Implementation adapted from [3]

2-1-2-1-2 Sinusoidal Modulation

This thesis focuses on the improvement of the New Phase Modulation technique by improving hardware control and changing the control signal from square waves to sinusoidal waves. The ideal modulation of the angle beta is the sinusoidal modulation.[6] The current I_1 and I_2 are now modulated using Equation 2-3 where f is the modulating frequency corresponding to β_1 and β_2. The currents are still applied to the direct and quadrature axes of the created synchronous generator as illustrated in Figure 2-5.

$$I1 = (I \times \sin(2\pi f t))$$
$$I2 = abs(I \times \cos(2\pi f t)) \quad \text{Equation 2-3}$$

There are two advantages for using sinusoidal modulations. The first stems from the resultant voltage vector Vs which rotates at an angular speed given by Equation 2-4 where ω_m is the angular velocity of the resultant voltage vector V_S, $\omega_0$is the synchronous angular speed and $\beta$is the phase angle of modulation.[6]

$$\omega_m = \omega_0 + \frac{d\beta}{dt}$$ **Equation 2-4**

The advantage lies in the fact that the derivative of a sinusoidal modulation is also a sinusoid.[6] This allows the created voltage V_S to vary its speed sinusoidally according to ω_m. This is an improvement over the square wave control implementation in [3] as it allows for smoother and more natural fluctuations in speed of the machine under test. This better mimics full load conditions of a physically loaded machine.

The second advantage to the sinusoidal modulation is that the resultant magnitude of vector V_S will always be constant as shown by Equation 2-5.[6] This advantage satisfies one of the characteristics identified in [5] as important to the synthetic modulation process. This is further described in the section dealing with Modulation Parameters.

$$sin^2(x) + cos^2(x) = 1$$ **Equation 2-5**

The two modulating advantages provide ideal modulating parameters. The physical setup for the experiment is the same as in [3]. The difference lies in the control hardware, software and signals itself. Initial simulation results of the Sinusoidal Modulation technique show a perfect power transfer between the test system and the recovery system shown in Figure 2-7. With the appropriate hardware and software control, it is expected that power fluctuations on the driver motor and the grid can be eliminated.

2-1-2-2 Modulation Parameters

Modulation parameter indentified by [5] as important for both the new phase modulation technique and the sinusoidal modulation technique are the frequency of modulation and the depth of modulation. These parameters are illustrated in Figure 2-8. The modulation depth is defined as the amount by which the frequency deviates from the natural frequency of 60Hz.[5] The modulation frequency is defined as the rate at which the modulation depths occur.[5] These deviations are needed to create equivalent temperature rise in the machine under test.

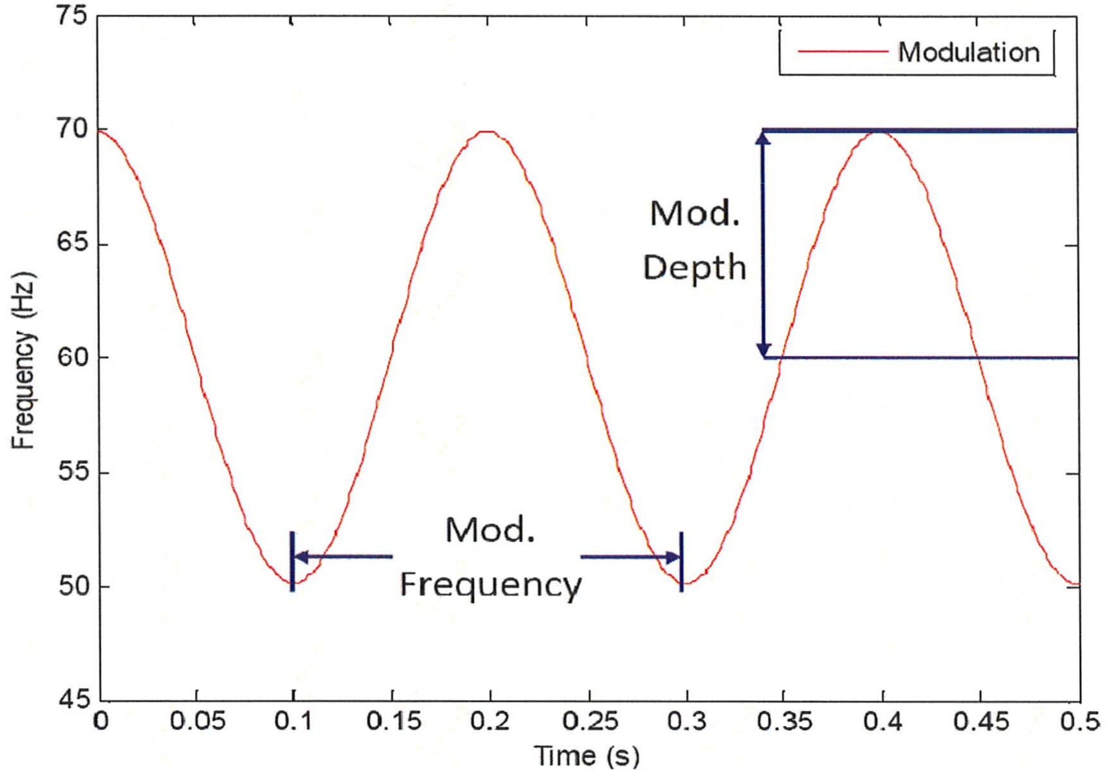

Figure 2-8 - Modulation Depth and Frequency Adapted from [5]

It was identified in [5] that the optimal modulation frequency and modulation depth for a single test machine as illustrated in Figure 2-6 is a 10Hz modulation frequency and a 5Hz modulation depth. These parameters were determined experimentally so that the machine under test achieved rated load conditions. These values were subsequently altered for optimal conditions to be reached in a five machine system as illustrated in Figure 2-7. However, care must be taken to keep the modulation depth small enough to keep the air-gap flux density at rated values.[5] This ensures that rated frequency and voltage are applied to the motor.[5] The smaller the modulation depth, the more uniform the voltage and frequency applied to the motor. The modulation frequency must also be adjusted to appropriate values. If the frequency is too low, the modulation depth will have to be increased to compensate and voltage fluctuations will be introduced.[3] If the modulation frequency is too high, then the rotor of the synchronous generator cannot properly follow the change in speed and the modulation will not achieve rated values in the test motor. As described in the above section, one of the advantages of the sinusoidal modulation technique is its ability to maintain a constant voltage magnitude during modulation.

Experimental results for the setup in the five machine setup depicted in Figure 2-7 revealed an optimal modulation frequency of 5Hz and a modulation depth of 10Hz. These values are depicted in Figure 2-8. Experiments were conducted using the modulation values proposed in [5] but the results proved inconclusive.

Chapter 3: Mathematical Model

It is important to try and forecast the outcome of an experiment before implementing it physically. This can help predict the outcome and results and may help with design modifications aimed at preventing unforeseen damage to the equipment under test. A good way to predict the outcome of an experiment is through the implementation of a good mathematical model. This chapter aims at explaining the principles behind the mathematical model presented in [3] and illustrating the modifications made to the model in order to simulate the sinusoidal phase modulation technique.

3-1 Reference Frame Theory

3-1-1 Background

The performance of electric machines can be described with the aid of differential voltage and torque equations. These equations can simply be dependent on speed or they can be time-varying in the case of differential voltage equations. As such, a change of variables is proposed to reduce the difficulty of these equations and help with the process of mathematical modeling.[13]

The idea of a variable change for analysis of synchronous machines was first proposed by Park [14] in 1920. Park referred the variables describing the stator windings to a frame of reference fixed in the rotor.[13] This proved extremely useful as it removed all time varying variables from the differential voltage equations. Subsequently Stanley [15] used the variable change technique to refer the rotor winding variables to a reference frame fixed with the stator. Kron [7] established a change of variables for symmetrical induction machines which referred both the stator and the rotor time varying variables to a synchronously rotating reference frame. Brereton established a change of variables for symmetric induction machines which referred the stator variables to a reference frame fixed on the rotor. It was subsequently discovered that a general transformation could remove all time-varying inductances in an induction machine by referring both the stator and the rotor to a reference frame which rotated in an arbitrary reference frame.[13] However this is not the case for the synchronous machine for which the transformation introduced by [14] proves to be most advantageous.[13] It is obvious that there exists an optimal variable substitution which is best utilized for induction machine and one for synchronous machines.

3-1-2 Equations of Transformation

The motive behind the change of variable technique stems from the complex differentially time-varying voltage equations which are used to describe the actions of the rotor and stator of both induction and synchronous machines. We can then refer these equations to an arbitrary reference frame which remains stationary or rotates at any arbitrary speed denoted by ω. This transformation is illustrated in Figure 3-1 although it must be noted that it does not have any physical meaning as the variable changes are only mathematical in nature.[13] The variable `f` can take the place of a voltage, current or electric charge. The three black lines represent the three phases of an electric machine which are spatially aligned to be 120 degrees apart. The two red lines are at a right angle to each other and form the direct and quadrature axes. The subscript `s` is used to denote stationary circuits, `q` denotes the quadrate axis, `d` denotes the direct axis, `a`, `b` and `c` represent the three phases and `θ` denotes an angular displacement.

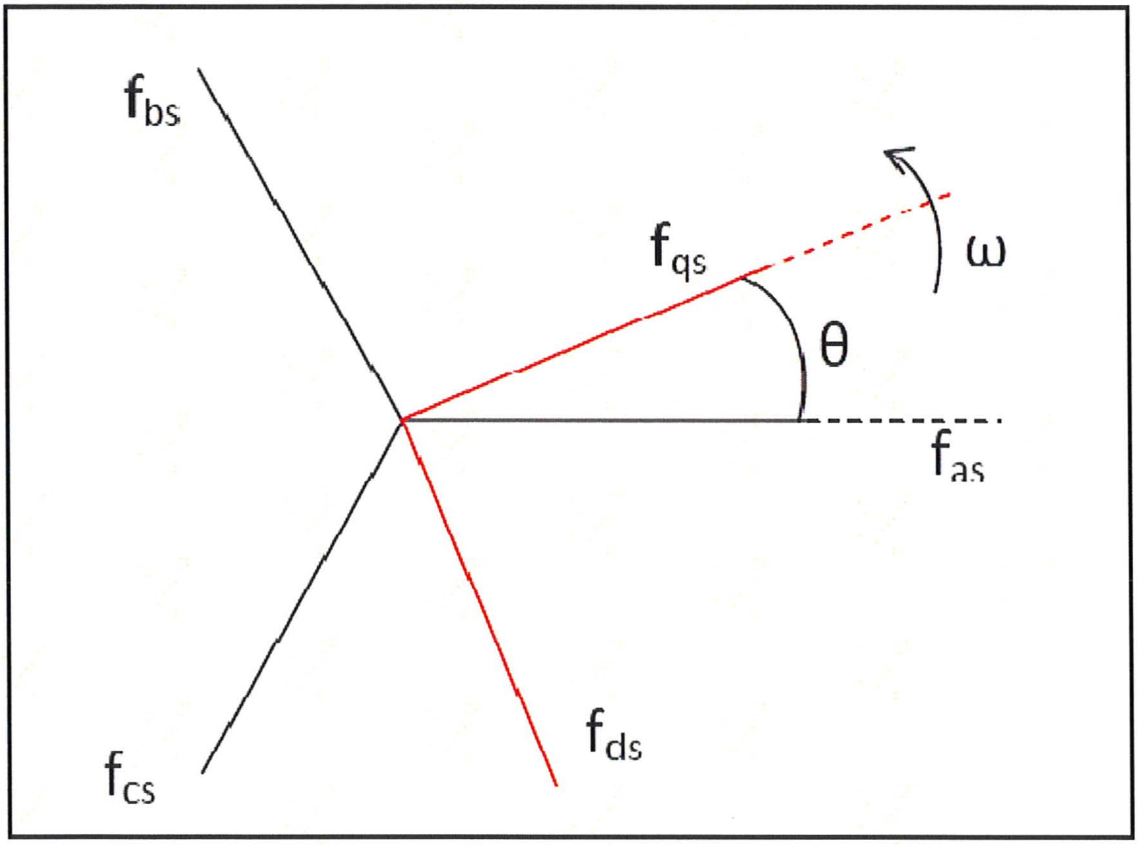

Figure 3-1 - Transformation for Stationary Circuits using Trigonometric Relationships

The mathematical representation for transformations of stationary circuits having ω = 0, is represented below:[13]

$$f_{qd0s} = K_s f_{abcs} \qquad \textbf{Equation 3-1}$$

Where

$$(f_{qd0s})^T = [f_{qs}\ f_{ds}\ f_{0s}]$$ **Equation 3-2**

$$(f_{abcs})^T = [f_{as}\ f_{bs}\ f_{cs}]$$ **Equation 3-3**

$$K_s = \begin{bmatrix} \cos\theta & \cos\left(\theta - \frac{2\pi}{3}\right) & \cos\left(\theta + \frac{2\pi}{3}\right) \\ \sin\theta & \sin\left(\theta - \frac{2\pi}{3}\right) & \sin\left(\theta + \frac{2\pi}{3}\right) \\ \frac{1}{2} & \frac{1}{2} & \frac{1}{2} \end{bmatrix}$$ **Equation 3-4**

$$(K_s)^{-1} = \begin{bmatrix} \cos\theta & \sin\theta & 1 \\ \cos\left(\theta - \frac{2\pi}{3}\right) & \sin\left(\theta - \frac{2\pi}{3}\right) & 1 \\ \cos\left(\theta + \frac{2\pi}{3}\right) & \sin\left(\theta + \frac{2\pi}{3}\right) & 1 \end{bmatrix}$$ **Equation 3-5**

$$\theta = \int_0^t \omega(\zeta)d(\zeta) + \theta(0)$$ **Equation 3-6**

The superscript `T` refers to the transpose of a matrix, the superscript '-1' refers to the inverse of a matrix and `$\zeta$` is a dummy variable of integration.[13] The beauty of this transformation is that the change of variables can be so altered from the stationary representation above to any arbitrary angular velocity ω. As such, the transformation can be used to simplify the rotor and stator circuits of both induction and synchronous machines making further calculations and mathematical modeling a lot simpler.[13]

3-2 Squirrel Cage Induction Motors

The equivalent circuit for a three phase, wye connected symmetrical squirrel cage induction machine is illustrated in Figure 3-2. The stator windings are illustrated on the left hand side of Figure 3-2 and are 120 degrees out of phase. Both the resistance r_S and the equivalent turns ratio N_S are equal for all three phases. The subscript `s` denotes values associated with the stator. The rotor windings are illustrated on the right hand side of Figure 3-2 and are also 120 degrees out of phase. The windings are also identical with the resistance r_r and the equivalents turns ratio N_r equal for all three phases. The subscript `r` denotes values associated with the rotor.

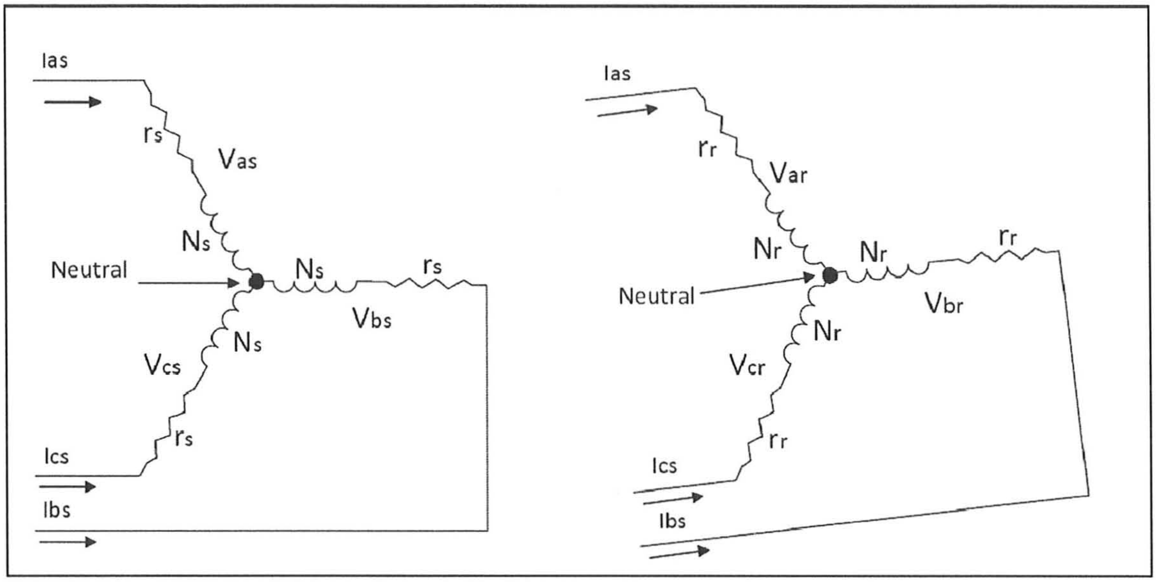

Figure 3-2 - Symmetrical 3-Phase Induction Machine Circuit

The following voltage equations described in [13] represent the stator and rotor of the symmetrical induction machine. The variables of the rotor have been referred to the stator. The ' is used to represent values referred from the rotor to the stator in all further work.

$$\boldsymbol{v}_{abcs} = \boldsymbol{r}_s \boldsymbol{i}_{abcs} + \frac{d}{dt}\boldsymbol{\lambda}_{abcs}$$ **Equation 3-7**

$$\boldsymbol{v}'_{abcr} = \boldsymbol{r}'_r \boldsymbol{i}'_{abcr} + \frac{d}{dt}\boldsymbol{\lambda}'_{abcr}$$ **Equation 3-8**

The bold values represent matrices. The flux linkages are described in [13] and shown in Equation 3-9 for magnetically linear systems.

$$\begin{bmatrix} \lambda_{abcs} \\ \lambda'_{abcr} \end{bmatrix} = \begin{bmatrix} \boldsymbol{L}_s & \boldsymbol{L}'_{sr} \\ (\boldsymbol{L}'_{sr})^T & \boldsymbol{L}'_r \end{bmatrix} \begin{bmatrix} \boldsymbol{i}_{abcs} \\ \boldsymbol{i}'_{abcr} \end{bmatrix}$$ **Equation 3-9**

The above voltages in Equation 3-7 and Equation 3-8 can be transformed to the arbitrary reference frame through the use of variable changes. By mathematical manipulation and the use of the Park transform described in [13] and section 3-1-2 we arrive at the following voltage equations which describe the original squirrel cage induction machine in the arbitrary reference frame.

$$\boldsymbol{v}_{qd0s} = \boldsymbol{r}_s \boldsymbol{i}_{qd0s} + \omega \boldsymbol{\lambda}_{dqs} + \frac{d}{dt}\boldsymbol{\lambda}_{qd0s}$$ **Equation 3-10**

$$v'_{qd0r} = r'_r i'_{qd0r} + (\omega - \omega_r)\lambda'_{dqr} + \frac{d}{dt}\lambda'_{qd0r}$$ **Equation 3-11**

The equivalent circuit obtained from Equation 3-10 and Equation 3-11 is illustrated in Figure 3-3. All original 'abc' phase variables have been replaced and translated to the 'qd' axes.

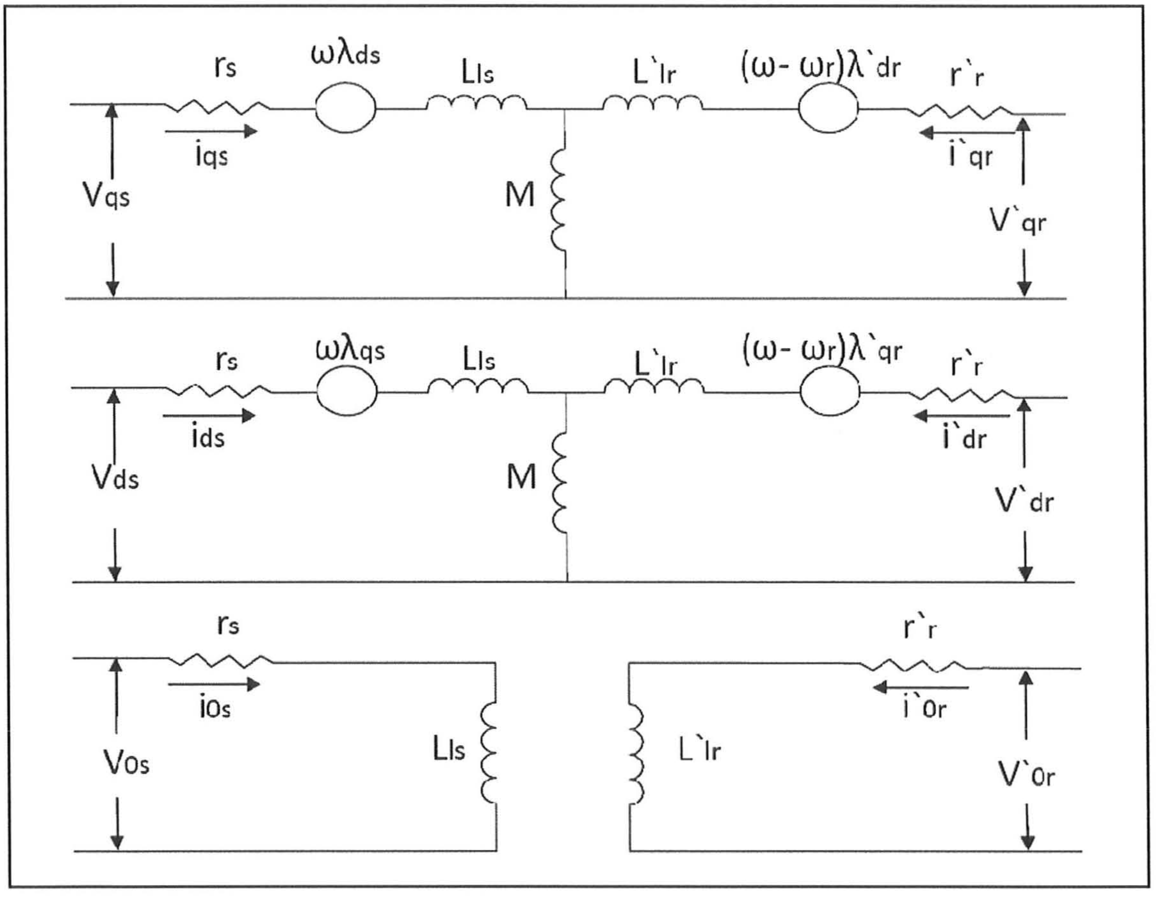

Figure 3-3 - Equivalent 3-Phase Symmetrical Induction Machine Circuit in the Arbitrary Reference Frame

To fully describe the induction machine using mathematical equations we have to translate the created electromagnetic torque T_e to the 'dq' axes. The expression for electromagnetic torque is defined in [13] as the sum of the inertial torque and load torque and is given by Equation 3-12.

$$T_e = J\left(\frac{2}{P}\right)\frac{d}{dt}\omega_r + T_L$$ **Equation 3-12**

The electromagnetic torque thus depends on the inertia of the machine J, the number of poles P, the derivative of the angular velocity of the rotor ω_r and the load torque T_L on the shaft of the machine. By rearranging Equation 3-12 we can express the load torque in terms of the derivative of the angular velocity. This is expressed in Equation 3-13.

$$\frac{d}{dt}\omega_r = \left(\frac{P}{2J}\right)T_e - T_L$$ **Equation 3-13**

Further substitutions from [13] allow us to describe the derivative of the angular velocity in terms of stator and rotor currents. This is expressed in Equation 3-14 and its use will be apparent in a later section.[3]

$$\frac{d}{dt}\omega_r = \left(\frac{P}{2J}\right)\left(\left(\frac{3P}{4}\right)M\left(i_{qs}i'_{dr} - i_{ds}'i_{dr}\right) - T_L\right)$$ **Equation 3-14**

3-3 Synchronous Generators

The sinusoidal phase modulation technique utilizes a wound rotor synchronous machine as a generator to supply modulated current to the motor under test. As was explained in section 2-1-2-1-2, one rotor phase of the wound rotor machine is supplied from a modulated sinusoid while the other two phases are connected in series and supplied from a modulated cosinusoid. This arrangement produces a 90 degree spatial alignment between the two newly created phases which produce a flux along the direct and quadrature axes respectively. The equivalent circuit for the 2-phase synchronous generator is shown in Figure 3-4.

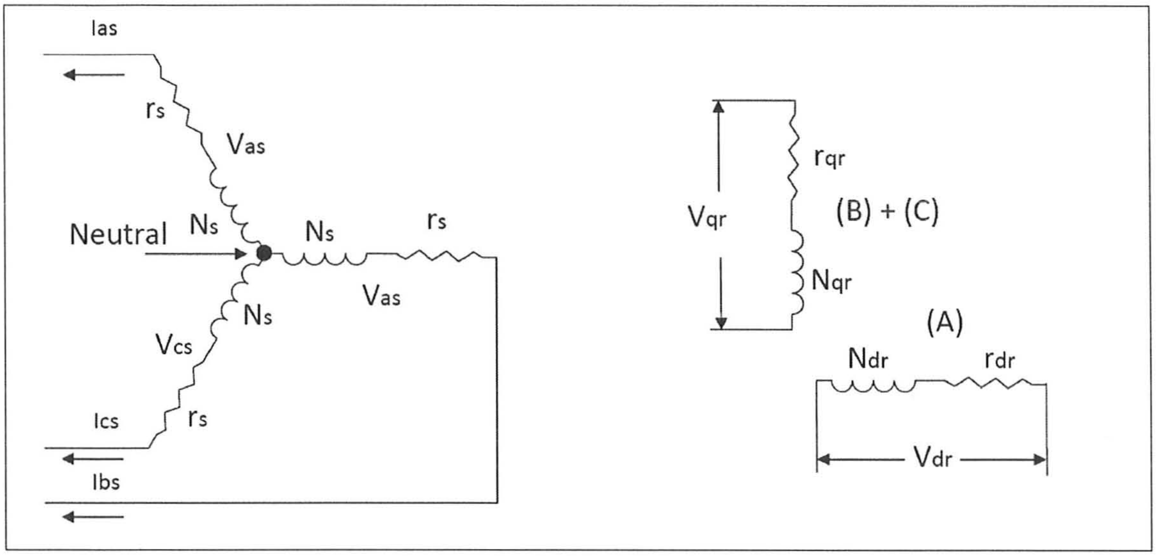

Figure 3-4 - Equivalent 2-Phase Synchronous Generator Circuit

The upside of this representation is that the rotor variables are already in the rotor reference frame which simplifies matters enormously in terms of mathematical complexity.[14] There are also a few key differences between the induction machine described in the previous section and the synchronous machine shown in Figure 3-4. Firstly, since we are dealing with a generator, the flow of current is out of the stator instead of into the stator.[3] Secondly, if we continue the assumption that all phases are symmetric in the stator and rotor, then we can conclude that the direct axis has an equivalent resistance of $r_{dr} = r_r$ and the equivalents turns ratio $N_{dr} = N_r$. This leads to the conclusion that the quadrature axis has an equivalent resistance of $r_{qr} = 2r_r$ and an equivalent turns ratio of $N_{qr} = 2N_r$. This leads to the following voltage equations as described in [14] which represent the stator and rotor of the synchronous machine. The variables of the rotor have once again been referred to the stator.

$$\boldsymbol{v}_{abcs} = -\boldsymbol{r}_s \boldsymbol{i}_{abcs} + \frac{d}{dt}\boldsymbol{\lambda}_{abcs}$$ **Equation 3-15**

$$\boldsymbol{v}'_{abcr} = \boldsymbol{r}'_r \boldsymbol{i}'_{abcr} + \frac{d}{dt}\boldsymbol{\lambda}'_{abcr}$$ **Equation 3-16**

Making sure to account for the proper flux linkage and expressing the voltage equations above in the rotor reference frame as described in [14] leads to:

$$\boldsymbol{v}_{qd0s} = -\boldsymbol{r}_s \boldsymbol{i}_{qd0s} + \omega \boldsymbol{\lambda}_{dqs} + \frac{d}{dt}\boldsymbol{\lambda}_{qd0s}$$ **Equation 3-17**

$$v'_{qd0r} = r'_r i'_{qdr} + \frac{d}{dt}\lambda'_{qdr}$$ **Equation 3-18**

The equivalent circuit illustrated in Figure 3-5 is drawn based on the above equations.[3]

As with the induction motor, a torque equation must be established before fully being able to mathematically describe the system. The electromagnetic torque for the synchronous generator is very similar to that of the induction machine however a negative sign is added in front of the inertial torque to depict the generator action.[3] Equation 3-19 describes the electromagnetic torque for the synchronous generator.

$$T_e = -J\left(\frac{2}{P}\right)\frac{d}{dt}\omega_r + T_L$$ **Equation 3-19**

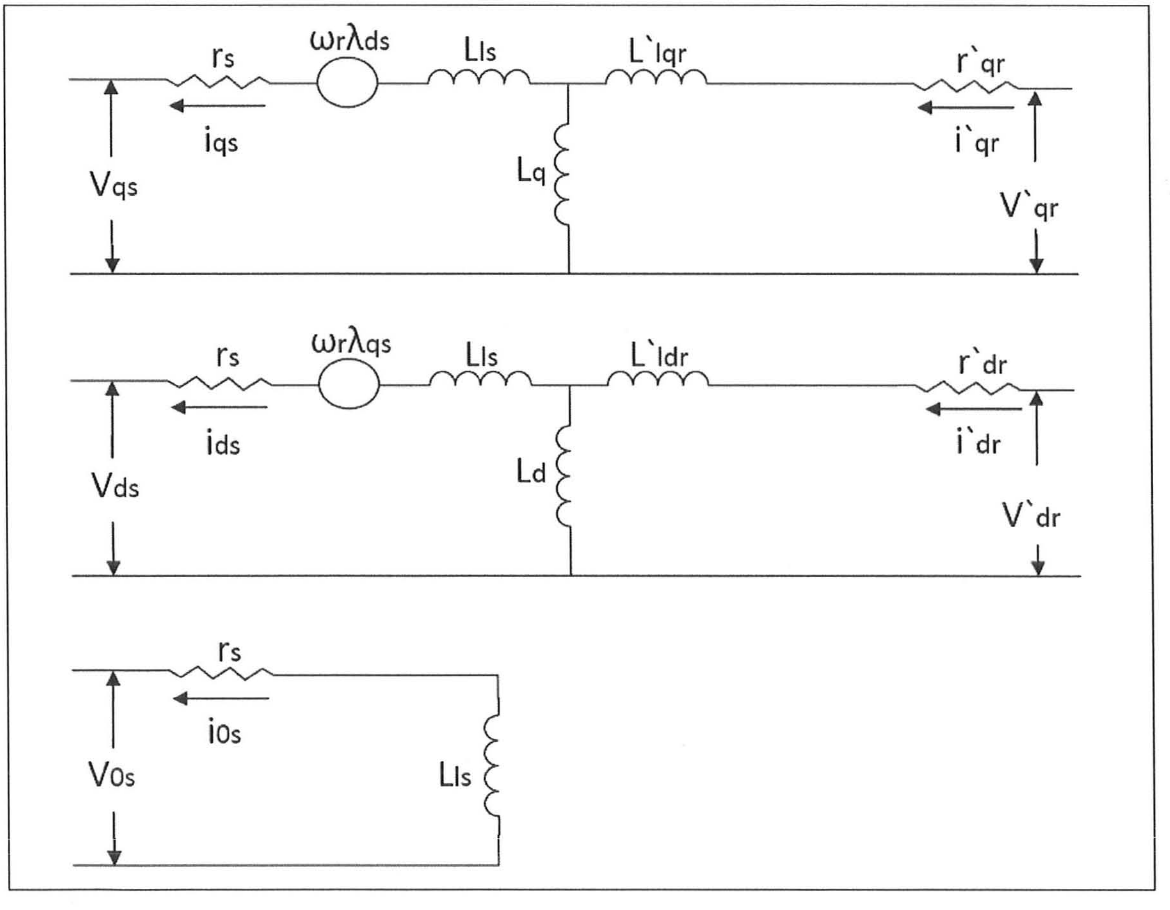

Figure 3-5 - Equivalent Synchronous Machine Circuit in the Rotor Reference Frame

As with the induction machine, the electromagnetic torque equation can be expressed in terms of the derivative of the angular velocity. This is described in Equation 3-20 and its use will once again be apparent in a later section.[3]

$$\frac{d}{dt}\omega_r = \left(\frac{-P}{2J}\right)\left(\left(\frac{3P}{4}\right)\left[L_d(-i_{ds} + i'_{dr})i_{qs} - L_q\left(-i_{qs} + i'_{qr}\right)i_{ds}\right] - T_L\right)$$ **Equation 3-20**

3-4 Complete Mathematical Model

The complete mathematical model is illustrated in Figure 3-6 and represents the equivalent circuit for a single system as illustrated in Figure 2-6 in Chapter 2. The driver motor in Figure 3-6 is coupled mechanically to the generator via the shaft. As it reaches full speed it rotates at an angular velocity ω_{r0}. To simplify calculations, the driver motor equations have also been transformed to the rotor reference frame. As such, the generator produces a voltage proportional to ω_{r0}. The test motor however is not coupled mechanically thus cannot utilize the same reference frame as the generator and driver motor and thus would rotate with its own angular velocity ω_{rm}. This problems is solved by setting the test motor to the synchronous rotating reference frame with $\omega_{rm} = \omega_{r0}$. This makes the voltage seen by the motor to rotate and an angular velocity equal to ω_{r0} - ω_{rm}.[3]

Since the generator and test motor are connected via the stators we can equate Equation 3-10 with Equation 3-17 and Equation 3-11 with Equation 3-18 to complete our model. By expansion we develop all necessary voltage equations.

$$\begin{aligned}\boldsymbol{v}_{qd0sg} &= -\boldsymbol{r}_s\boldsymbol{i}_{qd0sg} + \omega_{r0}\boldsymbol{\lambda}_{dqsg} + \frac{d}{dt}\lambda_{qd0sg} = \boldsymbol{v}_{qd0sm} \\ &= \boldsymbol{r}_s\boldsymbol{i}_{qd0sm} + \omega_{r0}\boldsymbol{\lambda}_{dqsm} + \frac{d}{dt}\boldsymbol{\lambda}_{qd0sm}\end{aligned}$$

Equation 3-21

$$\begin{aligned}\boldsymbol{v}'_{qd0rg} &= \boldsymbol{r}'_r\boldsymbol{i}'_{qdrg} + \frac{d}{dt}\boldsymbol{\lambda}'_{qdrg} = \boldsymbol{v}'_{qd0rm} \\ &= \boldsymbol{r}'_{rm}\boldsymbol{i}'_{qd0rm} + (\omega_{r0} - \omega_{rm})\boldsymbol{\lambda}'_{dqrm} + \frac{d}{dt}\boldsymbol{\lambda}'_{qd0rm}\end{aligned}$$

Equation 3-22

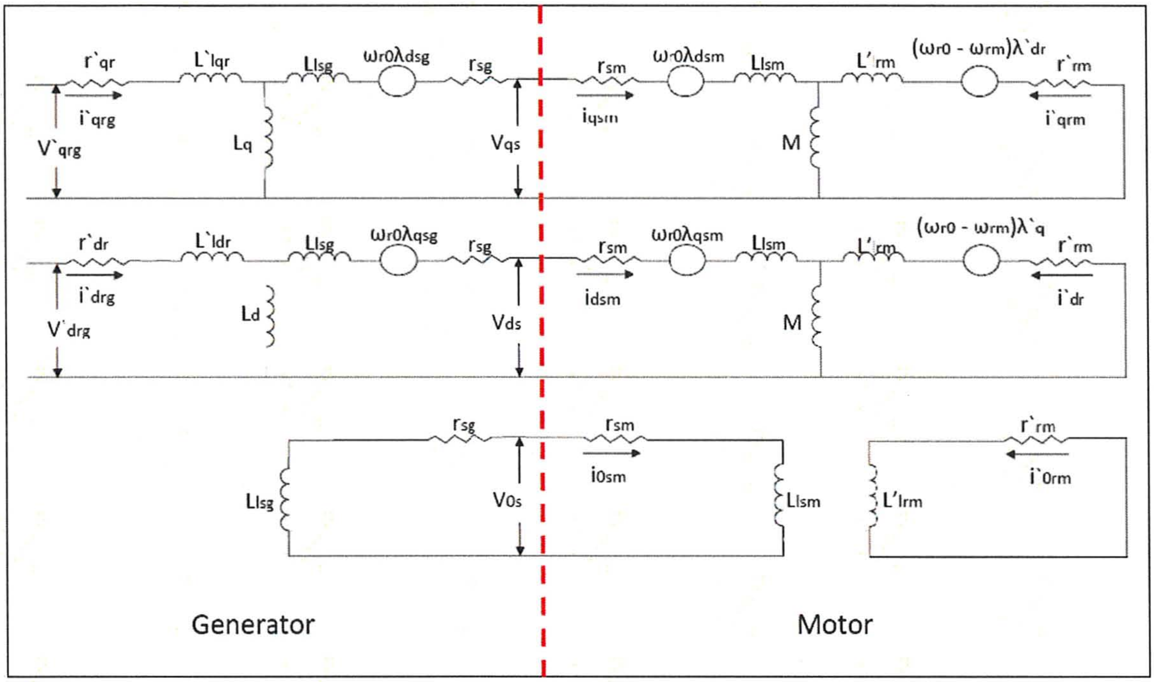

Figure 3-6 - Equivalent Single System Circuit

The last equation necessary to describe the entire system is the load torque equation for the driver motor D0.[3] The full system comprises of five electric machines of which three are connected mechanically; one induction machine and two generators. Therefore the load torque on the driver motor is affected by both mechanically connected generators and their angular velocities. Equation 3-23 describes the load torque T_L as derived in [3].

$$T_L = \frac{1}{H_0 + H_{g1} + H_{g2}} \left[T_{e0}\left(H_{g1} + H_{g2}\right) + H_{m0}\left(T_{eg1} + T_{eg2}\right) \right] \qquad \textbf{Equation 3-23}$$

Therefore the mathematical model of one of the five machines can be described by a combination of seven voltage equations, an angular velocity equation and two torque equations.

3-5 State Space Representation and Mathematical Simulation

A state space model was created in [3] to simulate the five machine system described by the equivalent equations in sections 3-2 to 3-4. As is typical in state space models, the equations used to describe electrical machines are either currents or flux linkages. [3] chose to depict his state space model using currents. As such, all voltage equations had to be rearranged through mathematical manipulation to be in terms of currents. Torque equations have also been rearranged in terms of angular velocities, where appropriate.

Table 3-1 describes the number and type of state space equations necessary to describe each machine.

Table 3-1 - State Space Varaibles Summary for the Five Machine Setup

State Space Variables					
	Stator	**Rotor**	**Angular Velocity**	**Torque**	**Total**
Driver Motor D0	qs,ds,0s	qr,dr,0r	ω_{r0}	T_e, T_L	9
System 1	qs,ds,0s	qs,qr,ds,dr	-	T_e	8
System 2	qs,ds,0s	qs,qr,ds,dr	-	T_e	8

A total of 25 state dependant state space equations we implemented and solved in Matlab using a fourth order Runge-Kutta numerical methods solver. Figure 3-7 from [3] depicts the program flow.

The top portion of the diagram depicts the state space model of the driver motor. The utility source voltages and currents are input to the system, transformed to the rotor reference frame via the Park transform and output as inputs for the two systems under test. The two systems are depicted in the lower portion of the diagram and operate identically. Each system solves for its specific voltage, current and torque equations and outputs those variables as results or as driving factors in the case of the created torque and angular velocity. The torques and angular velocities are in turn used to derive the load torque on the driver motor and its angular velocity which is used to drive the system. Once the simulation has concluded, all stored variable are referred back using the inverse Park transforms for numerical and graphical analysis.

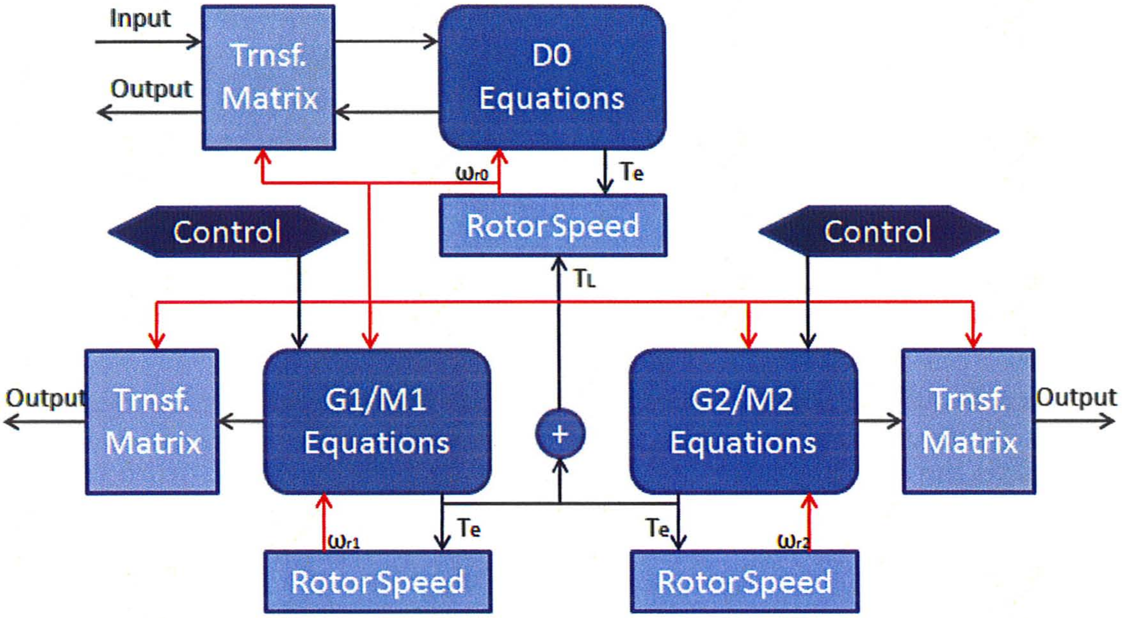

Figure 3-7 - Matlab Simulation System Flow Chart from [3]

3-5-1 Control Algorithm

The creation of a new control algorithm was necessary for simulation purposes of the sinusoidal phase modulation technique. The outcome of the simulation was necessary in deriving whether the technique was viable and whether physical experiments should be undertaken at all. The algorithm was implemented based on the theory introduced in [6] and in section 2-1-2-1-2. Sinusoidal and cosinusoidal modulations were introduced into the system to replace the previous square wave and DC modulations. Special care was taken to utilize the appropriate machine parameters and not to exceed machine specifications and guidelines proposed in [5] and [16]. The modifications increased the complexity of the algorithm and thus the runtime. Initial simulations produced positive results which matched theory expectations. Final simulation results are discussed in Chapter 5.

Chapter 4: Experimental Setup

4-1 Printed Circuit Board Design

Since the sinusoidal new phase modulation depends on precisely controlled DC sources, it is necessary to ensure that the equipment and components used for control are precise and accurate as well as rugged and able to withstand the high voltages and currents required of them. The circuitry itself must be reliable to ensure the continuous operation and safety of the components themselves, the machines they are controlling and the people that are operating them. This section of the thesis deals with the design of the two printed circuit boards used for control and measurement.

4-1-1 Building Blocks

4-1-1-1 Operational Amplifiers

The operational amplifier (op-amp) is one of the most commonly used components in electronics today. Its functionalities are diverse and in most cases easy to use. The measurement board and the control board designed for this thesis use many forms of the op-amp to create the final circuit. As such, a quick review of the basics of the op-amp will help explain the design of the circuit boards.

The op-amp is essentially a differential amplifier that amplifies the voltage difference between its two input terminals.[17] Ideally, op-amps have a very high input resistance, low output resistance and a high voltage gain.[17] There are two assumptions which are made when analyzing an op-amp circuit which greatly reduce its complexity:

$$I_{in} = 0$$ **Equation 4-1**

$$V^- = V^+$$ **Equation 4-2**

A fundamental op-amp is represented in Figure 4-1. These two assumptions above are based on the ideal op-amp and will be used throughout the chapter to aid with analysis. The MC33079 quad 14 pin Integrated Circuit (IC) is used for all op-amp circuits except for specific comparison tasks where a separate comparator is utilized.

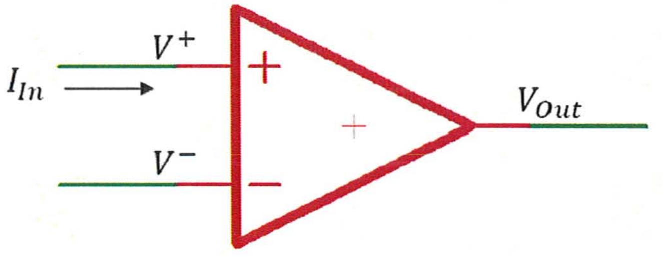

Figure 4-1 - Ideal Operational Amplifier

4-1-1-1-1 Impedance Buffer

A component used widely throughout the control board is the voltage follower or impedance buffer. The connections for the impedance buffer are shown in Figure 4-2. Based on the ideal op-amp principles, the voltage applied on the positive terminal will be equal to that of the output. Since $V^+ = V^-$ and $V^- = V_{Out}$ due to the negative feed back loop then it follows that $V^+ = V_{Out}$. The high imput resistance of the op-amp allows for almost perfect isolation between the source input and the output of the amplifier.[17] This makes the impedence buffer an extremely important and useful componant when trying to isolate signals, minimize distortions and maintain accuracy.

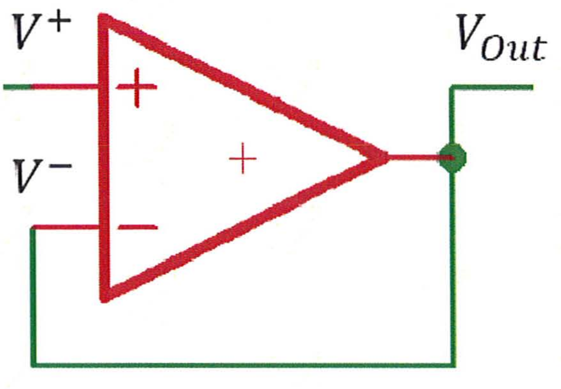

Figure 4-2 - Impedance Buffer

4-1-1-1-2 Level Shifter

Another useful circuit created with the aid of the op-amp is the differential amplifier or level shifter. The circuit is illustrated in Figure 4-3 and can be split up into two sections for the purpose of analysis.

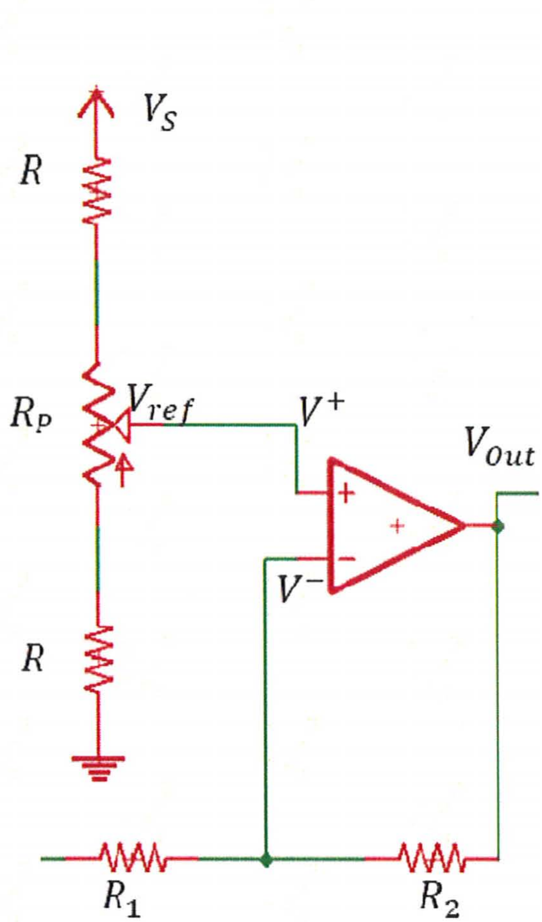

Figure 4-3 - Level Shifter

The mini circuit entering the negative terminal of the op-amp is simply a non-inverting closed loop gain circuit described by Equation 4-3and illustrated in Figure 4-4. Therefore, the appropriate selection of R_1 and R_2 can satisfy a wide number of gains assuming that the gain levels remain below the rail voltage of the op-amp.

$$V_{Out} = V^+ \times \left(1 + \frac{R_2}{R_1}\right) \qquad \textbf{Equation 4-3}$$

The mini circuit entering the positive terminal of the op-amp is an adaptation from a standard level shifter which would employ a precise DC source to regulate the offset. However, this adds cost to the circuit and does not allow for close control. One can create a controllable voltage reference V_{ref} by using two matched resistors R, a potentiometer R_P, and the already existing power supply required to power the op-amp.[17]

$$\mathrm{Vref} = \frac{\mathrm{R} + \Delta \mathrm{R}}{2\mathrm{R} + \mathrm{R_P}} \times \mathrm{V_S} \qquad \textbf{Equation 4-4}$$

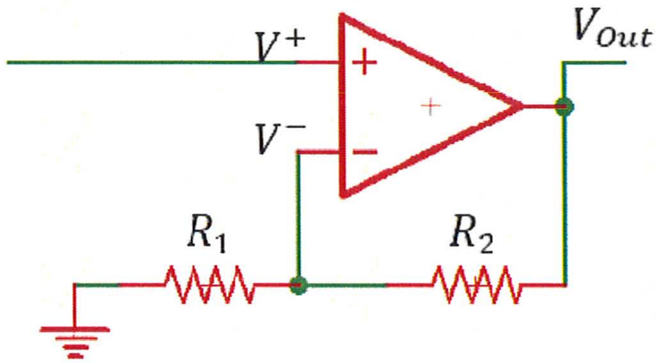

Figure 4-4 - Non Inverting Closed Loop Gain Circuit

V_{ref} is described by Equation 4-4 where ΔR is the adjustment ratio of the potentiometer. Therefore, any voltage reference V_{ref} between zero and V_S can be achieved by adjusting the potentiometer to the appropriate level. The complete circuit in Figure 4-3 is the level shifter with gain.

4-1-1-1-3 Integrator

Op-amps can also be used to differentiate or integrate a signal. Figure 4-5 shows the op-amp configuration for an integrator.

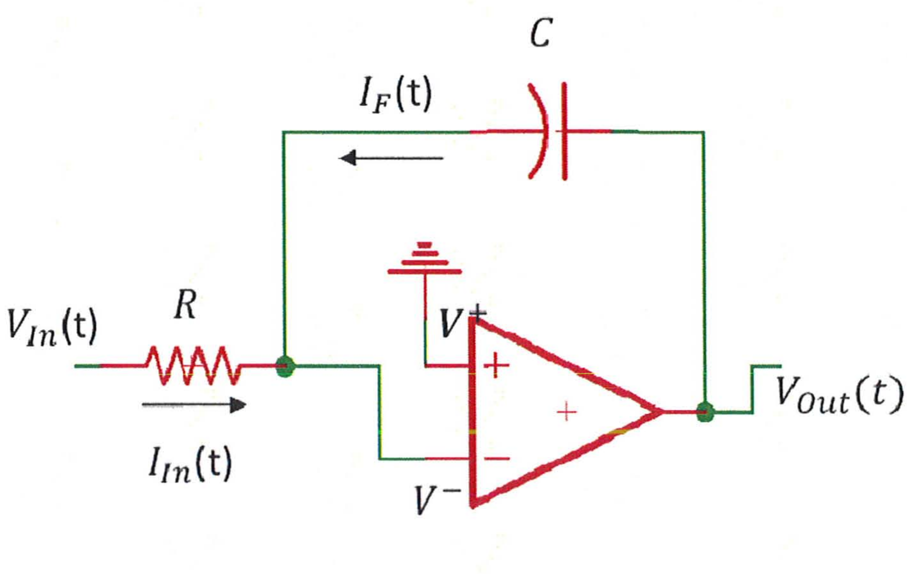

Figure 4-5 - Op-Amp Integrator

The analysis of the integrator circuit begins by realizing that $I_{In}(t) = -I_F(t)$ where

$$I_{In}(t) = \frac{V_{In}(t)}{R}$$ **Equation 4-5**

$$I_F(t) = C \times \frac{dV_{Out}(t)}{dt}$$ **Equation 4-6**

By equating the two currents, rearranging the equation and integrating both sides we end up with:

$$V_{Out}(t) = -\frac{1}{RC}\int_{-\infty}^{t} V_{In}(t')dt'$$ **Equation 4-7**

Equation 4-7 states that the output voltage is an integral of the input voltage, thus achieving the required integration action.

4-1-1-1-4 Digital Comparator

The digital comparator is another useful utilization of an op-amp. The comparator is shown in Figure 4-6. A basic comparator compares the input of the V^+ and V^- terminals and return a results based on the difference. The comparator is described by Equation 4-8 where A is the gain of the op-amp. It is important to note that since the open loop gain of op-amps is so large, any small difference between the two terminals will cause the op-amp to saturate to the supply voltage level. For example, if the voltage at V^+ is greater than V^- then V_{Out} is the saturation voltage of the op-amp $V_S{}^+$. Vice versa, if the voltage at V^- is greater than V^+ then V_{Out} is the saturation voltage of the op-amp $V_S{}^-$. This can be a useful feature especially when generating switching waveforms.[17]

$$V_{Out} = A \times (V^+ - V^-)$$ **Equation 4-8**

There are a few modifications that can be made to a basic comparator for the purpose of this thesis. Firstly, one of the input terminals of the op-amp has been connected to a reference voltage creator as with the level shifter described in the section above. This allows control over the reference between the positive and negative terminals of the comparator creating the ability to switch the positive or negative edge of the trigger to a desired value. Secondly, the LM311 specific integrated circuit has the advantage of an open collector output.[17] This, combined with a pull up resistor R and a +5V creates a switching waveform between 0 and 5 volts. This is an optimal way for creating digital signals or control logic.

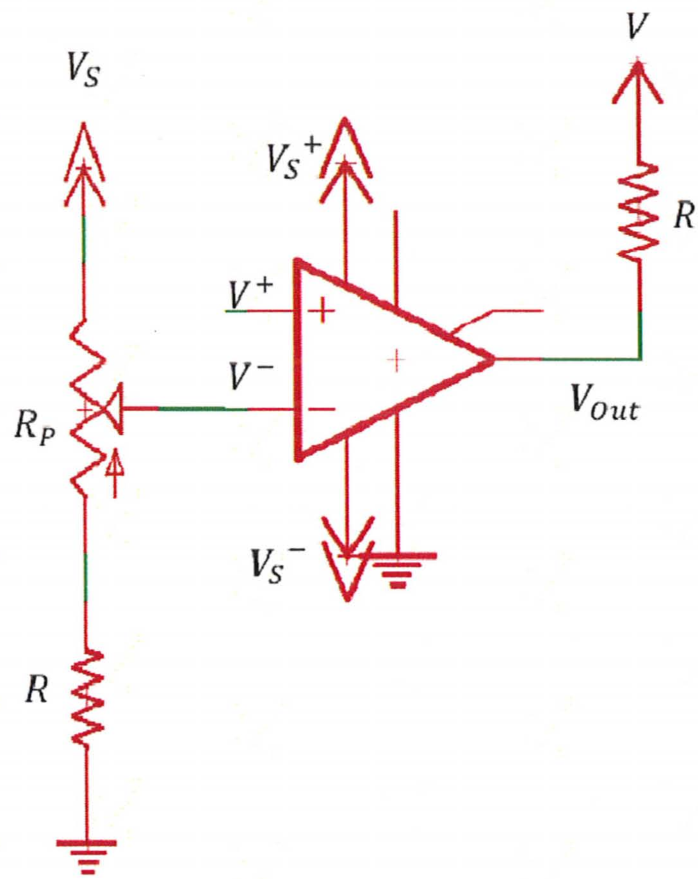

Figure 4-6 - Digital Comparator

4-1-1-2 Monostables

The CD4047BC 14 pin integrated circuit multivibrator is utilized in this thesis as a monostable with either a positive edge or negative edge trigger. A positive edge triggered monostable is shown in Figure 4-7.

The monostable receives an input value V_{In} and emits a rising edge trigger for a specified time period based on the time constant determined by RC. The signal is then output on the output terminal of the integrator circuit Q and $\overline{Q}$ where $\overline{Q}$ is the inverse of Q. The output has a 0 to 5V value and is perfect for digital logic and control circuits. With a wiring change to the monostable integrated circuit the trigger can be altered from a positive edge trigger to a negative edge trigger as required.

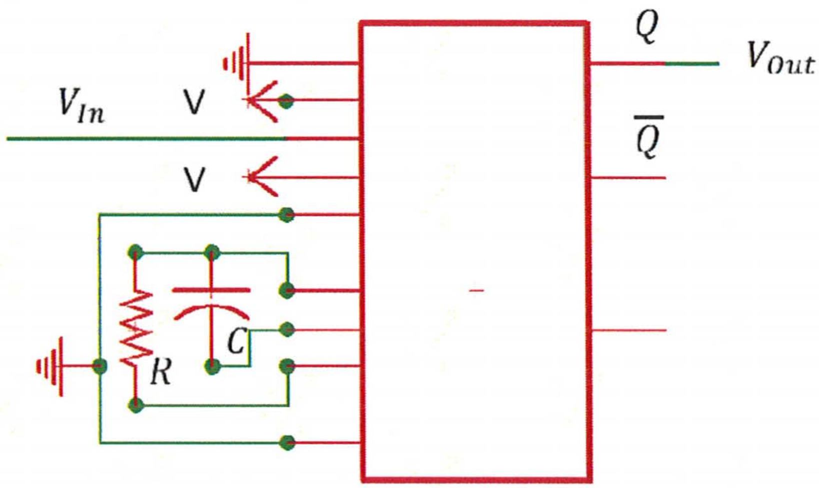

Figure 4-7 - Monostable

4-1-1-3 Set-Reset Flip Flops

The HEF4027B 16 pin, double Set-Reset Flip Flop integrated circuit is used as a timing circuit in this thesis. One of the two flip flops on the circuit is shown in Figure 4-8. The flip flop utilizes the inputs from the negatively and positively edge triggered monostables to switch, or flip flop, between its two states. The Set-Reset flip flop is connected in a set-reset mode with the output taken from pin Q and used to create a square wave with a 0 to +5V amplitude and a 50% duty cycle.

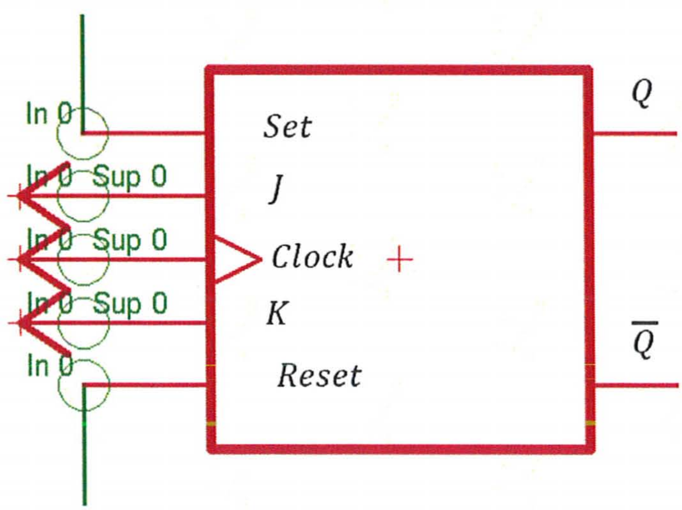

Figure 4-8 – Set-Reset Flip Flop

4-1-1-4 IGBT IC

The IRAMX20UP60A integrated circuit from International Rectifier (IR) is an isolated, high voltage, three phase motor driver IC. For the purpose of this thesis, the IC was reconfigured to act as a high voltage, high current isolated H-bridge able to drive the electric machines necessary for the experiment. Alterations to the suggested connections were made to ensure that only two of the three phases of the circuit were used at any given time. The external packaging of the IC can be seen in Figure 4-9.

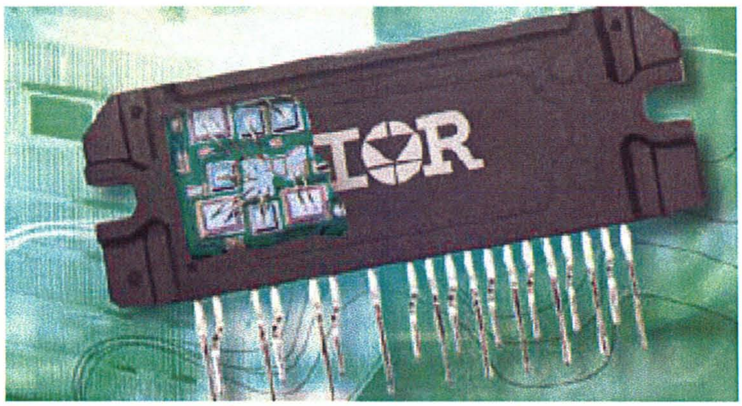

Figure 4-9 - IRAMX20UP60A IC External Package [18]

The IC is a combination of an H-Bridge and H-Bridge gate driver in one. The requirement of an H-Bridge inverter is determined based on the required phase angle of modulation β introduced in Section 2. The sinusoidal modulation technique is based on a positive and negative phase angle which can easily be implemented through the use of an H-Bridge inverter.

To further understand the operation of the IC we must first review the operation of an H-bridge. Figure 4-10 shows a simple H-Bridge design which we can analyse. The main use of the H-Bridge in this thesis is to create a positive and negative signal output from a fixed DC bus through the use of a control signal, effectively creating an inverter. The H-Bridge is comprised of a pairing of two Integrated Gate Bipolar transistors (IGBTs) for a total of four ITGBTs. Each IGBT is ladled 'H' in the diagram. The device under operation is connected in between the pairs, H1-H2 and H3-H4, and is used as a load. To achieve a positive signal H1 and H4 are turned on and H2 and H3 are turned off. This allows the current to flow through H1, through the load, through H4 and back out to the source following the blue path in Figure 4-10. The notation of a positive signals stems from the left to right flow of current through the device under test. If we wish to have a negative flow of current we turn on H2 and H3 and turn off H1 and H4. This creates a negative current flow from the source, through H3, through the load, through H2 and back to the source following the red path in Figure 4-10. All other switching combinations produce unwanted results and thus are not implemented in this work as they either short circuit the DC source (H1-H2 on or H3-H4 on) or bypass the load (H1-H3 on or H2-H4 on). Diodes are used in the H-Bridge design for protection against unwanted reverse load currents.

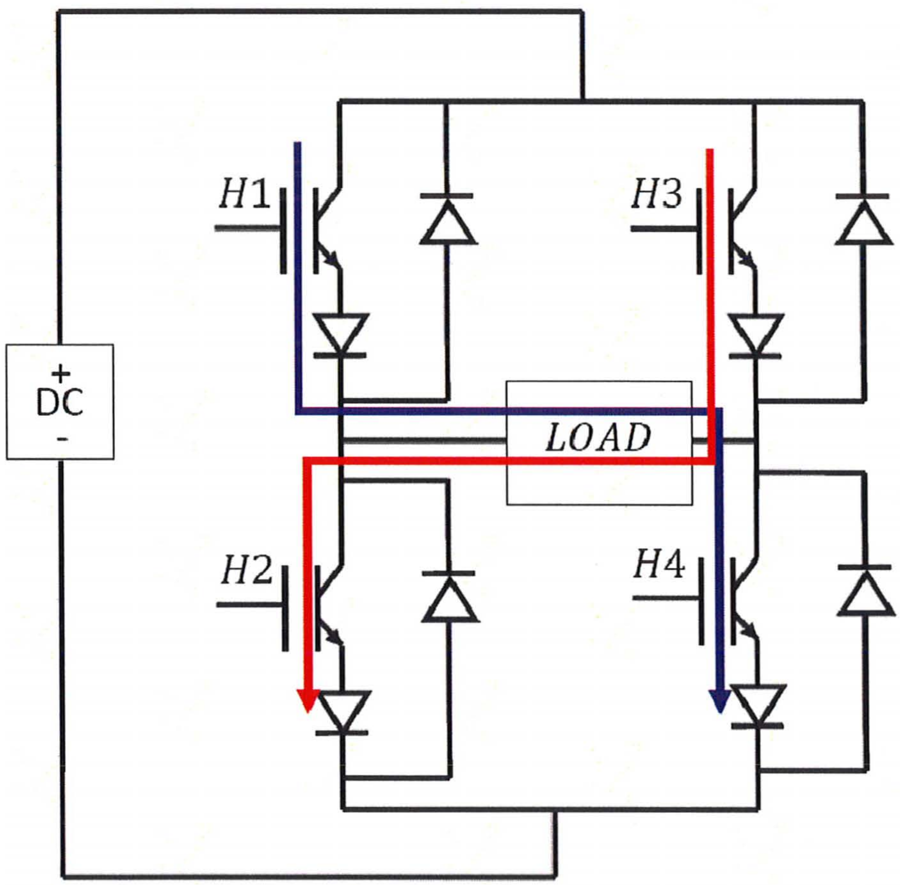

Figure 4-10 - H-Bridge Circuit

Many H-Bridge circuits are designed from scratch, especially in the case where a whole control circuit is also designed. However, through past experience it was decided that the IR IC was a good solution to bypass the hardships experienced in [3]. The IRAMX20UP60A was chosen based on its 20A current and 600V voltage ratings. These ratings were deemed sufficient to withstand the 10A current and 120V voltage ratings of the machines under test. The IC further provided isolation up to 2000Vmin which negated having to design and use optical couplers to isolate the low side form the high side in the circuit. The IC gate driver allowed the switching of the IGBTs at a speed of up to 20KHz which is more than sufficient for the scope of the thesis and the operation of each machine.

The pins of the IR IC are illustrated in Figure 4-11. Pins one to six represent the output connections of the two halves of the H-Bridge and are connected to the load. The use of boot strap capacitors in between pins one and two and in between pins four and five was necessary to ensure the appropriate voltage level was maintained for the duration of the 'ON' pulse. Pin ten is connected to the positive DC bus and pins twelve through fourteen are connected to negative DC bus. Pins fifteen through twenty represent the switching circuit control inputs that drive the H-Bridge. The IC is designed for three phases, and the sinusoidal phase modulation technique requires only two phases leaving the two IGBTs connected to pins seven and eight unused. The control signal for those these two IGBTs are on pins fifteen and eighteen and are set to 'high' ensuring that the two IGBTs stay off at all times. Pins sixteen and twenty drive one side of the H-Bridge while pins seventeen and nineteen drive the other side. Pins twenty-two and twenty-three are the +15V and common terminals that power the IC respectively. The pin numeration used by IR counts a pin even if there is no physical pin (empty space) thus creating twenty-three pins for the IC which only has nineteen physical pins.

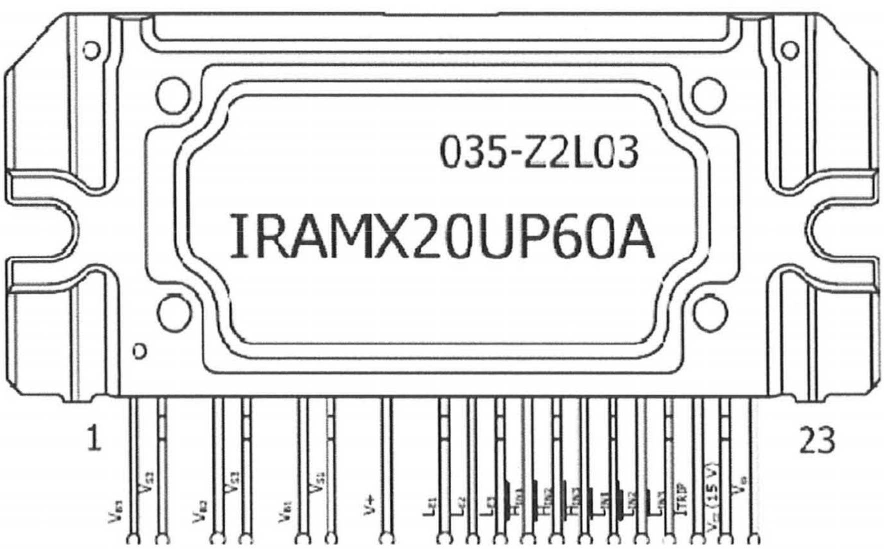

Figure 4-11 - IRAMX20UP60A Pin Configuration[18]

Heat sink selection for heat dissipation was determined based on [19]. It was determined that a close selection match could be achieved with the use of a standard CPU heat sink and operating fan. The heat sink was slightly altered by drilling holes in the appropriate positions to allow for a good fit. Thermal paste was used to couple the IC and the heat sinks. Screws were used to hold the two together. It was determined that the fan was necessary only for prolonged experiments at higher voltage and current levels although it was used at all times for safety purposes. The heat sinks attached to the back of the IR IC can be seen in Figure 4-12.

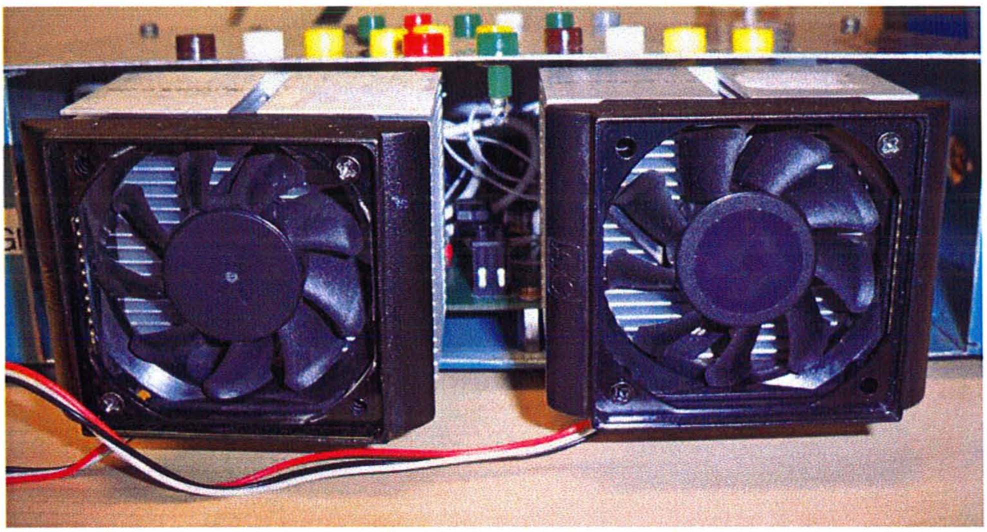

Figure 4-12 - IR IC Heat Sink and Fan

4-1-1-5 Voltage and Current Measurement Components

An important part of the data acquisition (DAQ) process is the scaling down of high voltage and current waveforms to low values appropriate for the data acquisition card (DAC). The PT is accurate to 4% and the output signal is conditioned through software. Figure 4-13 shows the schematic of the 3FS-310 50/60Hz 120V power transformer (PT).

The output of the power transformer can be connected either in series or in parallel depending on the desired voltage output. For the purpose of this thesis, the output of the PT was connected in series which dropped the voltage value on the secondary side to 10V. This output value corresponds to the maximum input value to the data acquisition card utilized for measurement. A potentiometer was placed at the output of the series connected PT to allow for fine voltage level adjustments to ensure uniformity across all PTs.

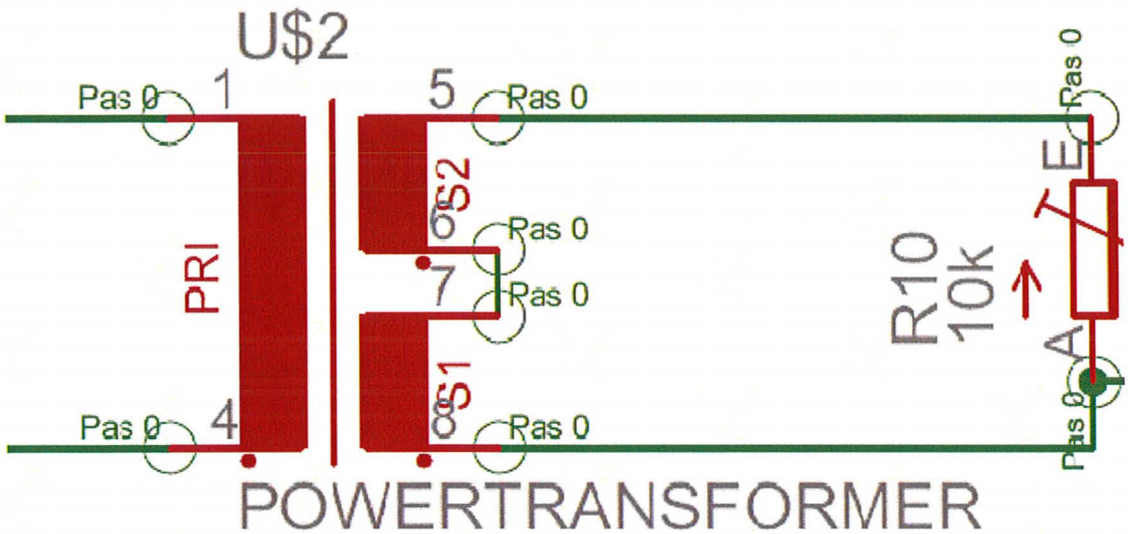

Figure 4-13 - Power Transformer

Figure 4-14 shows the HX 20-P 20A primary current transformer (CT). The CT comes pre-packaged with its own conditioning circuit which provides a very clean and accurate signal to convert the input current to a ±4V output within 1.5%. The output is then passed through a positive gain op-amp to raise the level to ±10V to correspond with the input range available on the DAC. The CT output signal is further conditioned and phase corrected using software to ensure the signal accuracy.

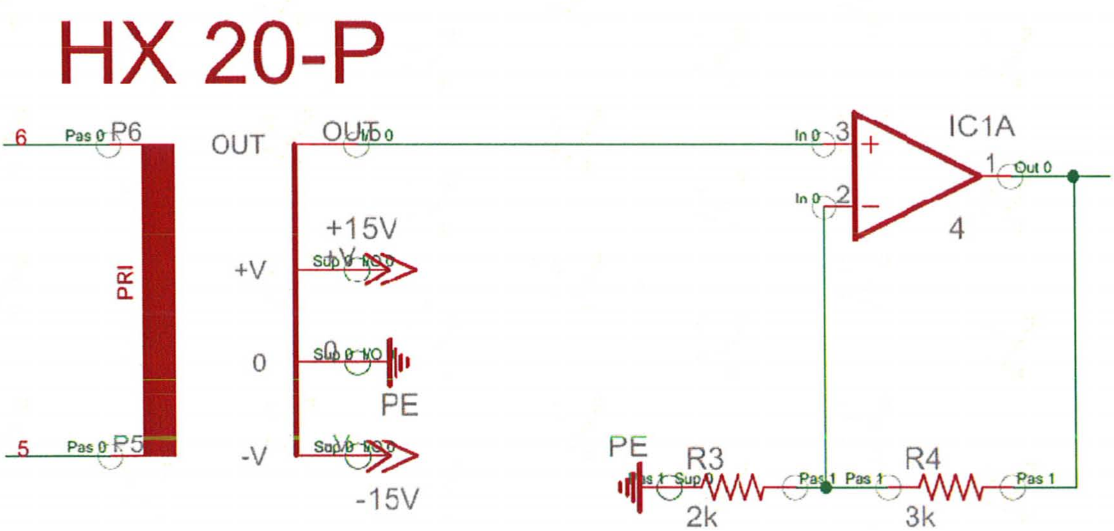

Figure 4-14 - Current Transformer

4-1-2 Carrier Wave Creation

Part of the driving force of the control board is the creation of the carrier wave. The design of the carrier wave is shown first in block form for conceptual purposes. Figure 4-15 shows the interrelation of these buildings block.

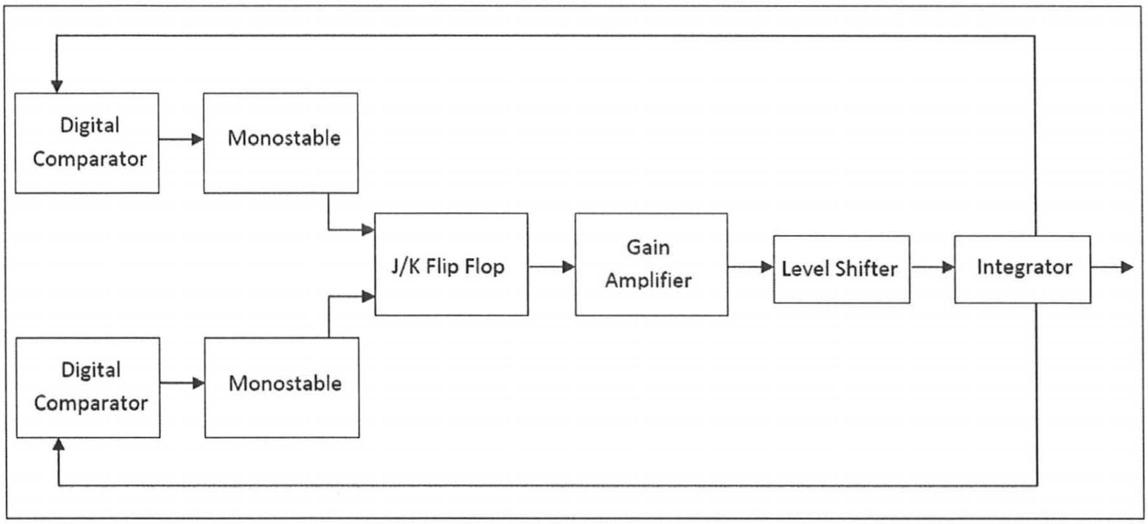

Figure 4-15 - Carrier Wave Creation Block Diagram

The block diagram above uses digital comparators, monostables, a J/K flip flop, a level shifter and an integrator block described in section 4-1-1. The J/K flip flop is used to create an alternating square wave output based on the HI/LOW signal received from each monostable. This square wave is passed on to a gain amplifier which increases the magnitude of the signal and a level shifter which is used to add a negative DC offset such that the square wave is symmetrical around zero. This square wave is then integrated to produce a fast changing triangular wave. This signal is used both as a carrier wave and driver for the J/K flip flop. The triangular wave is then passed on to the two digital comparators which are used as drivers for the two monostables. When the triangular wave reaches its positive peak, the first digital comparator switches HI which triggers a pulse output from the monostable. This pulse output is used to alter the output signal on the J/K flip flop. When the triangular wave reaches its negative peak, the second digital comparator signals the second monostable which resets the signal of the J/K flip flop. This cycle continues indefinitely. Please note that voltage followers are placed between blocks to ensure signal integrity.

Figure 4-16 illustrates the schematic and its components used to create the carrier wave in three separate sections. Section 1 of Figure 4-16 shows the connection of the level shifter, digital comparator, monostable and SET-RESET flip flop to produce a 0 to

+5V square wave with a 50% duty cycle. The square wave is then passed on to Section 2 of Figure 4-16 where it is amplified to 0 to +10V using an op-amp gain circuit and the appropriate value of resistors. From there the circuit uses a voltage follower to maintain integrity before it is passed through a level shifter to obtain a square wave from -5V to +5V. From there signal is again passed through another voltage follower before it is integrated in Section 3 of Figure 4-16. The integrator provides us with a triangular wave between -15V and +15V. The frequency of this triangular wave is dependent on the choice of capacitor and resistor which combined gives us the time constant τ. The frequency of the created carrier wave is 7.96 kHz. However 8 kHz is a very good approximation when considering the component error margins of both the capacitor and resistor used for integration.

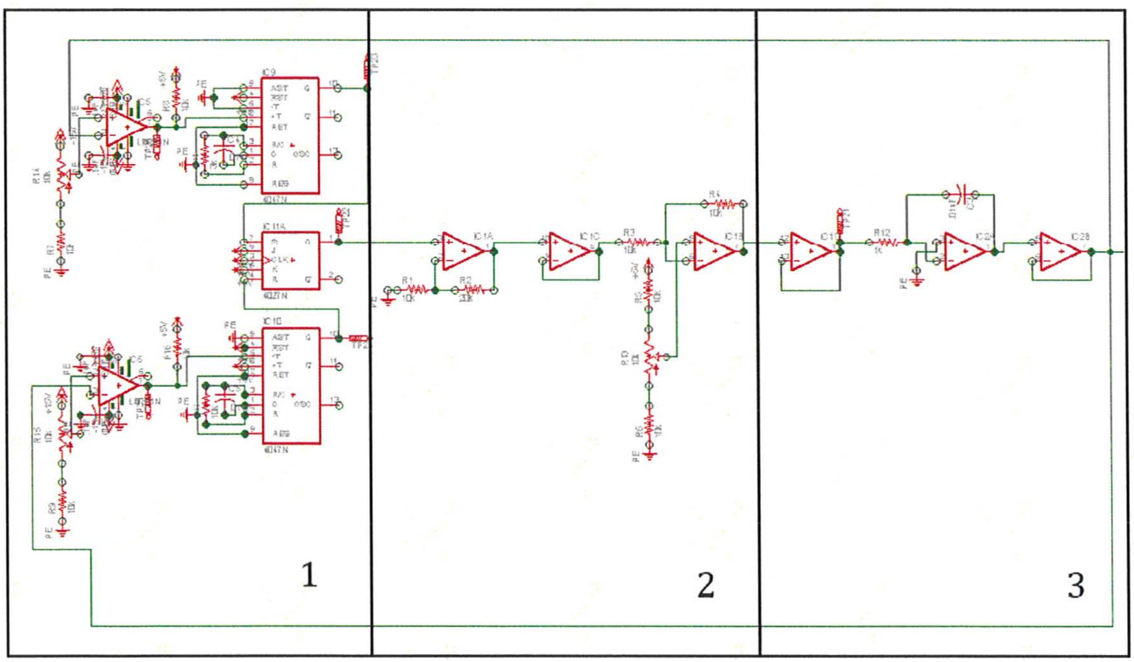

Figure 4-16 - Carrier Wave Creation Block Diagram

Please note that this circuit is self driving. The peak of the triangular wave generates a pulse from the monostable which switches the output of the flip flop. This in turn creates the shifted square wave which in turn is integrated to create the triangular carrier wave. For this to occur we require two monostables in the circuit, one positively edge triggered and the other negatively edge triggered monostable. The monostables drive the Set-Reset flip flop which is set at the top peak and reset on the bottom peak. By integrating the square wave we attain the triangular wave carrier signal. For this circuit to function accurately, the threshold on the digital comparator is set to a value smaller than the peak of the triangular carrier wave. This ensures that the flip flop will switch once for every half cycle.

4-1-3 Pulse Width Modulation Signal Creation

A common driving force behind H-Bridge circuits is a pulse width modulated (PWM) signal. A common way to create such a signal is to compare the desired signal with a carrier wave of a higher frequency. This method is illustrated in Figure 4-17. The amplitude of the sinusoid is compared with the amplitude of the triangular carrier wave. If the amplitude of the sinusoid is larger, the comparator outputs high, conversely, if the amplitude of the sinusoid is smaller the comparators outputs low. This creates the red PWM signal shown in Figure 4-17. It must be noted that the carrier wave should be at least ten times the frequency of the signal wave with which it is being compared. The newly created PWM signal can now be used to drive the switching circuits of the H-Bridge.

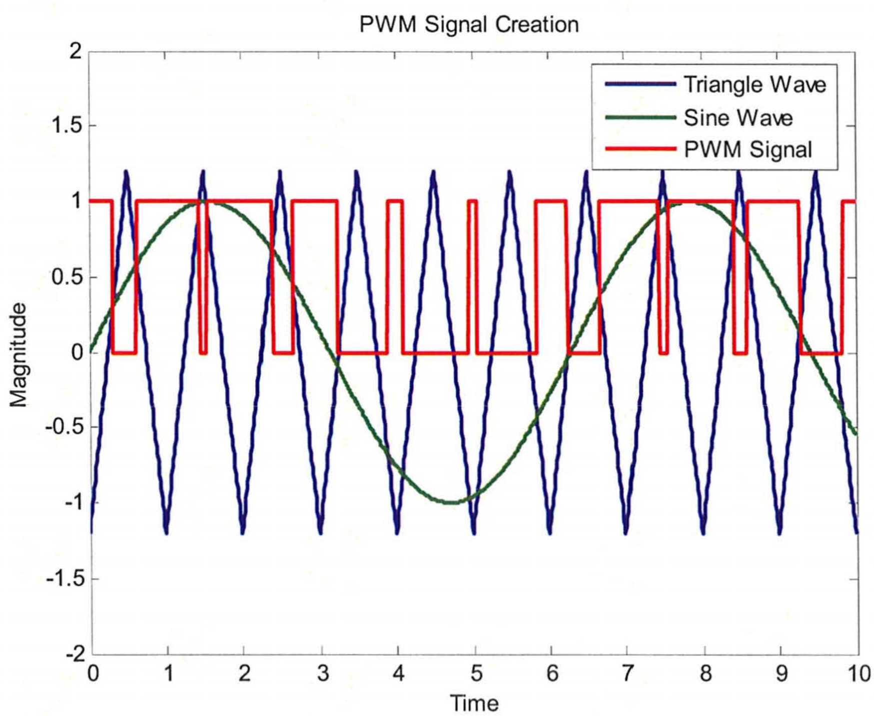

Figure 4-17 - PWM Signal Creations through Comparison

The design of the PWM wave is shown first in block form for conceptual purposes. Figure 4-18 shows the interrelation of these buildings block. The creation of the PWM signal itself is straight forward. The voltage follower is used to ensure a clean carrier wave signal is passed on to the digital comparators. The clean carrier wave can then be compared with the aid of a digital comparator to a signal of choice operating at a lower frequency. The signal is then passed on to the condition phase of the circuit. For the purpose of this thesis, the conditioning phase includes a series of AND gates and NOR gates as well as amplifiers to ensure the PWM output signal is appropriately conditioned for the driver circuit it needs to control. The output to PWM block is a 0 or +5V pulse. Please note that a generic conditioning block is shown in Figure 4-18 since two separate PWM signals are required for the thesis, each with its separate conditioning.

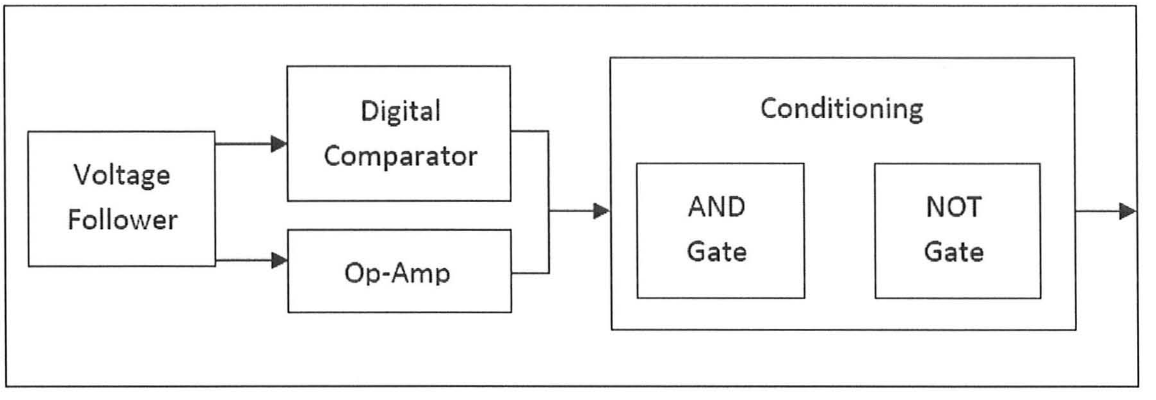

Figure 4-18 - PWM Signal Creation Block Diagram

Figure 4-19 shows the components and mini circuits used in the creation of the PWM signal separated in three sections. The control signal is applied at 1a in Figure 4-19. In this case, the modulated sinusoidal control pulse is the control signal. The signal is passed through a series of impedance buffers aimed at preserving the signal and splitting it into its positive and negative halves. The two signals are then compared using a comparator circuit and thus creating the PWM signal described in Figure 4-17. In Section 2 of Figure 4-19, the newly created PWM signal is passed through an AND gate along with a scaled down version of the original half sinusoid. The AND gate is used to flip the state of the PWM; all high values become low and all low values become high. This is done in conformance with the logic low driving circuit of the IR IC, however more signal conditioning is required. The extra NOT gate in the bottom half of Section 2 is there to correct for the negative half of the control signal. The signal is then passed through another impedance buffer before exiting Section 2. In Section 3 of Figure 4-19 the signal is passed through another AND gate which compares the signal to a +5V fixed signal. This is done to ensure the PWM is at the right amplitude level for a digital signal. The last step of Section 3 is to pass the signal through a NOT gate. This is the last step in ensuring the logic low switch driver performs correctly. Without the NOT gate the PWM signal would have its proper shape but it would be inverted meaning the gate would be open when it should be closed and closed when it should be open. From there, the signal is passed through another voltage follower and on to the appropriate gate driver pin on the IR IC.

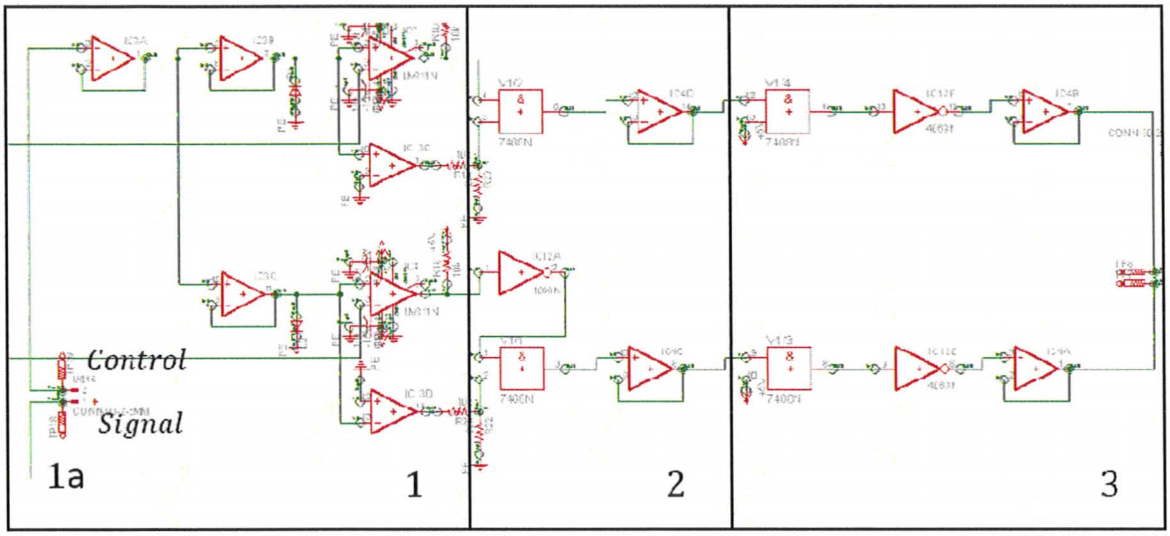

Figure 4-19 - PWM Creation Circuit

4-1-4 Board Designs

The final board designs are shown below in schematic, layout and physical forms. Each board was encased in a grounded metal box aimed at reducing noise. Connections to the two boards were made with banana plugs. Each board was manufactured and populated twice; to drive and record measurements for each of the two systems under test.

4-1-4-1 Measurement Board

The schematic of the measurement board is shown in Figure 4-20. The measurement board has three PTs and four CTs. This allows for a total of six simultaneous voltage measurements and eight simultaneous current measurements when combining the two boards. Each individual PT and CT was calibrated manually and through software to ensure uniform measurement results. The measurement board requires a single 300mA ±15V isolated power supply to operate.

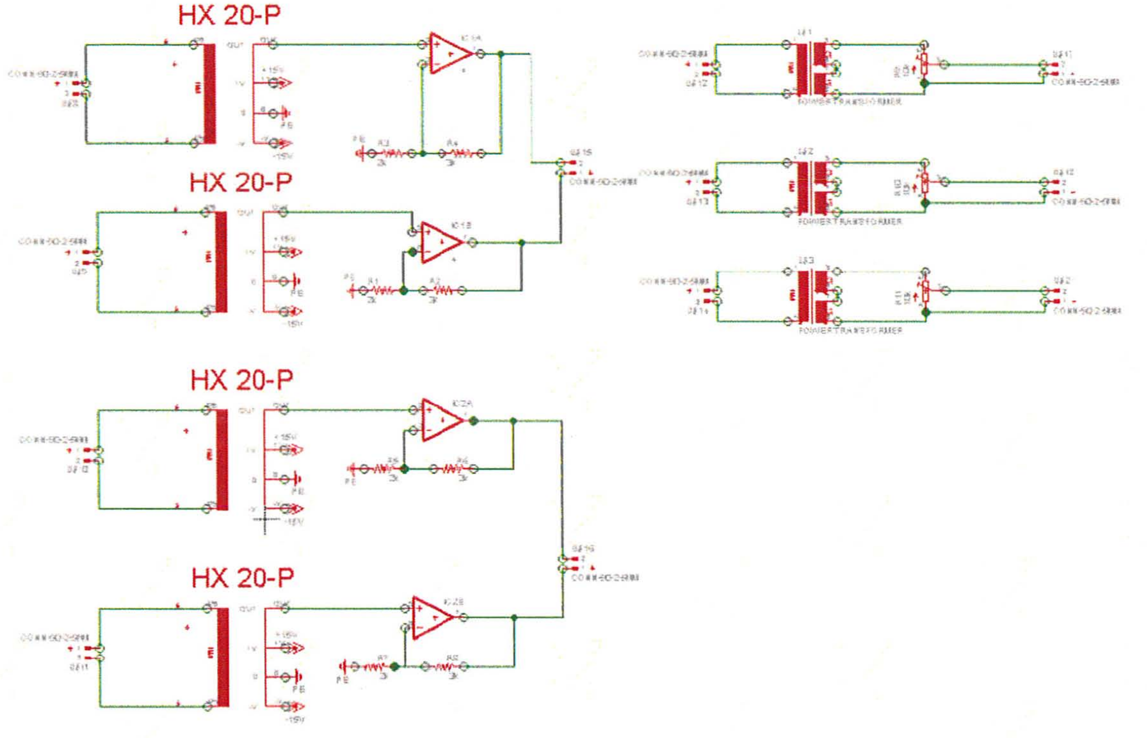

Figure 4-20 - Measuring Board Schematic

The layout design of the measurement board is shown in Figure 4-21. The dimension of the single sided board is 27cm by 10cm. A ground plane shown in dashed lines was used to help reduce noise.

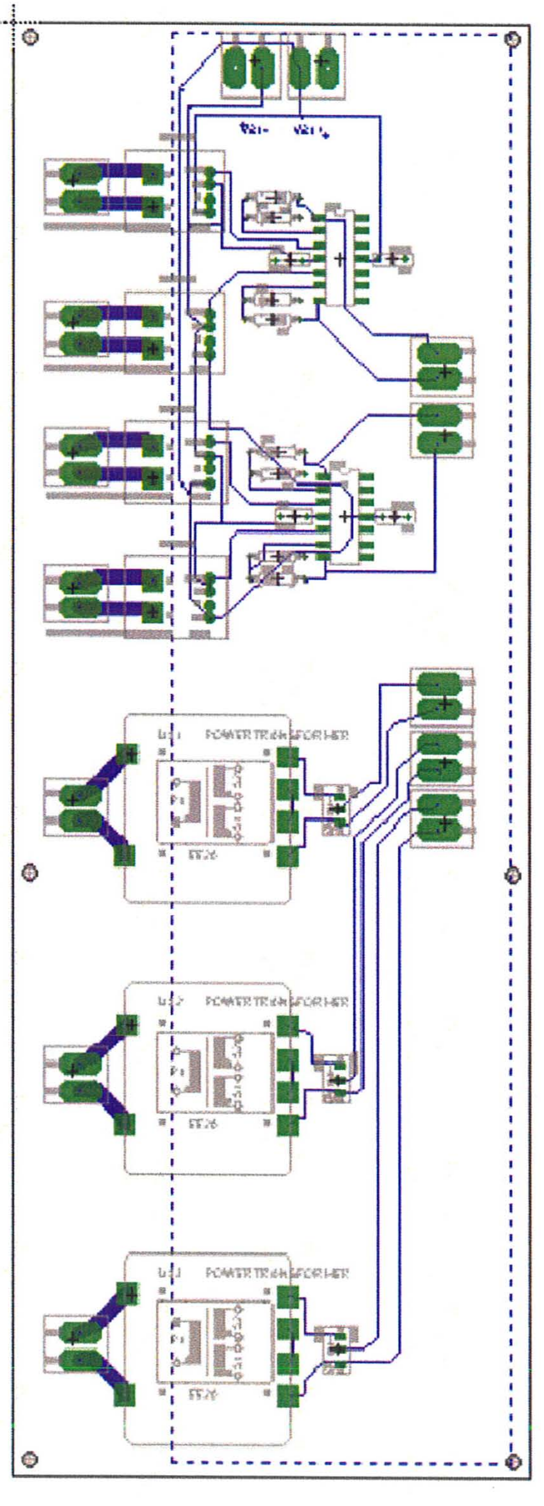

Figure 4-21 - Measurement Board Layout

The physical encasement and printed circuit measurement board can be seen in Figure 4-22 and Figure 4-23 respectively. Please note that the second figure only has three CTs instead of four CTs. This was done on purpose to minimize cost as only seven simultaneous current measurements were necessary for this experiment.

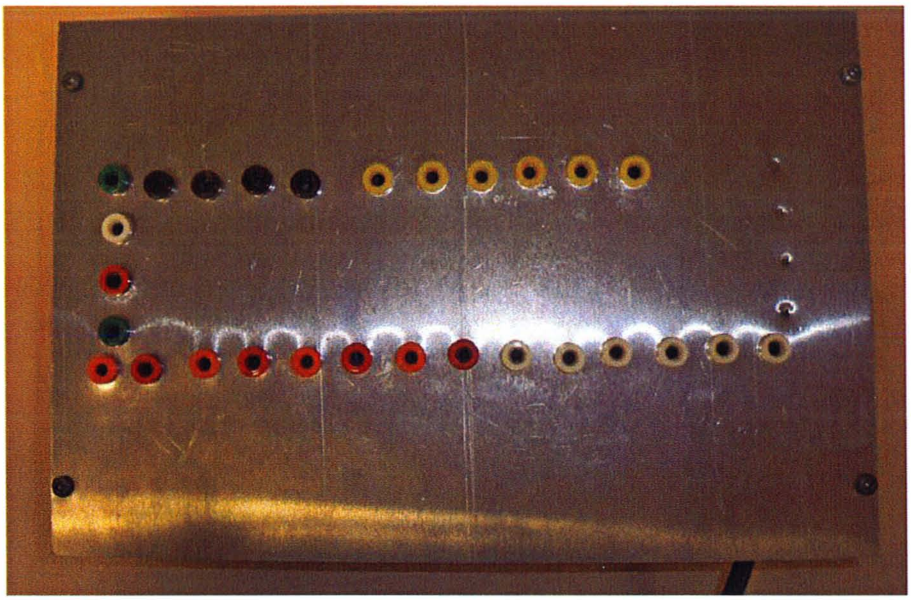

Figure 4-22 - Measurement Board Top View

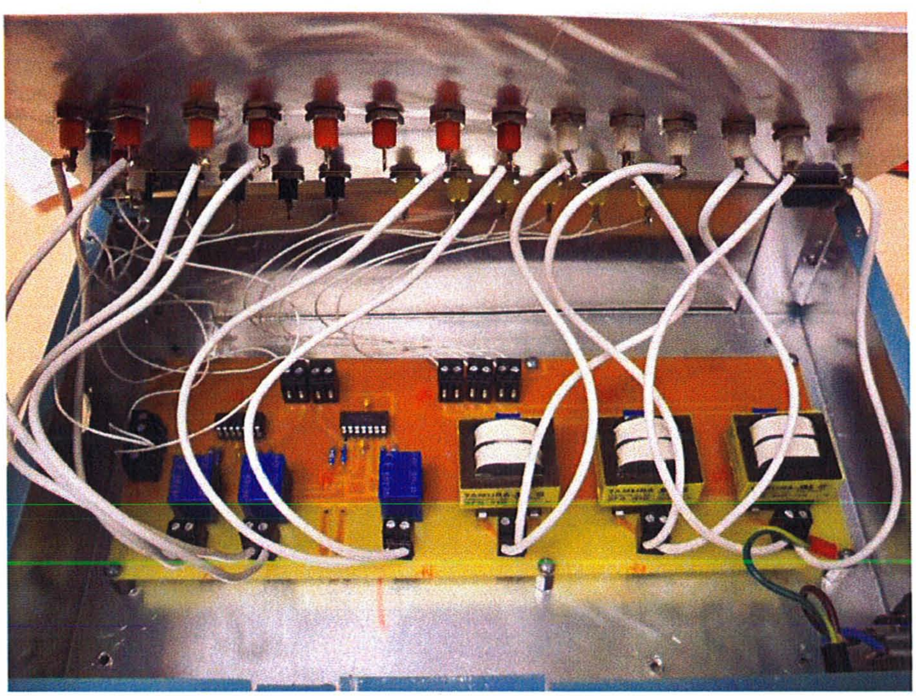

Figure 4-23 - Measurement Board Interior View

4-1-4-2 Control Board

The initial design phase of both the measurement and control boards were begun on breadboards. Figure 4-24 shows the final bread board design of the control board. Each mini circuit described in Section 4.1 was developed and tested to ensure it worked as it was designed to. The design process encompassed numerous steps till it reached the final stage shown in Figure 4-24.

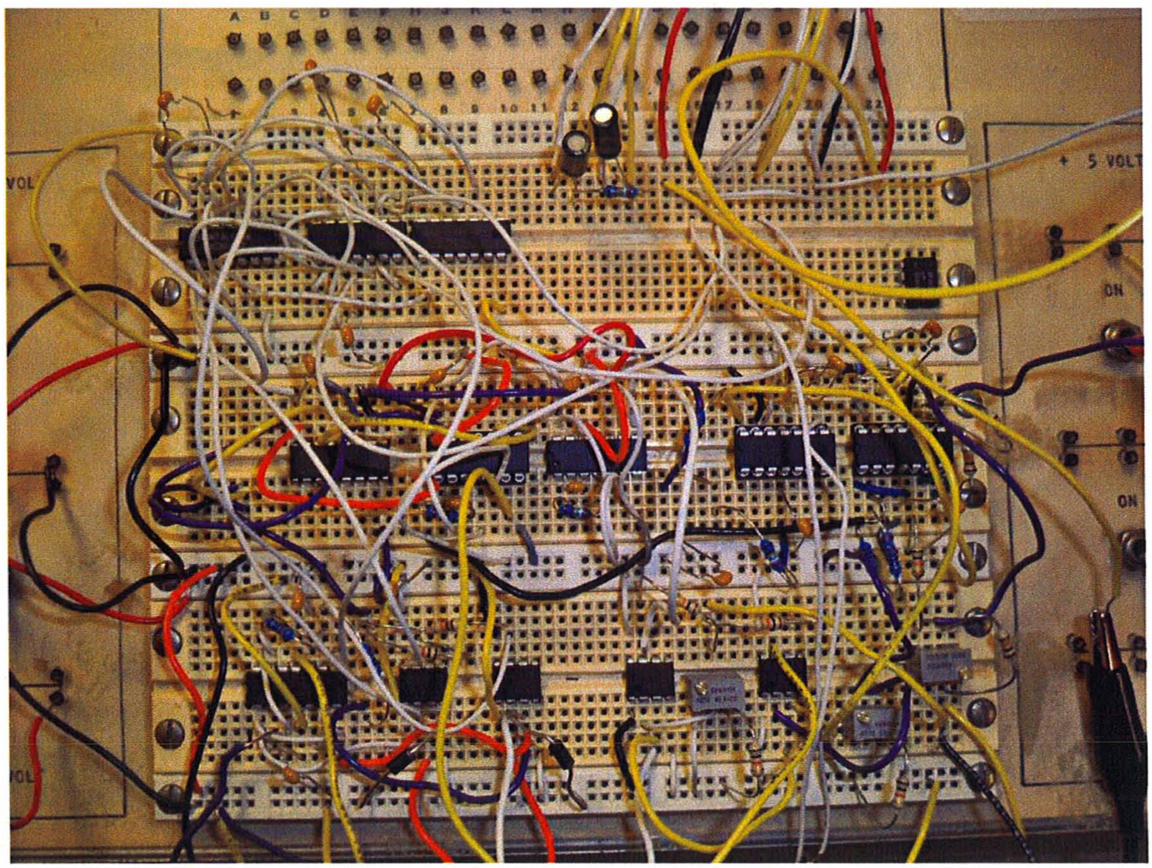

Figure 4-24 - Control Board Breadboard Design

The schematic of the control board is shown in Figure 4-25. The control board has a total of twenty-two ICs and twenty input and output connections. Each board was calibrated manually to ensure the carrier wave and resultant PWM signals matched. The control board requires a 300mA ±15V isolated power supply and a 300mA +5V power supply to operate.

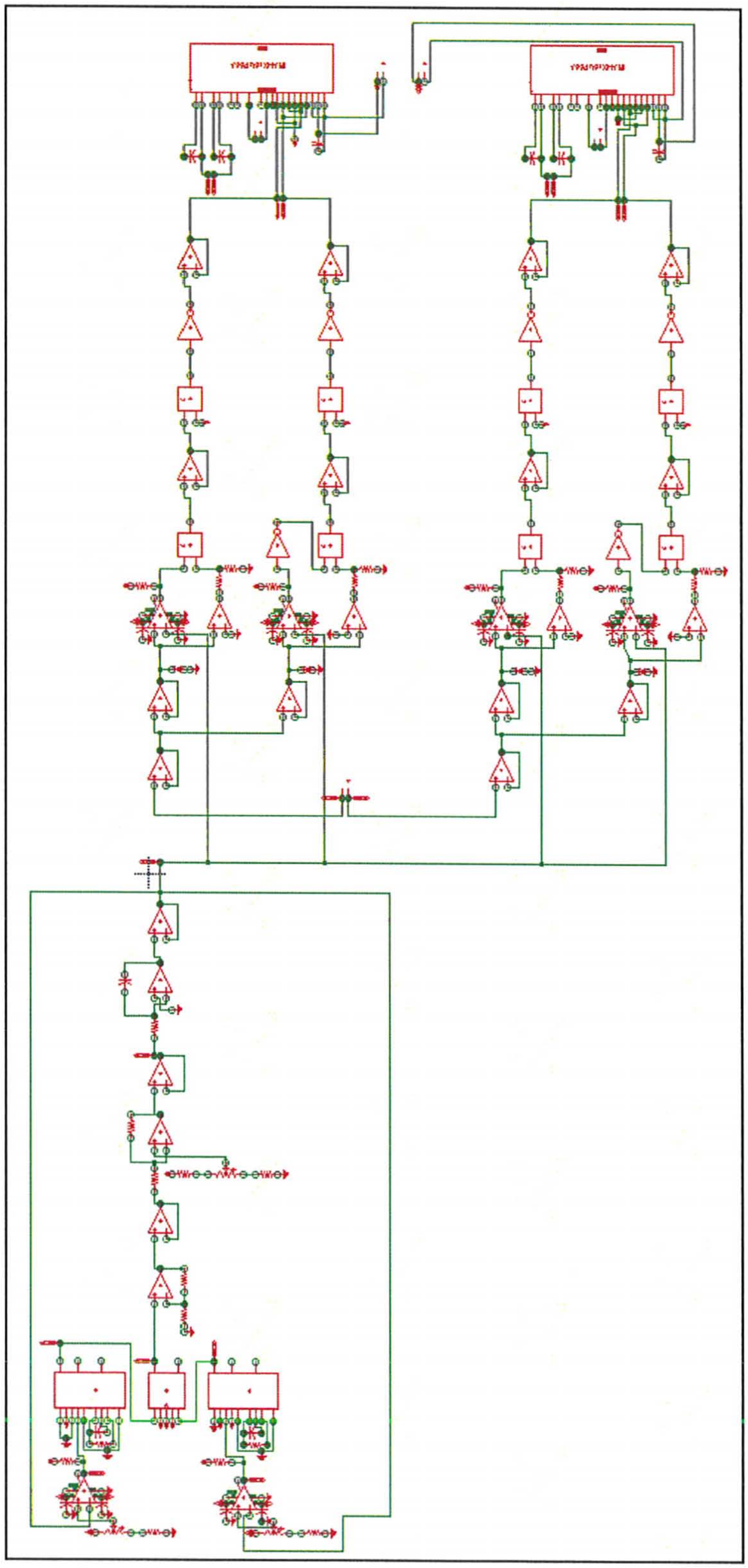

Figure 4-25 - Control Board Schematic

The layout design of the control board is shown in Figure 4-26. The dimension of the double sided board is 20cm by 12cm. The bottom side traces are shown in blue and the top side traces are shown in red. Thicker traces are used for higher current carrying signals. Again, ground planes are shown in dashed lines and are used to help reduce noise.

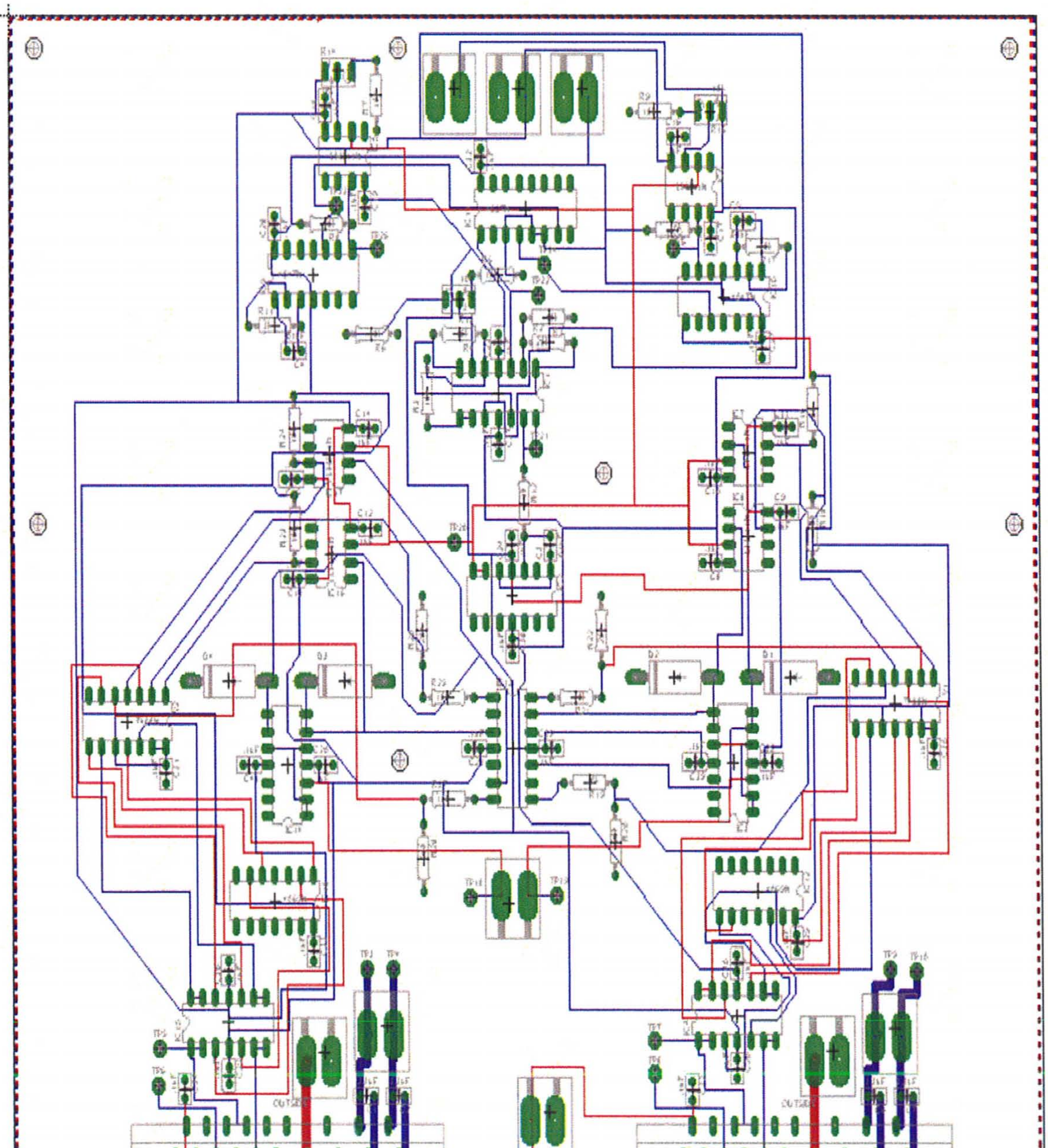

Figure 4-26 - Control Board Layout

The physical encasement and printed circuit control board can be seen in Figure 4-27 and Figure 4-27 respectively.

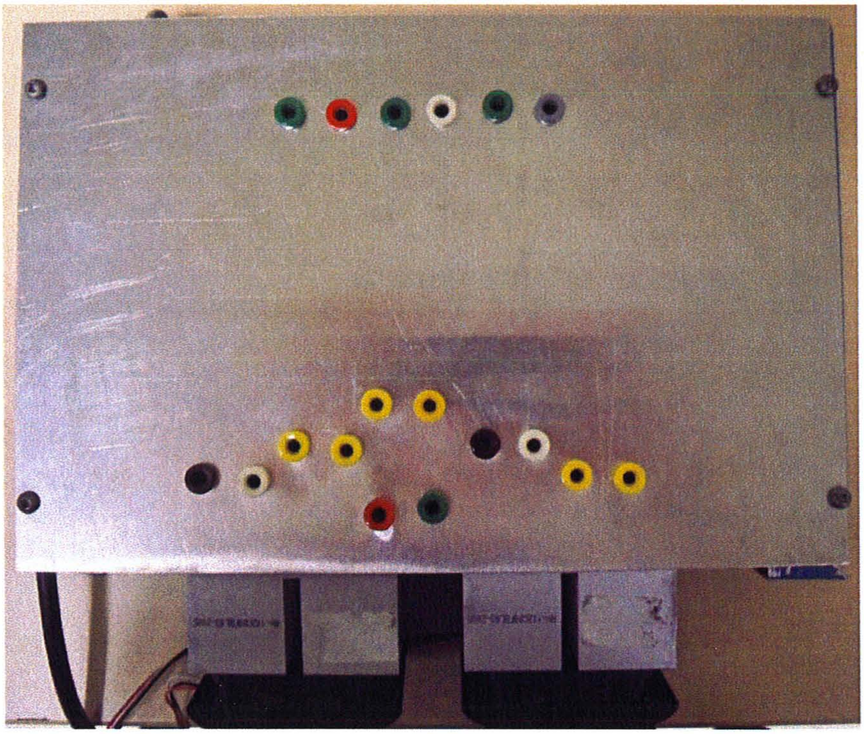

Figure 4-27 - Control Board Top View

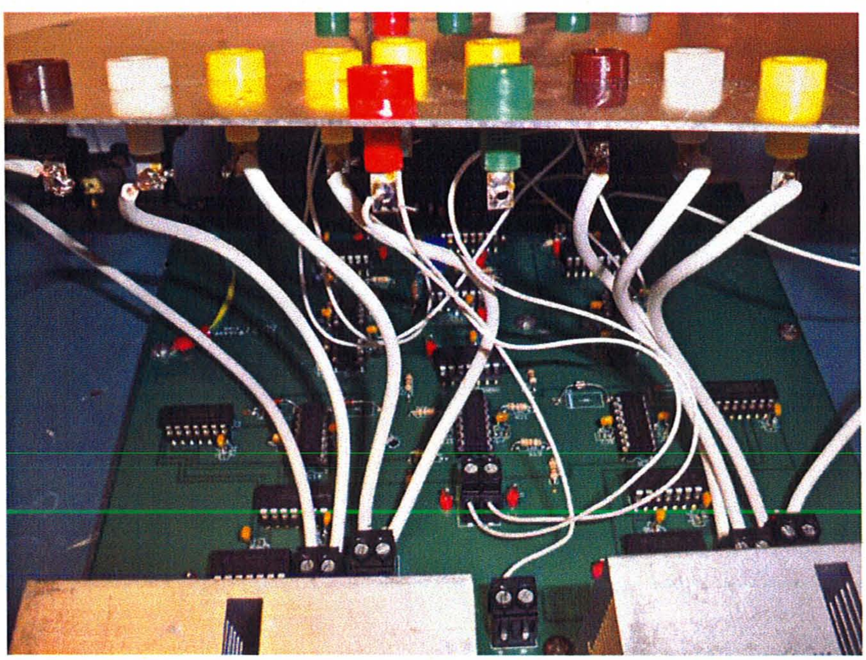

Figure 4-28 - Interior View

4-2 Software Implementation with LabView

The following section aims to describe the software design and implementation of the experiment. The software utilized for this purpose is LabView which is manufactured by National Instruments. LabView Student Edition 8.0 was used for the design.

4-2-1 Software Objectives

The objective of the software program is to create a modulated sinusoidal signal based on user specifications and apply this signal to the control board designed in Section 4.1. The goal of the signal is to minimize power fluctuations in the driver motor D0. The program must have an easily accessible user interface. It must allow for many degrees of freedom in construction of the control signal but must ensure the signal stays within safety boundaries defined by both software and hardware. The program must send, acquire, display and store real time data in an efficient and accurate manner. This means that changes can be made to the program without interference and the program must remain stable at all times to ensure the safety of the hardware and equipment. The program must also be able to control the modulation signal automatically to acquire and display the best set of modulation parameters.

4-2-2 Implementation and Design

The flow chart in Figure 4-29 describes the high level interface and functionality of the LabView program. The program is initially designed to take in user input pertaining to the modulation parameters of the control signal. This information is passed along to the mathematical algorithm as input variables. The algorithm produces a single period of the modulated sinusoidal and cosinusoidal signals required for modulation and pass the information down to the DAQ. The DAQ processes these signals as analog outputs and transmits them to the control board where the appropriate PWM signal is created. The PWM signal is then applied to the five machine system and measurements are taken via the measurement board. The measurement board passes these signals back to the DAQ via the DAQ's analog inputs. These signals are then displayed to the user as well as stored for future reference. At this time the user can chose to manually adjust inputs or allow a control algorithm to find the optimal parameters which minimize power fluctuations in D0. The program can be split into four main parts in order to achieve the above results. These four sections will be described below in detail.

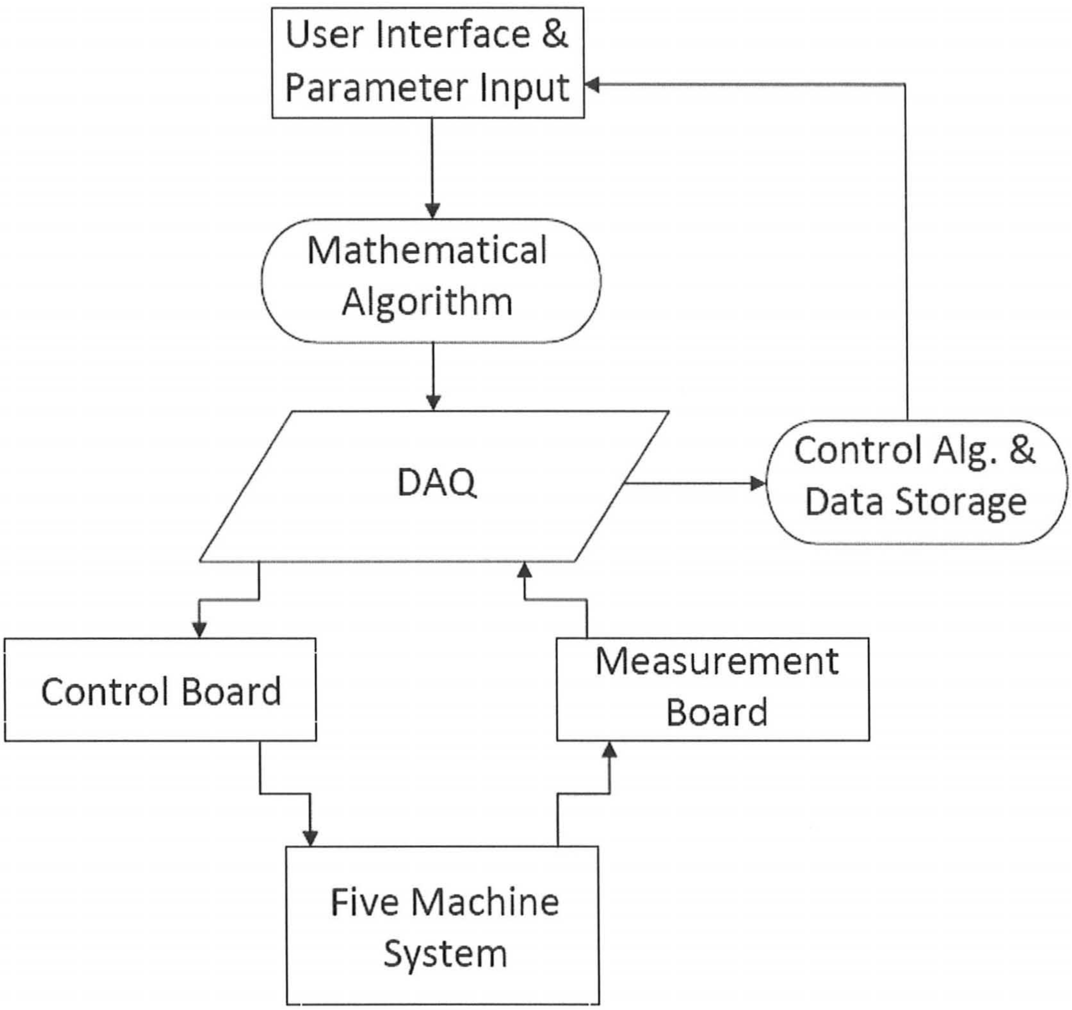

Figure 4-29 - LabView Software Integration in High Level Form

4-2-2-1 Control Signal Algorithm

The control signal algorithm is based on Equation 4-9 which states that the modulation angular velocity ω_m is equal to the synchronous angular velocity ω_0 plus the derivative of the phase angle β with respect to time. If the phase angle is sinusoidal then its derivative is sinusoidal and the addition of the two sinusoids in Equation 4-9 creates a sinusoidally modulated angular velocity.

$$\omega_m = \omega_0 + \frac{d\beta}{dt}$$ **Equation 4-9**

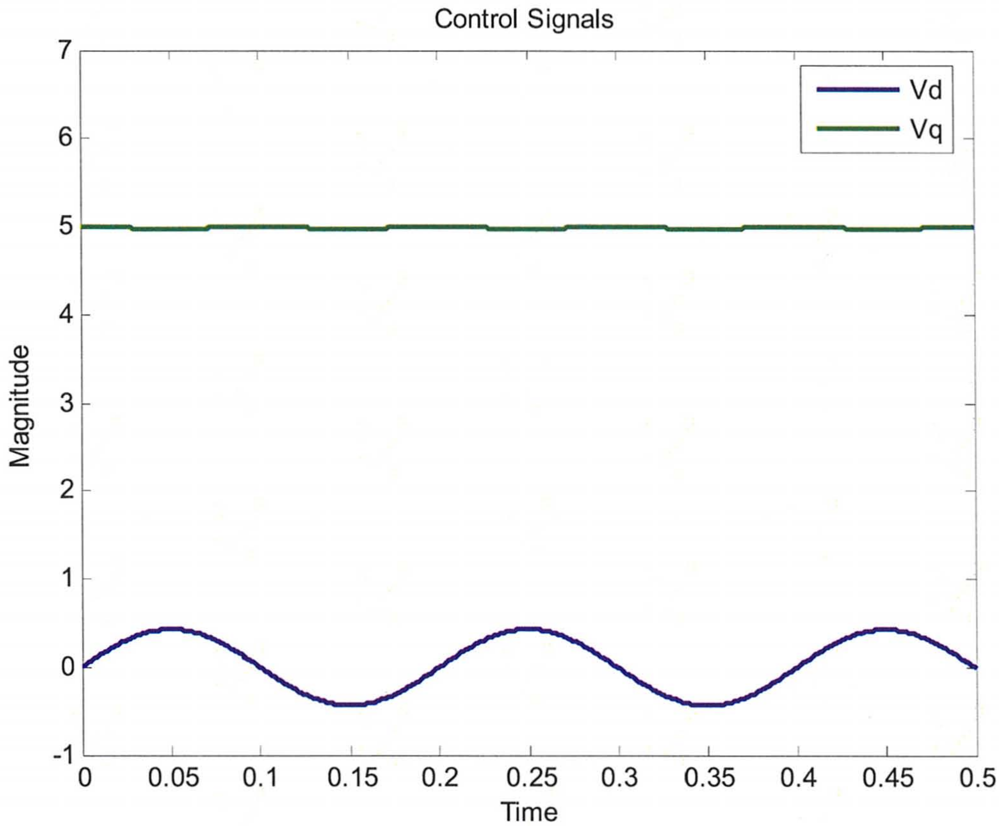

Figure 4-30 - Sinusoidal and Cosinusoidal Modulation Signals

By taking into account the inductances and resistances of the phases and transforming the values to the direct and quadrature axes we can derive the two control signals. Figure 4-30 illustrates these two voltage signals. The blue sinusoidal signal is the direct axis modulation and the green cosinusoidal signal is the quadrature axis modulation. It is to be noted that the green signal has a magnitude variation of at most 1.5%.

The algorithm creates the two signals one period at a time depending on the modulation frequency, and stores the values in arrays. The arrays are then output to the DAC. If the input parameters are left unchanged, the algorithm will reproduce the same signal in the next iteration. If the input parameters are altered the algorithm will not be affected until the end of the period of the current modulated signal. As such, the delay of the algorithm varies with the modulation frequency and the application of the change. For the scope of this thesis, the maximum delay corresponding to 10Hz modulation is 0.1 second. This is an acceptable delay when considering the change in input is produced through human interface and machine response time.

4-2-2-2 Data Acquisition

Data Acquisition is achieved through the use of two synchronized National Instruments data acquisition cards. The PCI-6024E model card will be described below.

4-2-2-2-1 Characteristics

The E series model cards from National Instruments are fast, inexpensive and readily available in the lab at no extra cost. It offers a sampling rate of 200 kS/s with twelve bit resolution. It comes with sixteen single ended analog inputs or eight differential analog inputs and two analog outputs. Each channel was sampled at 3000 S/s which allowed for all channels to be sampled simultaneously and still ensure that the maximum sampling rate of the DAC was not reached.

4-2-2-2-2 Synchronization of Two Cards

For the purpose of this experiment we require a total of four analog outputs and thirteen analog inputs. For this reason, we required two 6024E model cards. To achieve accurate and matching inputs and outputs we must synchronize the two cards before inputting or outputting any signals. This was achieved through physical connections and software. Physical synchronization was achieved through a real time system integration (RTSI) cable with 32 wires which was hooked up to the RTSI bus of both cards. The software synchronization was implemented in LabView and utilized triggers and the internal clock rate of each card. One card was set to act as the ‘master’ and the other card was set to act as the ‘slave.’ The first task of the program, before executing any mathematical algorithms, was to send a trigger which initialized the same clock pulse on both cards. In this way, the two cards would have the exact same start clock time which was triggered simultaneously for both cards. Timing throughout program operation would remain constant through communication over the RTSI cable.

4-2-2-2-3 Data Recording

The acquired data needs to be analyzed both in real time and stored for later analysis. Data is analyzed in real time through the use of graphs and averaging algorithms. Voltages, currents, powers and averages are displayed onscreen using a LabView chart shown in Figure 4-31.

Data is saved to Excel spreadsheets for later analysis. The start and stop times of data recording are controlled by the user. The excel file is appended to if the file is not empty to ensure that no data is lost.

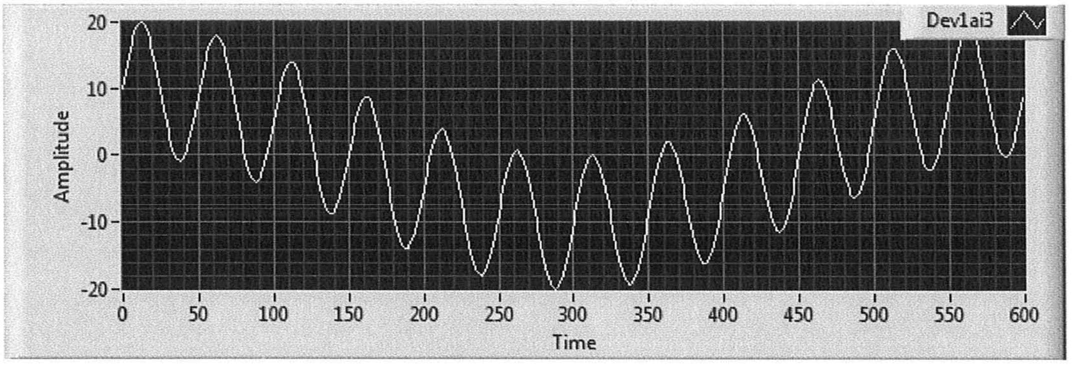

Figure 4-31 - LabView Chart for On Screen Display

4-2-2-3 Automated Control

The use of automated control was implemented in the program to add precision. The software compares the two incoming power signals by calculating the phase angle difference. Once the phase angle difference is found, the algorithm adds a phase shift to one of the power signals and compares the difference. When the power is 180 ±1 degrees out of phase the algorithm terminates. The synchronizing algorithm can also be turned on and off by the user at any time.

4-2-2-4 User Interface

The user interface is key to the successful operation of the sinusoidal phase modulation technique. The user interface main controls are shown in Figure 4-32. The bottom left part of Figure 4-32 shows the channel selection for each of the two data acquisition cards. Seven of the thirteen required analog inputs are measured on DAC one and the remaining six are measured on DAC two. Both DACs output two analog signals. The sampling rate was set to 3kHz which provides sufficient resolution while keeping the number of stored data points relatively low.

In the top left of Figure 4-32 are the start-up controls. To achieve start-up, we supply a DC signal to one phase of the generator until full speed is achieved. The amplitude of the sinusoid is not utilized in the start-up conditions. The magnitude of the cosinusoidal modulation is used as the amplitude of a square wave with a 100% duty cycle. The names appear misleading at first but are so given so that the operator knows which of the circuits and IR ICs are being utilized. Control shifts to the boxes labelled 'System 1' and 'System 2' once the 'MODULATE' button is pressed.

The right hand side of Figure 4-32 shows the user interface for creating and changing the modulated control signals. The modulation frequency and modulation depth are only displayed once since they are common to both systems. Each system has its own resistance and inductance values as well as separate magnitude controls. The magnitude control allows the user to tune power fluctuations depending on machine parameter imbalances. Each system also has a phase adjustment control. Phase control is utilized for fine control and can be changed manually and automatically.

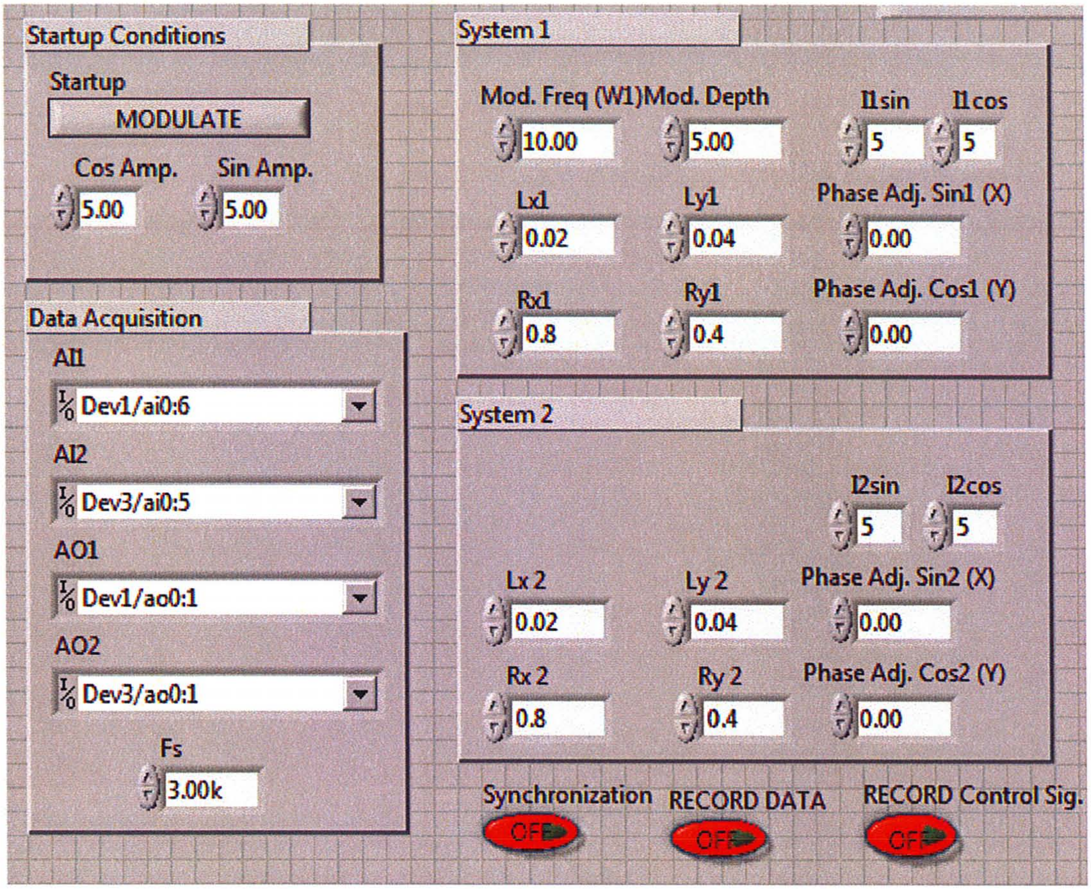

Figure 4-32 - LabView User Interface

Lastly, the user has the option of storing two types of data and initializing the synchronization algorithm. When pressed, these buttons activate their respective functions and do so until terminated by the user or by the algorithm they commenced.

4-3 Equipment Setup

A challenge for this experiment was to find an optimal way to arrange the experimental equipment in such a way to minimize space while maintaining functionality and access to the PC. This was made more difficult by cable length constraints for the Lab Volt power supplies. The solution and the physical connections of the experiment equipment will be explained in the sections to follow.

4-3-1 Power Supplies

A total of four large power supplies are utilized for this experiment; three variable DC supplies and one variable AC supply. The AC supply is connected to the driver motor D0 through an ammeter, a voltmeter and a switch. The connections are shown in Figure 4-33.

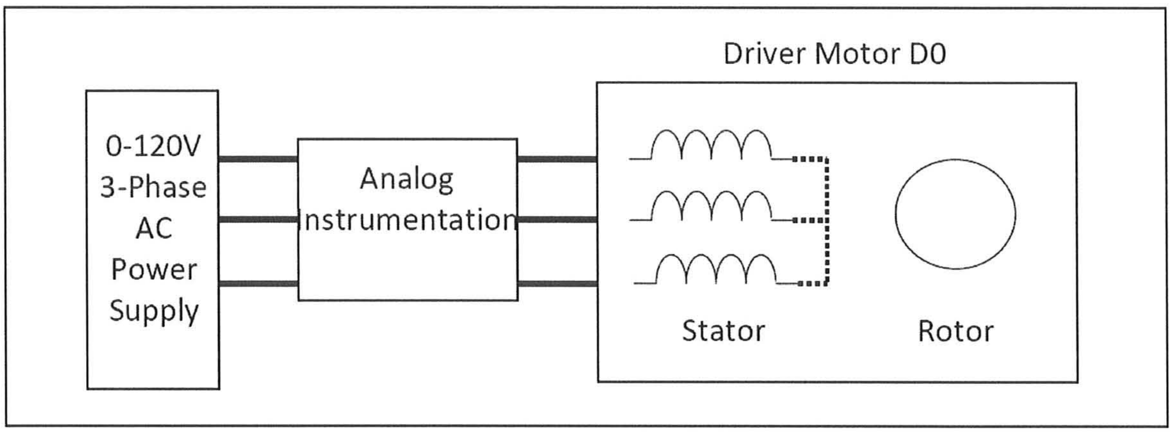

Figure 4-33 - Driver Motor Connections

The analog instrumentation is used to compare the actual experimental values with the DAQ values to ensure uniformity. The switch is used to protect the CTs on the measurement board. The switch is necessary since the driver motor was started by applying a 120V directly to the stator windings which causes high starting currents for a short period of time. Once the machine reaches rated speed the current drops to normal operating values. The switch is therefore used to bypass the current instrumentation during start up conditions since these starting currents are higher than the rated 20A of the CT. When machine reaches rated speed, the switch is flipped and the measurement instrumentation is connected to the stator windings. Since no data acquisition is required during the start up of the D0, there is no need for the current measurement circuit to be online.

There are two types of DC power supplies utilized during the experiment. The first is the Lab-Volt rectified variable DC supply terminal with an added LC filter on the output to minimize the voltage ripple. This type of supply is used to start the two generators. The starts up procedures are described in more detail later on in this chapter.

The second type of DC power supply is a rectified variable AC source. Two such power supplies are necessary, one for each generator. The connection for one such supply is illustrated in Figure 4-34.

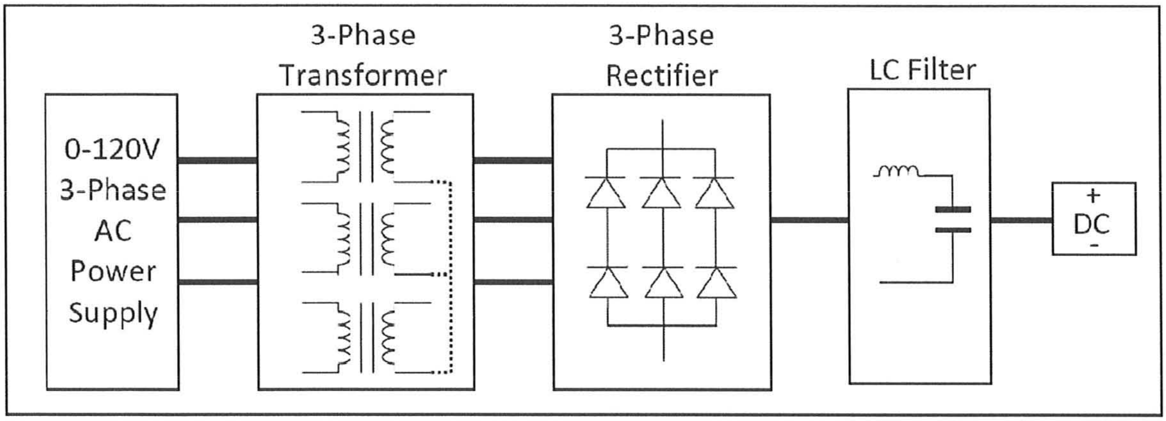

Figure 4-34 - Rectified and Isolated DC Signal

The setup in Figure 4-34 shows a three phase variable AC power supply manufactured by Lab-Volt which is connected to a three phase one to one transformer. The secondary windings of the transformer are connected together to form a floating neutral point. This isolates the power signal and allows for isolation between the generators. This is important in breaking the ground loop which is created when there is more than one power supply connected together. The ground loop can cause circulating currents which are detrimental to the experiment and can be harmful to both the machines and hardware running the machines.[3] The isolated, floating neutral point AC power signal is then passed through a three phase rectifier bridge composed of six diodes. The output of the bridge is fed to an LC filter and the result is an isolated variable DC power source.

4-3-2 Physical Machine Connections

The connection between the synchronous generator and the squirrel cage induction motor is shown in Figure 4-35. As described in section 2-1-2-1-2, the synchronous generator is fed by a sinusoidal and cosinusoidal signal. The modulated sinusoidal signal is created on one of the IR ICs on one of the two control boards. The signal is then output through analog instrumentation to verify the results on the measurement board and then passed to one of the windings on the rotor. The rotor winding is connected as is the load in the H-Bridge diagram in Figure 4-10. The other IR IC on the control board feeds a modulated cosinusoidal signal to the other two windings of the rotor which are connected in series. This creates the 90 degree spatially flux distribution required by the sinusoidal phase modulation technique. The modulated cosinusoidal signal is also passed through analog instrumentation for verification purposes. The stator of the newly created two phase synchronous generator is connected to the stator of the induction machine, again through analog voltage and current instrumentation. All these connections create one of the two systems used in the modulation technique experiment. An identical system is connected using the other two measurement and control boards, the second generator and the second induction motor.

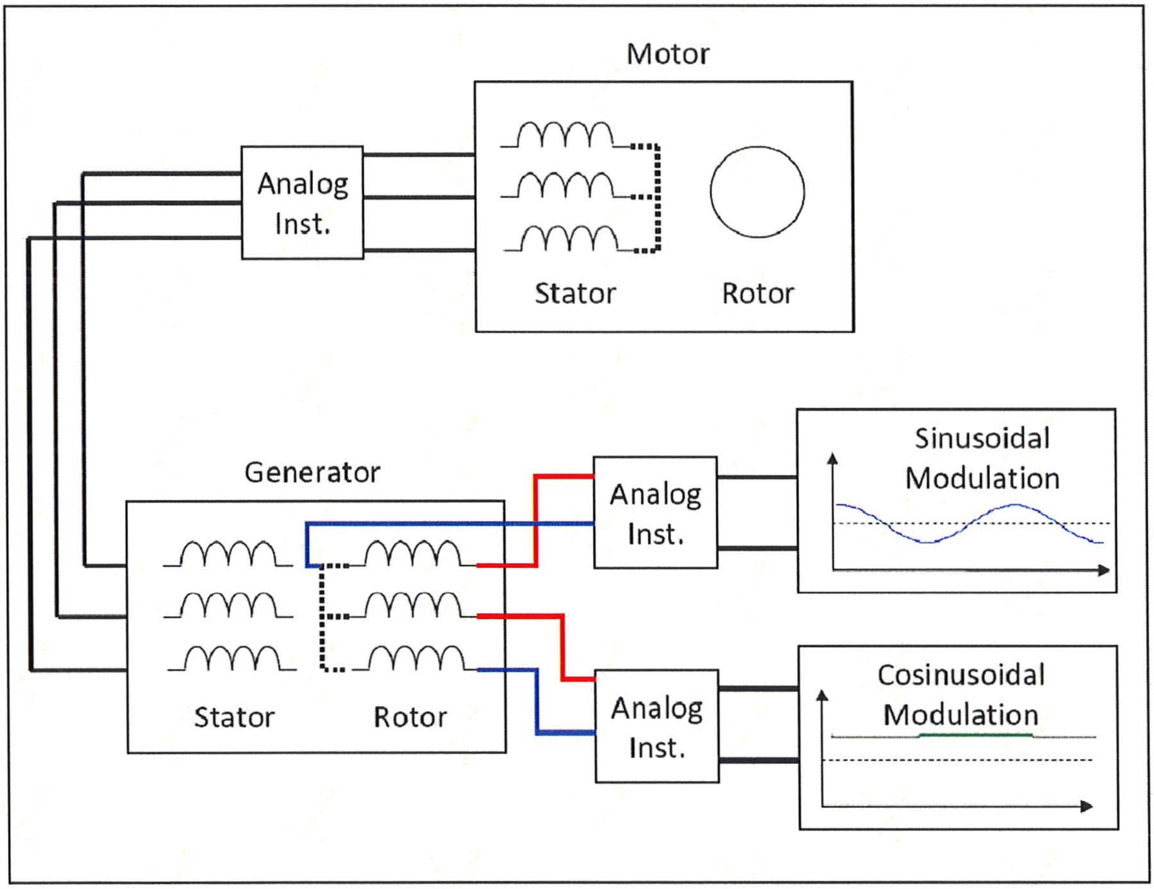

Figure 4-35 - Synchronous Generator and Induction Motor Connections

4-3-3 Start Up Procedures

Figure 4-36 shows the five machine setup and instrumentation used for start up and experimental procedures. Figure 4-36 shows the driver motor D0 connected shaft to shaft with the two generators and the stator to stator electrical connections between the two generators and their respective motors. The three DC sources and one AC source are also visible along with the two switches, the LC filter and the modulation hardware. Although the intent of the experiment was to use the almost fixed modulated cosinusoidal signal for start up and operation it proved to cause too much interference. Since the variations of the modulated cosinusoidal signal are only 1.5% at most based on the optimal modulation parameters it was decided to utilize a filtered fixed DC source for both operation and start up.

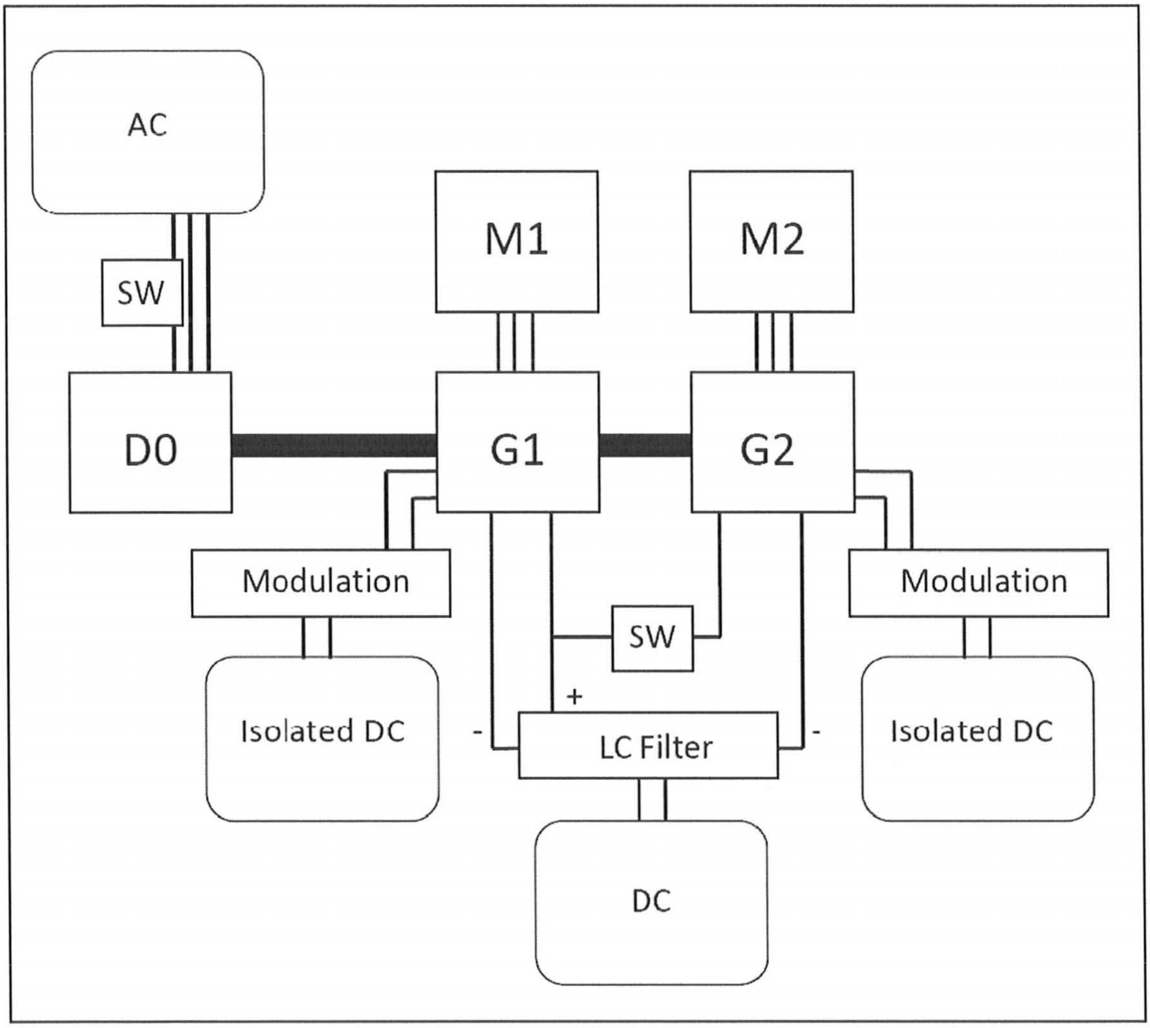

Figure 4-36 - Complete Five Machine System

The start up procedures requires one motor to start and to reach rated speed before starting the second motor. This action is achieved through the use of a switch. This procedure is necessary to prevent over current in the windings of the generators. Although over current is experienced by the generator which has reached rated speed when powering on the second motor, the current values are much smaller and rotational cooling aids in diminishing damage. The DC signal is applied to the two windings connected in series on the rotor of the synchronous generator.[3]

The switch is initially left open to start M1. This action provides a clean DC signal to G1 while cutting off any current to G2. Once M1 reaches rated speed, the switch is flipped and current is fed to both generators. It is important to note that the power supplies that power the modulation signals are left off during start up. Modulation can begin once both motors have reached full speed.[3]

4-3-4 Control and Measurement Connections

Figure 4-37 shows the placement of both analog ammeters and voltmeters as well as the connections of the measurement board.

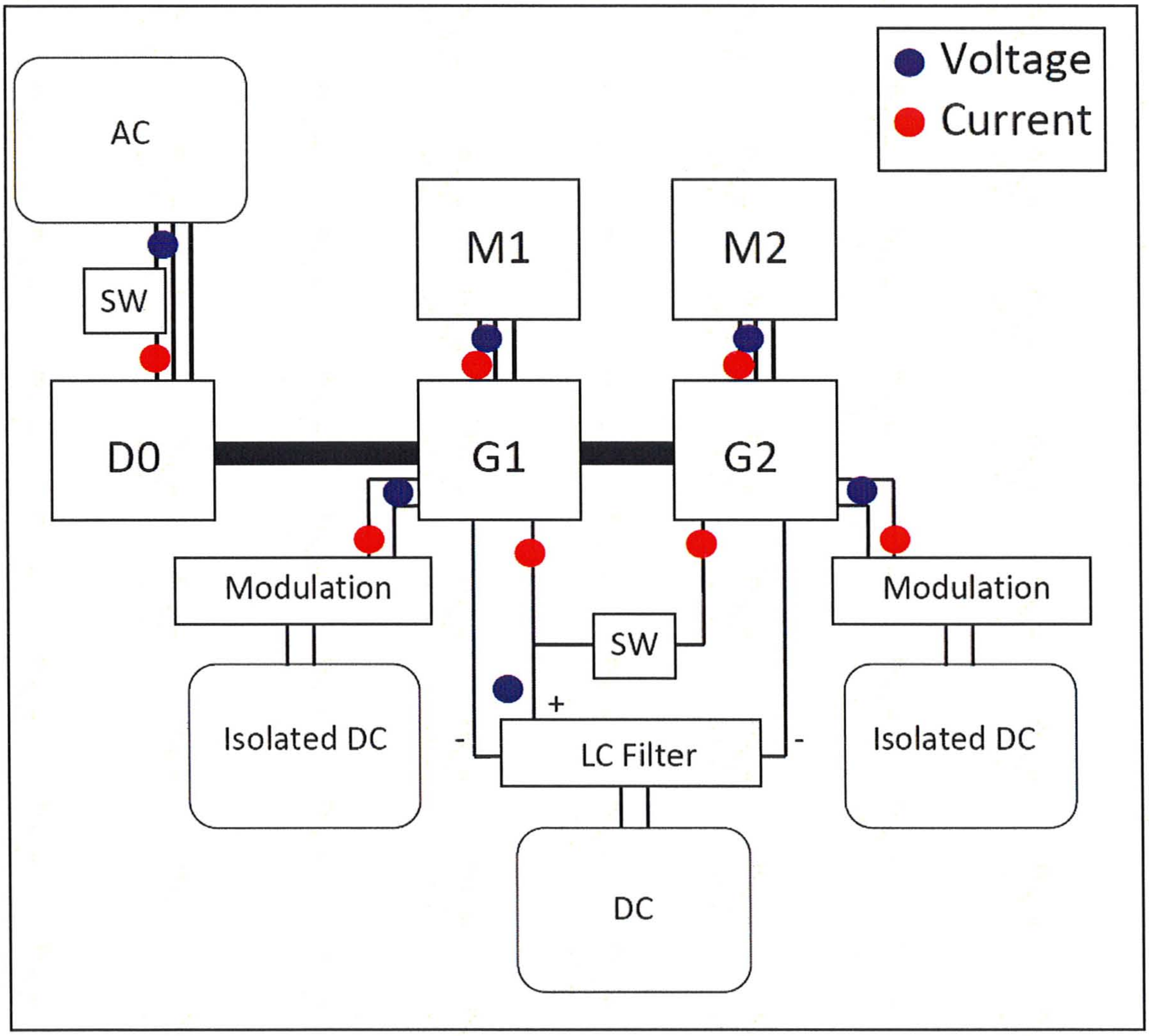

Figure 4-37 - PT and CT Placement for the Five Machine System

Voltage measurements are depicted by blue circles and current measurements are depicted by red circles. Of course, voltage measurements are taken in parallel and provide line to line values while current measurements are taken in series and provide line values. A total of six voltage measurements are necessary. One voltage measurement for each stator phase of the three motors. Two voltage measurements, one for each of the modulated sinusoidal signals applied to the rotor and one voltage measurement for the DC signal applied to both rotors. A total of seven current measurements are required. Three measurements for each stator phase of the three motors. Two current measurements, one for each sinusoidal modulation applied to the rotor of each of the two generators and two more for the two phases connected in series of the two generators. Measurements are taken on one phase of each machine only. This is assumed to give an accurate representation since the machines are assumed to be balanced.

4-4 Rotating Machine Setup

The overall experiment setup can be seen in Figure 4-38.

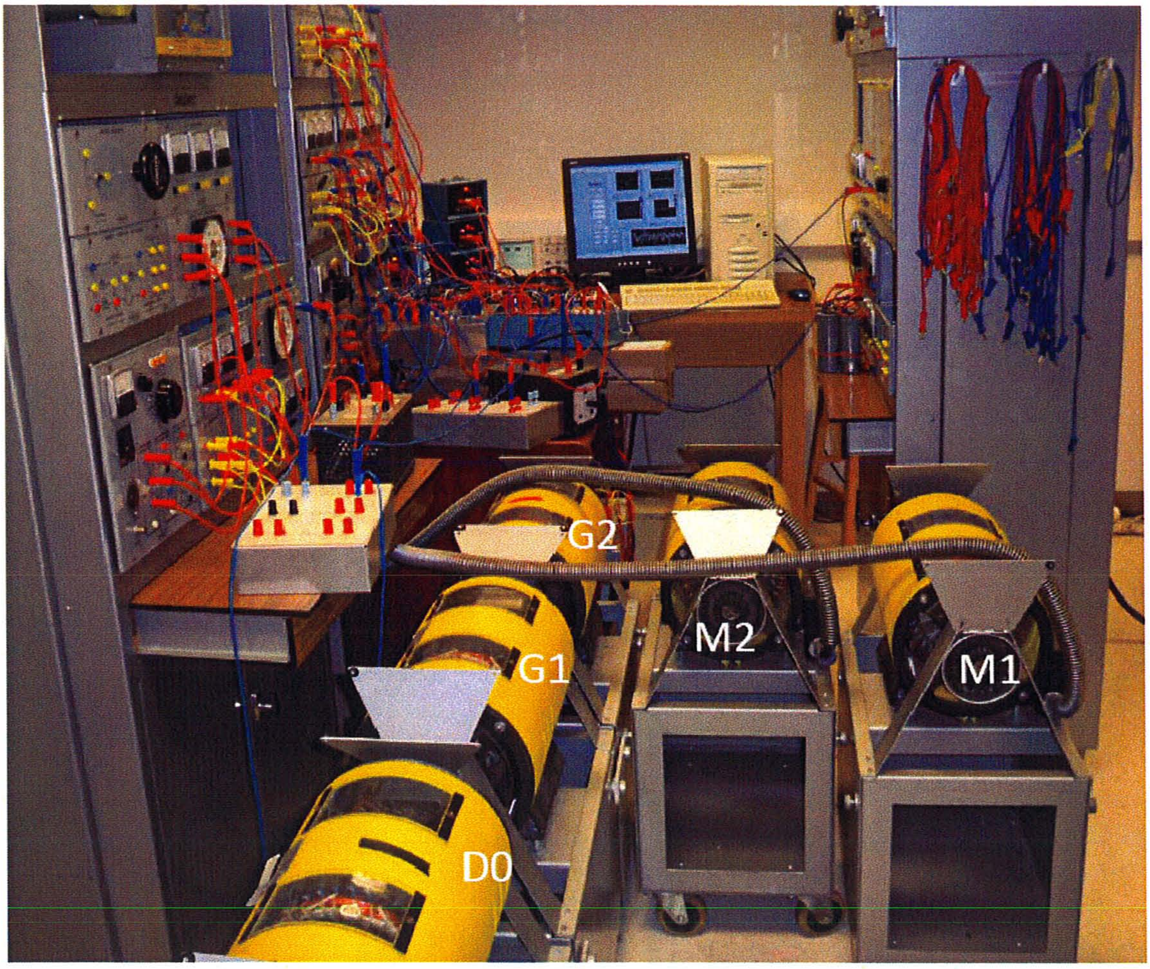

Figure 4-38 - In-Lab Experiment Setup

Readily available equipment manufactured by Lab Volt and used in the undergraduate machines laboratory is utilized as much as possible. The bottom of Figure 4-38 shows the physical arrangement of the five 2 kW electric machines; three squirrel cage induction machines used as motors and two wound rotor machines used as generators. On the left hand side of Figure 4-38 are the Lab Volt wiring modules and analog instrumentation equipment. On the right hand side of Figure 4-38 is the DC supply used for start up. In the background of Figure 4-38 are the two DACs and the PC used to drive the control systems and on the brown bench in front of the PC are the two measurement and two control boards.

Table 4-1 provides a list of all the equipment necessary for running the experiment.

Table 4-1- List of Equipment

Equipment List	
Type	**Quantity**
Squirrel Cage Induction Machine(SCIM)	3
SCIM Wiring Module	3
Wound Rotor Machines (WRM)	2
WRM Wiring Module	2
Power Supplies	4
3-Phase Transformers	2
3-Phase Bridge Rectifiers	2
LC Filters	3
AC Ammeters	3
AC Voltmeters	3
DC A/V Meters	5
Phase Switches	2
Control Boards	2
Measurement Boards	2
DACs	2
PCs	1
Oscilloscopes	2
+5V DC supplies	2
+- 15V AC Supplies	5

4-4-1 Machine Parameters

Proper machine parameters must be established before any accurate simulations can be conducted. The equivalent circuit of the induction machine with the rotor values referred to the stator is shown in Figure 4-39.

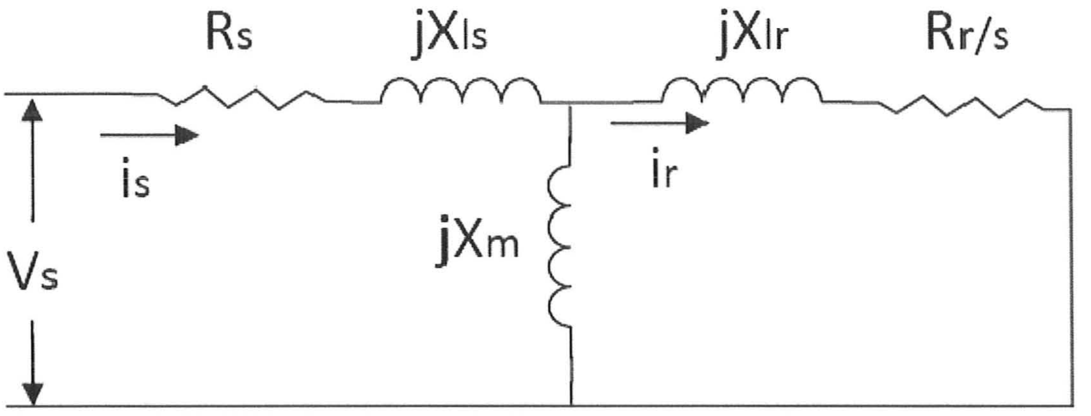

Figure 4-39 - Equivalent Induction Machine Diagram

The appropriate stator and rotor resistances and inductances must be calculated for each machine using the various techniques described below.

4-4-1-1 DC Resistance Test

The DC resistance test is run to find the equivalent, per-phase stator resistance.[3] The Lab Volt induction machine wiring module is connected with an ammeter in series and a voltmeter in parallel on each of the three phases. A DC source is connected to each winding and power is increased until rated current flows through each winding. The voltage is then measured and averaged over all three phases to find the equivalent DC resistance using Ohm's law. The skin effect for this test can be neglected since the wiring of each module is small enough to be able to neglect the skin effect.[3]

4-4-1-2 Blocked Rotor Test

The blocked rotor test is run to determine the equivalent, per phase stator and rotor leakage reactances Xm and Xls and Xlr as well as the equivalent rotor resistance.[3] The rotor is blocked and power is applied to all phases until rated stator currents are reached. Stator currents, voltages and input power are recorded. This test is performed as quickly as possible to ensure no damage is inflicted to the windings since there is no cooling from rotation.[3]

Since there is no motion during this test (slip=1), the magnetizing reactance Xm is very small and can be neglected for calculation purposes. This simplifies the circuit by removing Xm from calculations thus leaving a series circuit with an impedance composed of the sums of Rs, Xls, Xlr and Rr. Xls and Xlr can be considered equal for test purposes and are easily calculated from the above impendence. Rr can then be found by taking into account the Rs value calculated from the DC resistance test.[3]

4-4-1-3 No Load Test

The no load test is run to determine Xm, the magnetizing reactance of the equivalent circuit.[3] When the motor is run at rated speed without a load the slip is 0. When the slip is 0 there is almost no current flowing through Ir of Figure 4-39 thus creating an open circuit. This means that the remaining current flows down in Xm. We can determine the magnetizing reactance by recording the real power P, the apparent power Q and the total power S along with the no load currents and voltages.

4-4-1-4 Motor/Generator Characteristics

The above tests along with the nameplate values found on the induction machines provide the following two tables. Table 4-2 represents the name plate values of the two Lab Volt squirrel cage induction machines and

Table 4-3 represents the parameter values found using the above three test.

Table 4-2 - Squirrel Cage Induction Machine Name Plate Ratings

	Squirrel Cage Induction Machines	
	Machine 1	Machine 2
W	2000	2000
RPM	1770	1770
Volts	120/208	120/208
F.L. Amps	15.2/8.8	15.2/8.8
Phases	3	3
Hz	60	60
PF	0.77	0.77
Class	B	B

Table 4-3 - Squirrel Cage Induction Machine Parameters

	Squirrel Cage Induction Machines	
	Machine 1	Machine 2
Rs (Ω)	0.6	0.6
Rr (Ω)	0.4	0.4
Xls (Ω)	0.7	0.7
Xlr (Ω)	0.7	0.7
Xm (Ω)	23	23
J (kg-m^2)	0.0189	0.0189

Chapter 5: Comparison of Theoretical and Experimental Results

Theoretically, for the rotating flux created in the two generators to remain constant, we require both a sinusoidal and cosinusoidal modulations as explained in Chapter 2. Due to decoupling problems with the International Rectifier IC, supplying both modulations simultaneously was impossible. Since the cosinusoidal modulation only varies 1.5%, it was changed to a fixed DC as was done in [3].

Although it was stated in [5] that the ideal modulation parameters are 10Hz modulation frequency with a 5Hz modulation depth, this was the case when only one generator was attached to the shaft of the driver motor. This thesis is based on a five machine system which naturally contains different modulation parameters. Experiments were conducted based on [5] ideal parameters, but the power fluctuations were too small in magnitude to draw concrete conclusions. We have determined experimentally that a 5Hz modulation frequency with 10Hz modulation depth provides best results.

All experiments displayed in this chapter were achieved with a sinusoidal modulation and a fixed DC signal. All figures in this chapter are per phase representation unless otherwise specified.

5-1 No Load Conditions on D0

The no load conditions for the driver motor D0 refer to when there is no load on either of the two generators connected to the shaft of D0. As such, this is the base load with only the mechanical losses of the two generators running at full speed. Figure 5-1a shows the simulated power consumption and Figure 5-1b show the experimental power consumption on D0. The simulated result on the left shows no average power fluctuations and no ripple. This is to be expected as the power supply used in the experiment is ideal. The experimental result shows in Figure 5-1b displays slight fluctuations in power. These fluctuations can be attributed to slight voltage variations in the power supply. As such, the average power is not completely stable. These fluctuations however are random and small enough in magnitude to be neglected.

For more accurate comparisons, the generators were loaded with loads M1 and M2. A DC current was applied to the excitation winding on G1 first, until M1 reached synchronous speed. The switch was then closed, and M2 was brought up to synchronous speed in the same manner as described in Chapter 4-3-3. Figure 5-2a shows the simulated results and Figure 5-2b shows the experimental results for the loaded, but un-modulated power in D0. The two figures are almost identical to one another but Figure 5-2b achieves slightly higher power consumption with slightly more average power fluctuations. This may be due to the fact that the experimental case uses a constant feed as opposed to a cosinusoidal feed used in the simulated case. The average power in the experimental case fluctuates by a maximum of 4%. When taking into account 1.5% cosinusoidal fluctuation with another two percent maximum measurement error, the fluctuations in the experimental case can be neglected. Figure 5-2 also illustrates that both the actual and average powers are higher than in Figure 5-1 because there are more losses in the system with the introduction of M1 and M2. Driver motor D0 provides these losses.

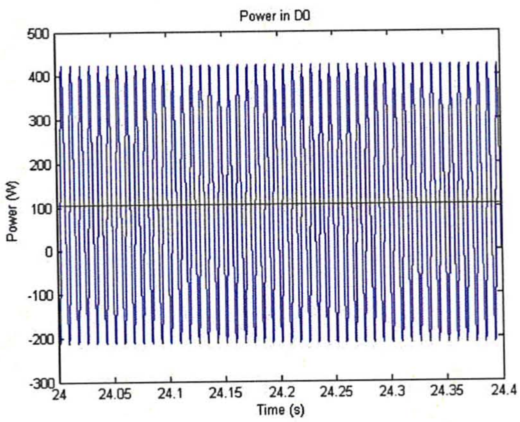

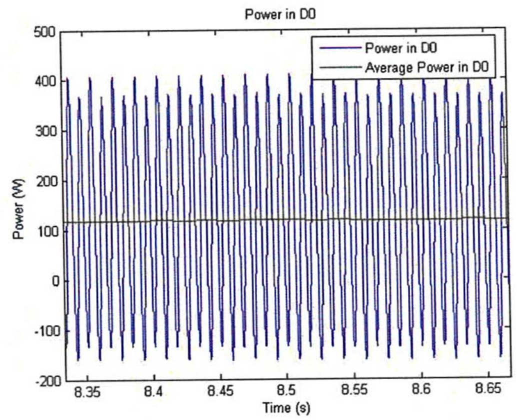

Figure 5-1a **Figure 5-1b**

Figure 5-1 - Simulated and Experimental Results for Unload Power on D0

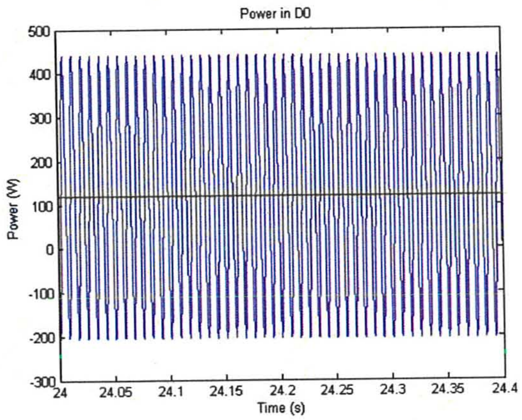

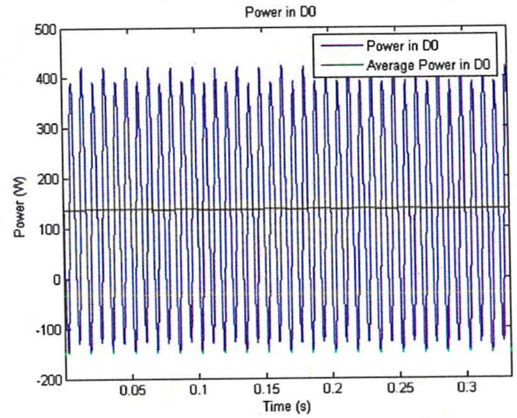

Figure 5-2a **Figure 5-2b**

Figure 5-2 - Simulated and Experimental Results for Load Power on D0

5-2 One Motor Load on D0

The next step was to load and modulate only half of the system and compare the simulated and experimental results to ensure that the experiment was working correctly. The system was started and the motor loads M1 and M2 were brought up to speed. At this time, only G2 received sinusoidal modulation. Figure 5-3 shows the simulated results of the sinusoidal modulation at 5Hz. As is to be expected, the field current in G2 is sinusoidally modulated at 5Hz as seen in Figure 5-3b. This creates a power oscillation in M1, seen in Figure 5-3c which is passed on to the driver motor D0 seen in Figure 5-3d.

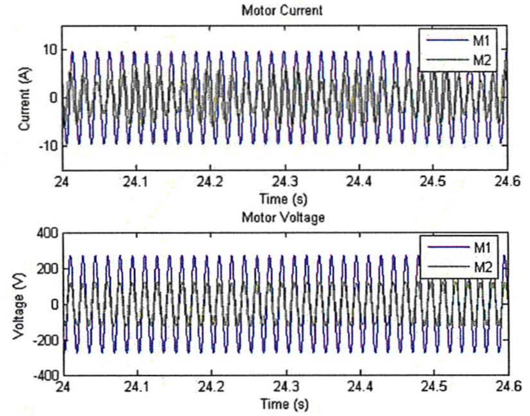

Figure 5-3a

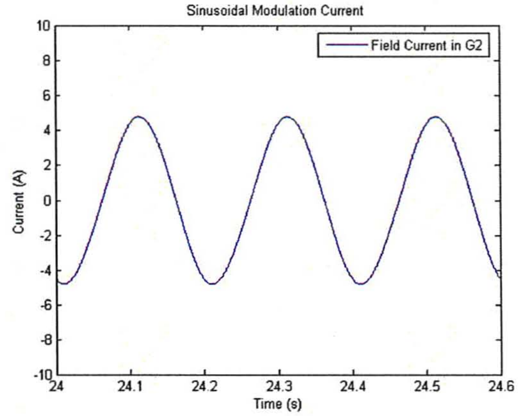

Figure 5-3b

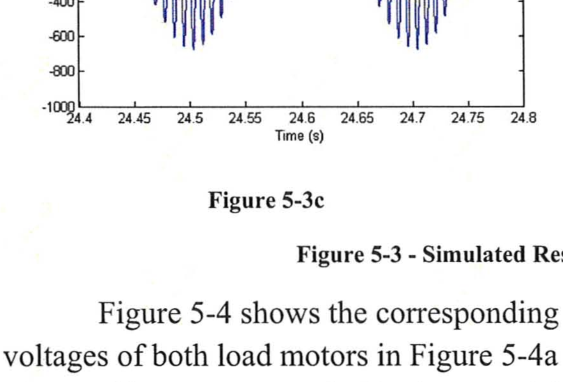

Figure 5-3c

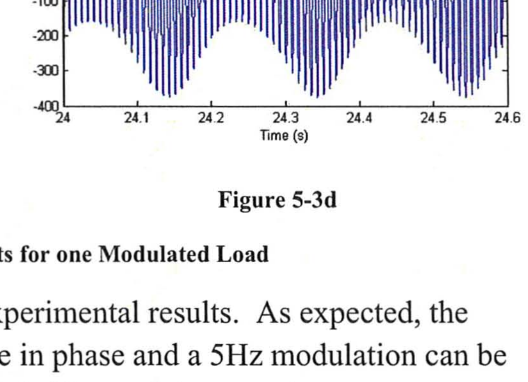

Figure 5-3d

Figure 5-3 - Simulated Results for one Modulated Load

Figure 5-4 shows the corresponding experimental results. As expected, the voltages of both load motors in Figure 5-4a are in phase and a 5Hz modulation can be observed in the current of M2. As a result M2, in Figure 5.4c, experiences a power

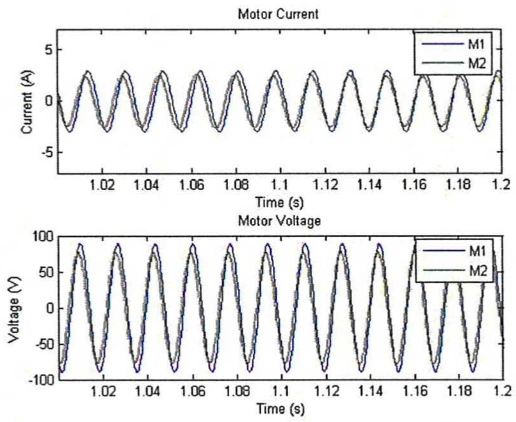

Figure 5-4a

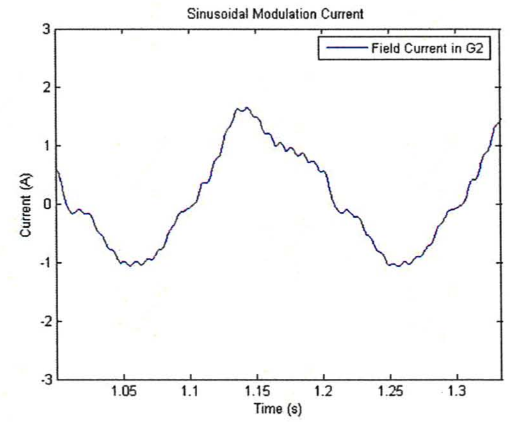

Figure 5-4b

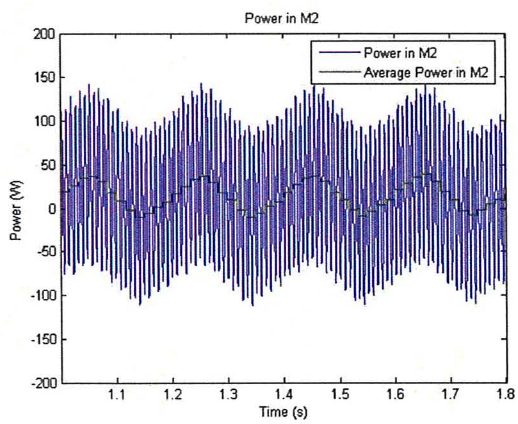

Figure 5-4c

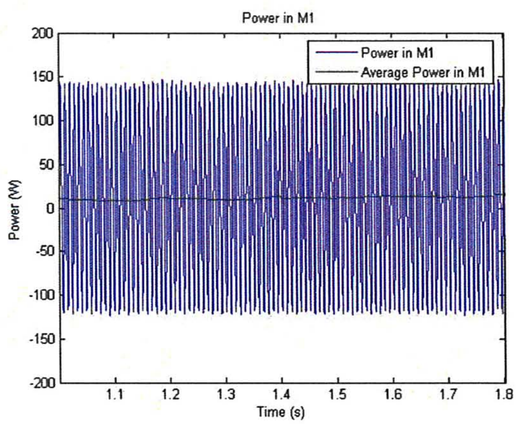

Figure 5-4d

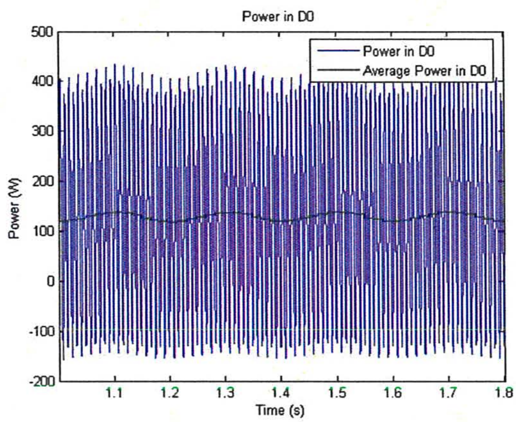

Figure 5-4e

Figure 5-4 - Experimental Results for One Modulated Load

fluctuation, and M1 in Figure 5-4d does not. We expect these fluctuations to be passed on to the driver motor, D0, which is the case as shown in Figure 5-4e. The field current modulation, shown in Figure 5-4b, is subjected to a sinusoidal modulation of 5Hz.

5-3 Two Motor Load on D0

To complete the experiment, the power fluctuations noticeable on D0 must be negated. As such, the G1/M1 pairing was modulated in opposition to the G2/M2 pairing. This was done so that when one of the pairings is creating power at a modulated frequency of 55-65Hz, the second pairing is consuming power at the same frequency. Theoretically this should negate the power swings exhibited on the driver motor and its power supply.

5-3-1 Balanced Loads

Simulation results, for a perfectly balanced system, with all machine parameters equal, showed a perfect correlation between theory and practice. Figure 5-5a shows that both loads are being modulated. Figure 5-5b shows a perfect sinusoidal modulated field current which result in equal and opposite power consumption by each of the two loads M1 and M1 (Figure 5-5c and Figure 5-5d). Figure 5-5e shows no power fluctuations on D0, which is the optimal and desired result. The small constant power is due to the power drawn by the driver motor D0, loaded with generators G1 and G2 attached mechanically to its shaft.

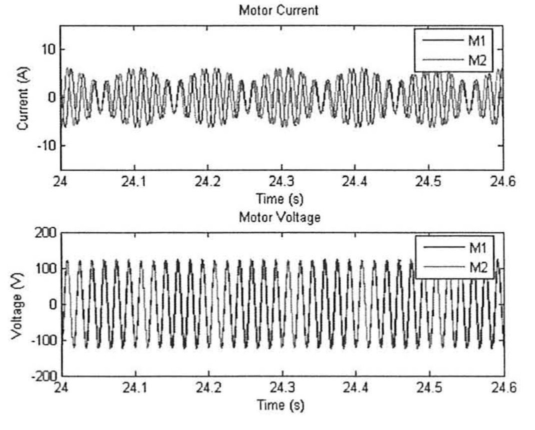

Figure 5-5a

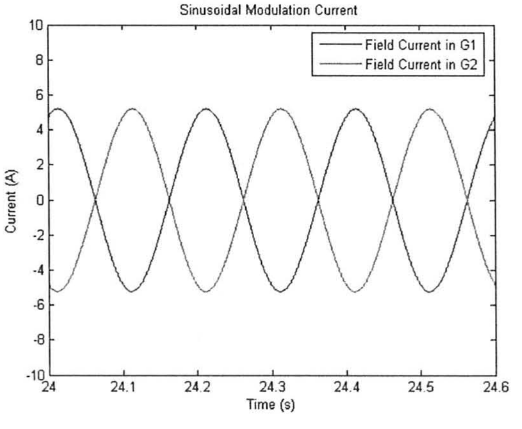

Figure 5-5b

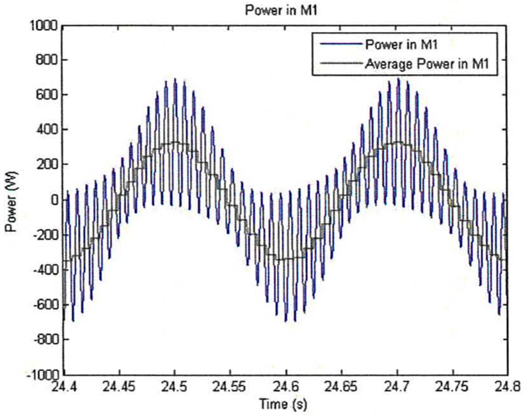

Figure 5-5c

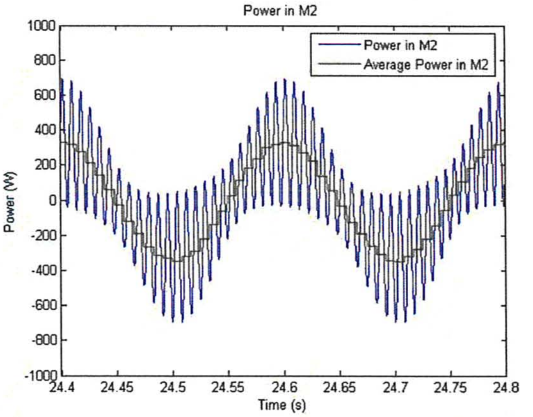

Figure 5-5d

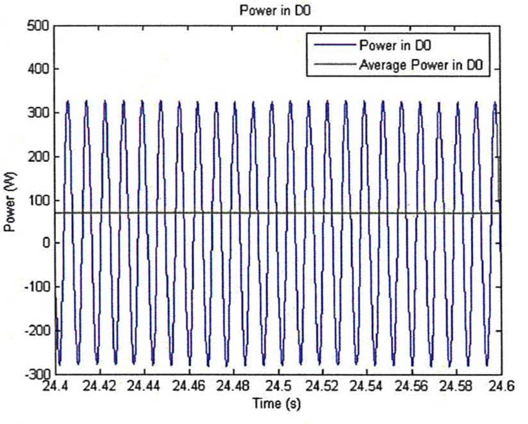

Figure 5-5e

Figure 5-5 - Simulation Results for Perfectly Balanced Loads

5-3-2 Unbalanced Loads

It is improbable in the real world to expect that two loads will be perfectly balanced. A more realistic and suitable simulation is a system with unbalanced loads. Figure 5-6b shows the sinusoidally modulated field currents for both generators under balanced modulation parameters. Balanced modulation parameters were fed into the program based on the assumption that both machines under test have the same characteristics, including resistances, inductances and inertias. It can be seen that the two currents are not 180 degrees out of phase and that there is a large magnitude discrepancy between the two currents. These two factors affect the instantaneous and average powers in the two motor loads as can be seen in Figure 5-6c and Figure 5-6d respectively. The loads are not consuming the same amount of power thus we expect to see a power fluctuation on the driver motor D0. This power fluctuation can be seen in Figure 5-6e

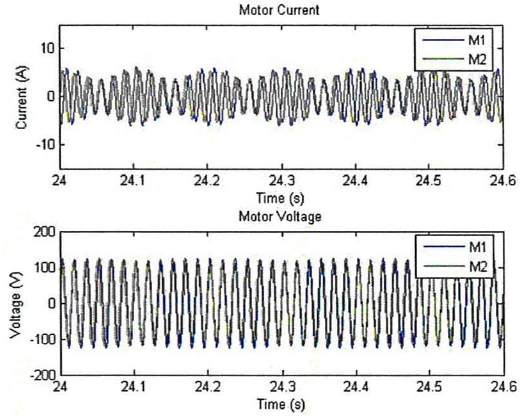

Figure 5-6a

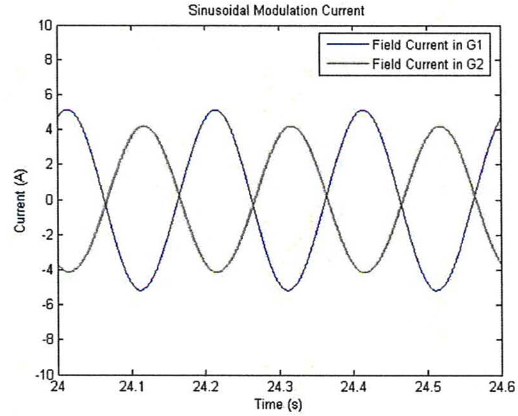

Figure 5-6b

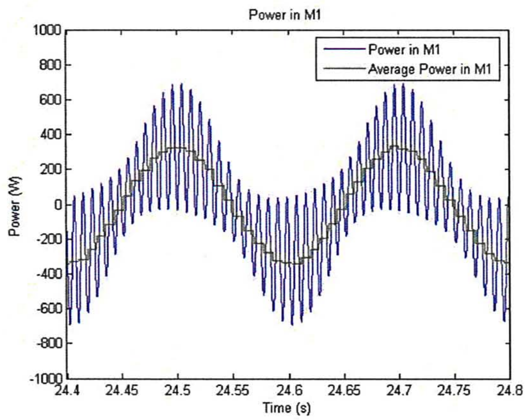

Figure 5-6c

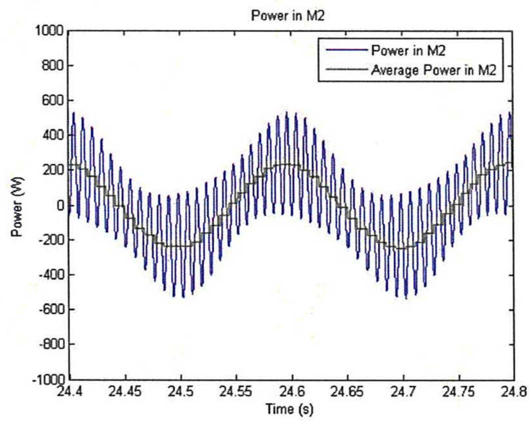

Figure 5-6d

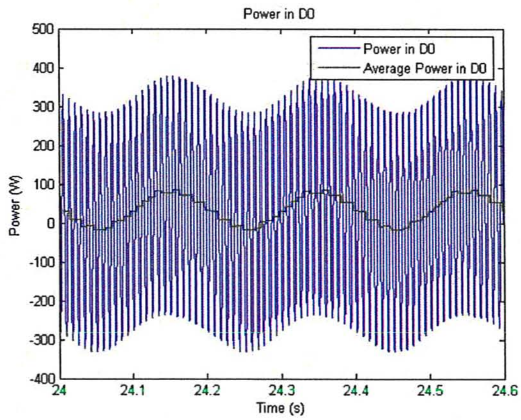

Figure 5-6e

Figure 5-6 - Simulation Results for Unbalanced Loads without Magnitude Adjustment

and is approximately 18% or 110W, and must be negated. Experimental results could not be investigated since two identical loads were not available.

5-3-2-1 Magnitude Adjustment

Figure 5-7 shows the simulated results for sinusoidal modulation with magnitude adjustment. Since the two loads are not equal, we can expect slightly different modulation currents for each machine. As expected, the modulation magnitudes of each generator are different as seen in Figure 5-7b. Furthermore, a slight voltage variation is visible in Figure 5-7a. This attributed to the power fluctuation noticeable in Figure 5-7e. Magnitude adjustment can diminish power fluctuations in D0 to a minimum of 8% or 50W. Although Figure 5-7c and Figure 5-7d appear to be 180 degrees out of phase, under closer investigation it can be seen that that is not the case. Furthermore, closer inspection of Figure 5-7b illustrated and Figure 5-7f demonstrate that, in fact, the modulation currents of unbalanced loads are not 180 degree out phase.

Simulation results prove that, magnitude adjustment alone cannot completely negate power fluctuations in the driver motor when the subject loads are unbalanced. To achieve better results, a slight phase adjustment must also be applied to compensate for machine imbalances.

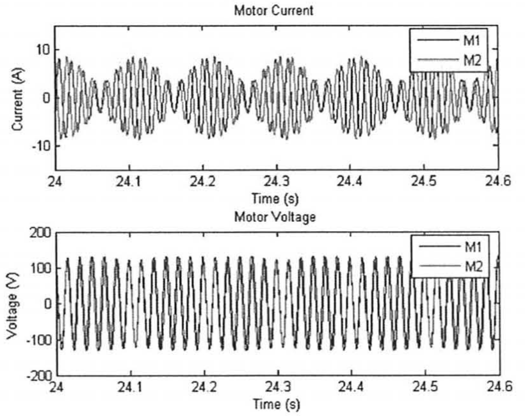

Figure 5-7a

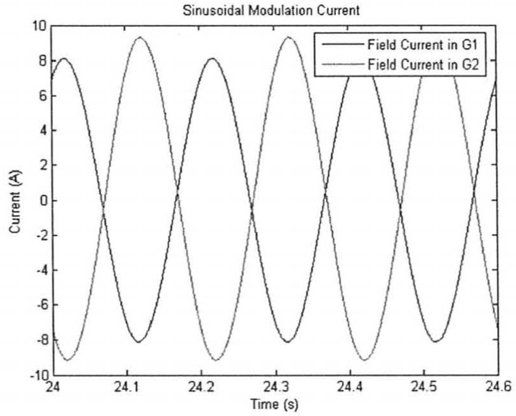

Figure 5-7b

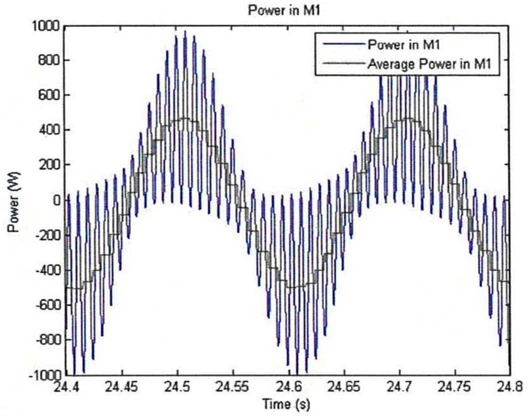

Figure 5-7c

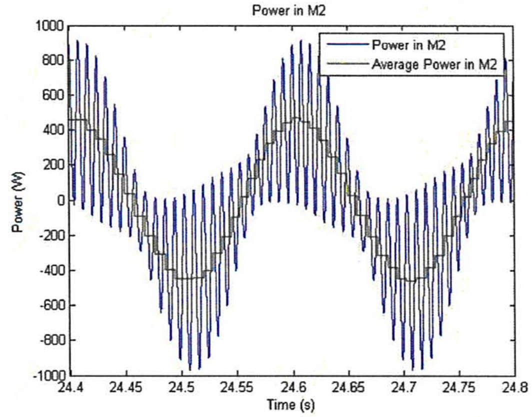

Figure 5-7d

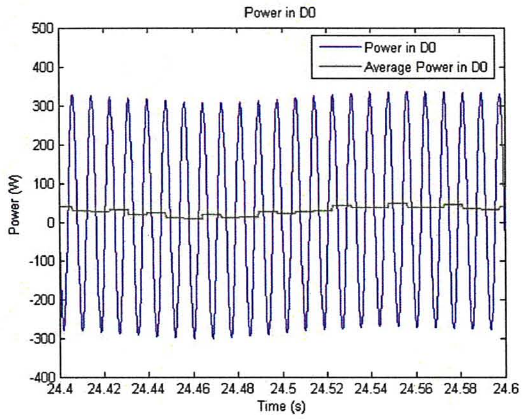

Figure 5-7e

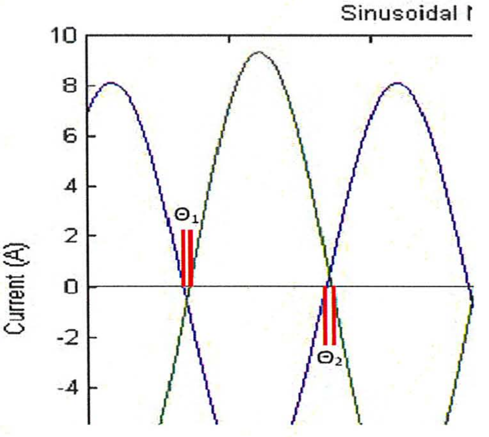

Figure 5-7f

Figure 5-7 - Simulated Results for Magnitude Adjustment of Unbalanced Loads

Experimental results for magnitude adjustment are shown in Figure 5-8. Figure 5-8b exhibits the expected sinusoidal oscillation at 5Hz. There is some noise present in the signal as well as a slight deformation when compared to a perfect sinusoid. These factors can be attributed to the control circuit. Even though noise was minimized as much as possible, there are a lot of wires in the setup and measurement circuits which intersect and cause possible interference. Therefore, some noise is to be expected. The signals also exhibit a small delay at each zero crossing. This can be attributed to the dead zone timing factor between each leg of the H-bridge. Without a sufficient dead zone, the IGBT's will have a shoot through current exceeding the safe functioning of the bridge.

The motor loads in Figure 5-8c and Figure 5-8d illustrate an almost equal and opposite power consumption, as such, the driver motor D0 exhibits only small power fluctuations. This small fluctuation is seen in Figure 5-8e and is in the order of 5%, or approximately 10W. These results conform to the simulation results achieved in Figure 5-7. It can be observed that the overall power fluctuation in D0 is lower in the experimental case than in the simulation. This result is observed based on absolute measurements taken on the power fluctuations of the driver motor. It can also be noted that the modulation currents in the experimental results also show a phase shift offset which is illustrated in Figure 5-8f. This puts further emphasis on exploring the effects of phase adjustment to diminish fluctuations in D0 when the loads are not balanced.

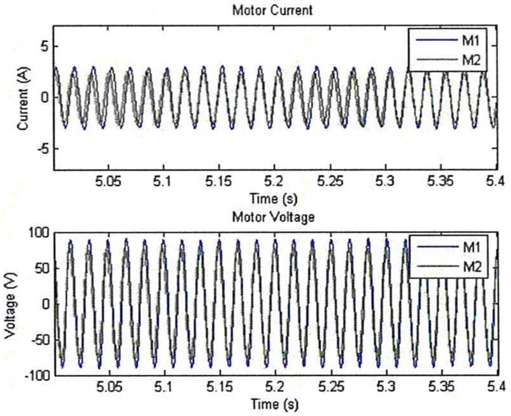

Figure 5-8a

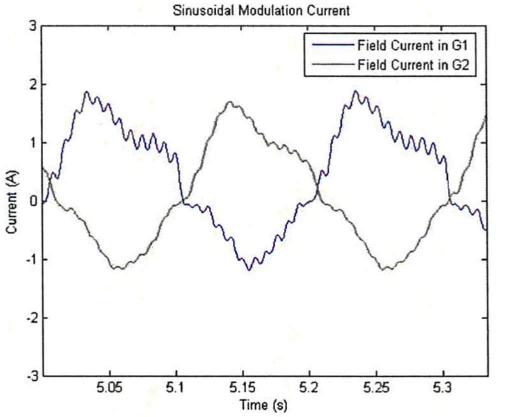

Figure 5-8b

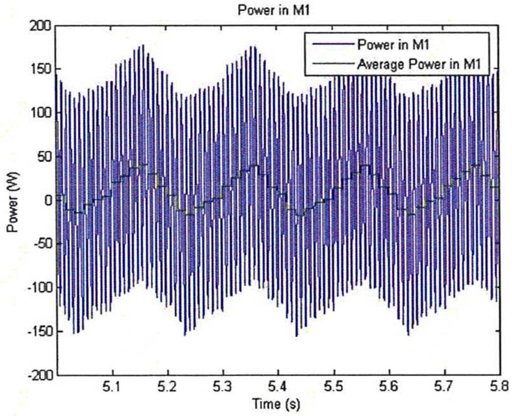

Figure 5-8c

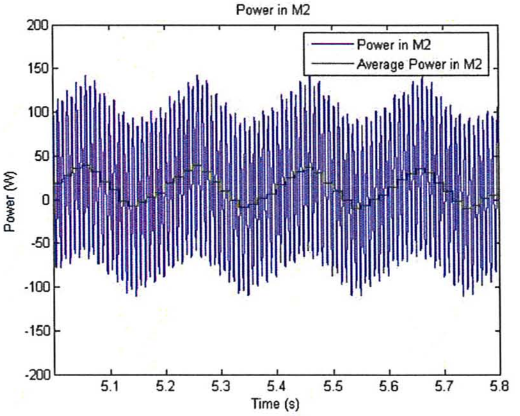

Figure 5-8d

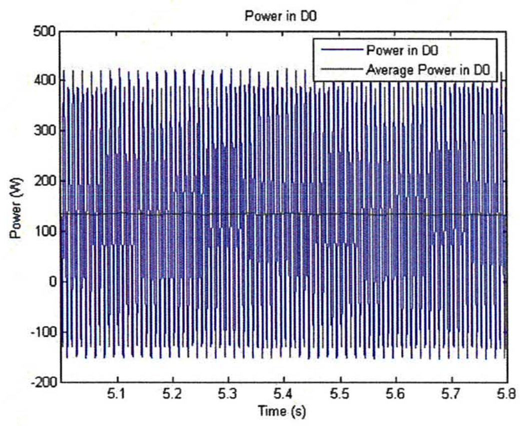

Figure 5-8e

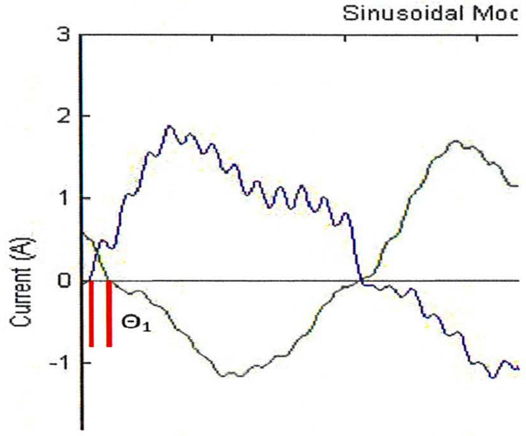

Figure 5-8f

Figure 5-8 - Experimental Results for Magnitude Adjustment of Unbalanced Loads

5-3-2-2 Magnitude and Phase Adjustment

It has been noted that magnitude adjustment alone does not achieve perfect results. It was proven in [3] that the mechanical axis alignment did not prove to be a factor in negating the power oscillations of the driver motor because axis adjustments could only be achieved at 15 degree intervals. This control is too coarse to show possible improvements. A fine electrical axis alignment made possible by the new control circuit may prove beneficial in negating these oscillations.

Figure 5-9 illustrates the case without phase correction. As can be seen, the two generator signals are exactly 180 degrees out of phase but the resultant flux, due to machine imbalances, is not. If a phase adjustment is added to the modulated signal in one of the generators, then the flux created should theoretically be offset by the same magnitude. Figure 5-10 illustrates the phase difference θ, between the two signals. With this offset, the resultant flux is 180 degrees out of phase thus negating the phase difference, Φ, in Figure 5-9.

The subsequent sections will look at phase adjustment as a possible method to improve stability in D0 on top of magnitude adjustment. Both manual and automatic phase adjustment techniques will be studied.

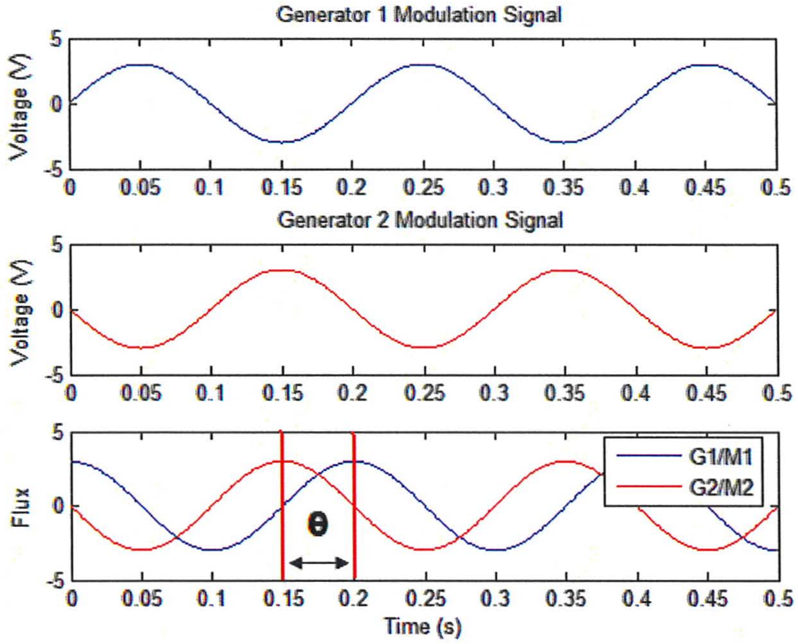

Figure 5-9 - Modulated Signals without Phase Correction

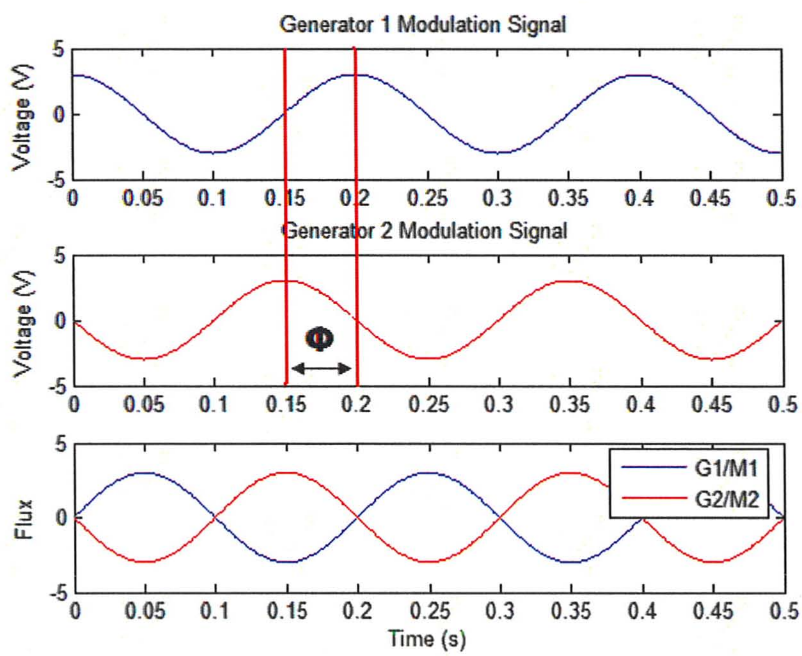

Figure 5-10 - Modulated Signals with Phase Correction

5-3-2-2-1 Manual Phase Adjustment

Manual phase adjustment was achieved by incrementing and decrementing the phase of the applied sinusoidal wave on one of the two generators. Immediate changes in phase adjustment could be compared with the ability to compute an online average power of D0. Figure 5-11a shows the per phase instantaneous and average power of driver motor D0. Figure 5-11b shows a zoomed in version of the instantenous power of D0. As can be seen, the fluctuations are almost non existant when a phase shift of two degrees is added to modulated current of G1. Furthermore, Figure 5-11c shows the two modulated field currents to be in perfect opposition. As observed, the power fluctuations drop from 8% to less than 2%. This is a power fluctuation of less than 6W for a 2KW machine.

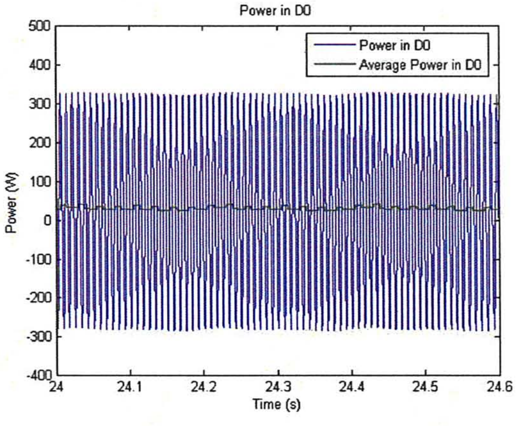

Figure 5-11a

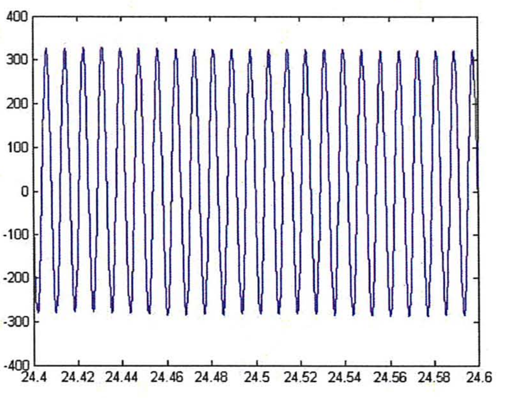

Figure 5-11b

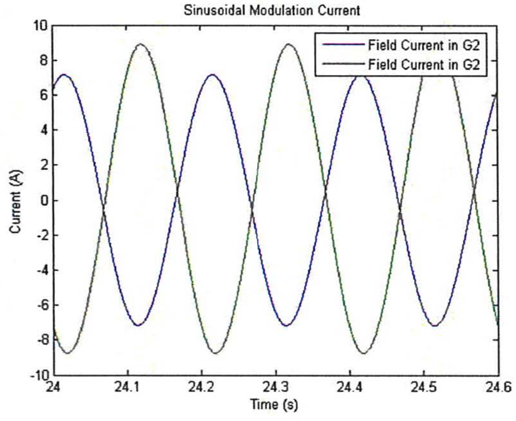

Figure 5-11c

Figure 5-11 - Simulated Results for Magnitude and Phase Adjustment of Unbalanced Loads

Experimental results mimic the simulated results for magnitude and phase adjustment although the improvements are not as drastic. Figure 5-12a shows the per phase instantaneous and average powers of the driver motor D0 with a phase offset of negative three degrees, effectively leaving the loads 177 degrees out of phase. Figure 5-12b shows a close up, or zoomed in version of Figure 5-12a. The effect of the phase change on the driver motor power fluctuation can further be examined in Figure 5-12c, a blown up version of the average power in D0. It can clearly be seen that fluctuations on the driver motor D0 are less than two percent. This is an improvement of more than 50% when compared to magnitude adjustment alone. Figure 5-12d further illustrates the improvement of phase correction by comparing the average power of D0 with and without phase shift correction. It can be determined that phase correction is a vital and necessary part of power oscillation elimination in the synthetic loading of induction machines and more specifically, the sinusoidal modulation technique.

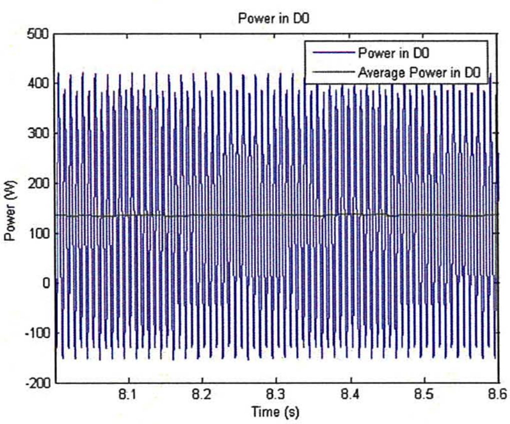

Figure 5-12a

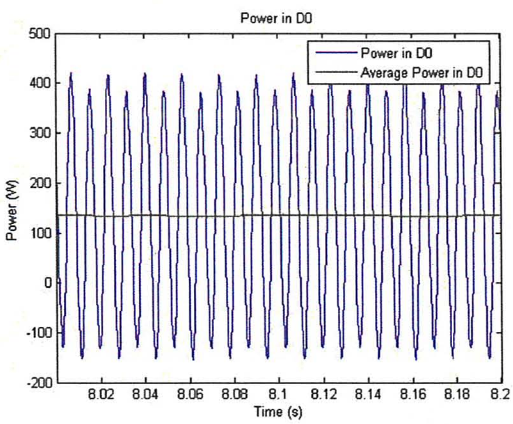

Figure 5-12b

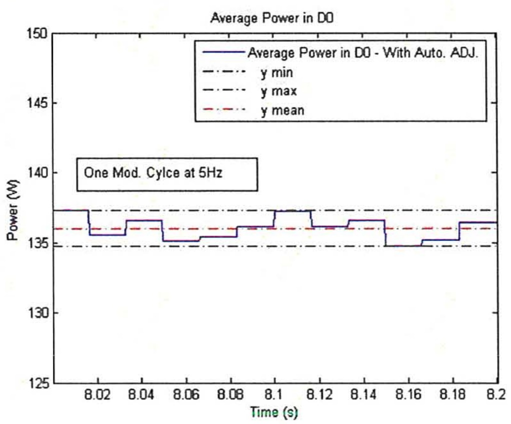

Figure 5-12c

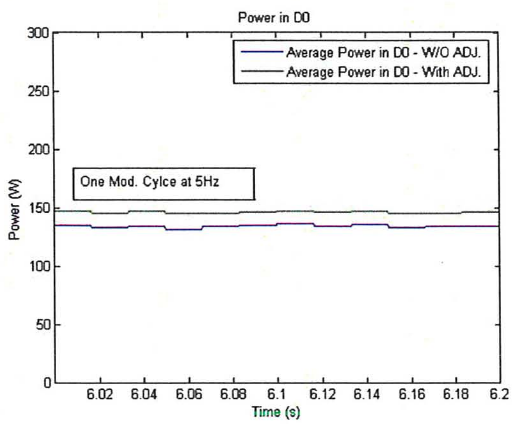

Figure 5-12d

Figure 5-12 - Experimental Results for Magnitude and Phase Adjustment of Unbalanced Loads

5-3-2-2-2 Automatic Phase Adjustment

Automation of the phase adjustment method was attempted in the hopes of improving the synthetic loading method and generalizing it for a wider range of test machines. The automatic computation of phase angle adjustment took into account the angle difference between the instantaneous powers of each of the loads and adjusted the phase of one load to try and achieve a 180 degree phase shift between the two. Therefore this method would prove useful for any two loads which may be more or less unbalanced within the range of unbalance of this experiment.

Figure 5-13 illustrates the results of the average power of D0 under automatic phase correction. The initial phase was set to zero degrees and changed up and down in steps of 0.5 degrees depending on the phase difference between the two motor loads. Several observations can be drawn from the experiment. Firstly, the phase angle appeared increased in the negative direction, as expected from the manual phase adjustments. However even though the trend was increasing in phase in the negative direction, the phase angle was continuously increasing and decreasing. This is seen as continuous oscillations in the average power in Figure 5-13. This could be due to the sampling rate on the DAQs not being high enough, or the two data acquisition cards may not be perfectly synchronized. This would cause an offset in the sampled data in each motor and thus completely inhibits the algorithm from working properly. Secondly, since the algorithm did not find a perfect 180 degree phase difference, it did not stop. This is seen in Figure 5-14. As the algorithm approaches the -3 degree phase offset, between time $t=12$ and $t=15$, the power in D0 is constant. As the phase offset increases in the negative direction, time $t \geq 15$, the oscillations become more prevalent.

Further work into the automated phase correction algorithm may be done to identify the exact problems and devise appropriate corrections to damp the ill effects of the practical system.

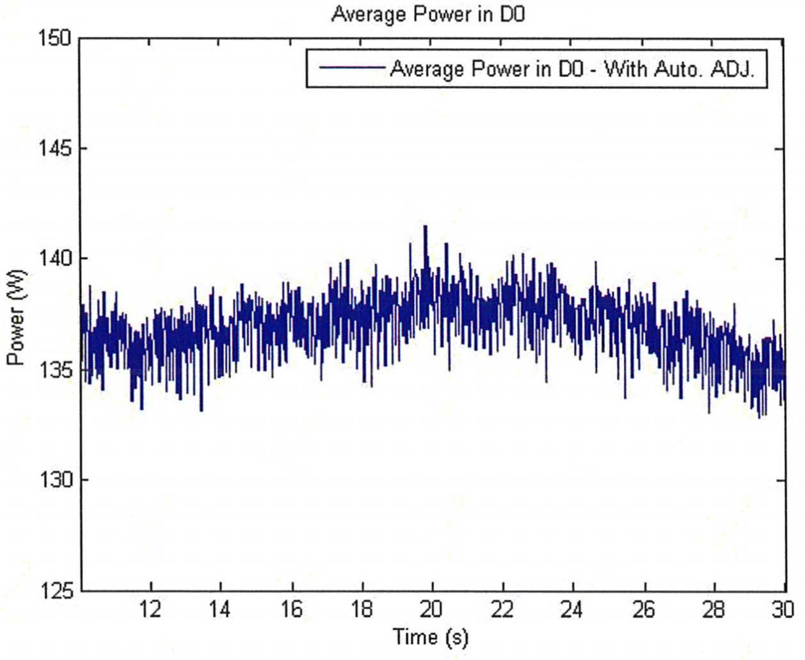

Figure 5-13 - Experimental Results for the Average Power of Automatic Phase Shift Correction of Unbalanced Loads

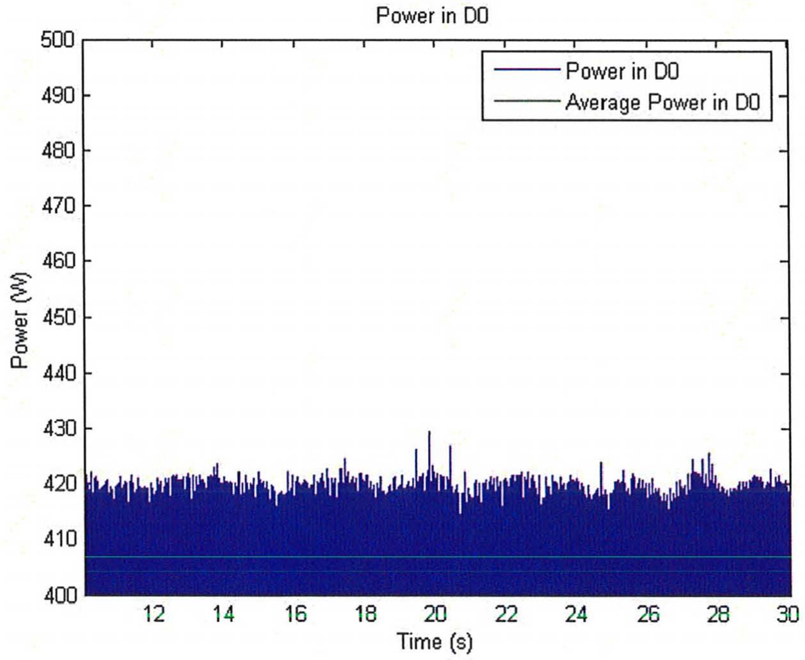

Figure 5-14 - Experimental Results for the Instantaneous Power Fluctuations for the Automatic Phase Shift Correction of Unbalanced Loads

Chapter 6: Conclusions and Recommendations

6-1 Conclusions

The objectives in this thesis were to improve on or negate the power fluctuations observed in [3]. Three major alterations along with many smaller changes were implemented to [3] to achieve this goal. Firstly, a sinusoidal modulation technique was developed instead of the previously used square-wave modulation technique. Secondly, new hardware and software was designed specifically for the control and application of the sinusoidal modulation technique to the five machine system. Thirdly, new hardware and software was designed for converting, measuring, controlling and storing the experimental results. The three alterations combined achieved the desired results of power oscillation negation on the driver motor.

The implementation of the sinusoidal modulation technique on the five machine system proved instrumental to the negation of power oscillation in the system. The electric machines used in the experiment were better able to follow the changes in modulation due to the nature of a sinusoid and its derivative properties. This allowed for sinusoidal voltage variations rather than exponential voltage variations which better suited the experiment. Additionally the sinusoidal modulation technique had the ability to provide five the machine system with constant voltage since the squares of a sinusoidal and cosinusoidal wave always add to one. Experimental results showed that the cosinusoidal variations were at a maximum of 1.5%. It was concluded that these variations were small enough to be neglected with the experimental and measurement system used in this thesis. A DC source was used instead of the modulated cosinusoidal component which greatly simplified the experiment while not deteriorating results.

The ability to precisely measure and control the system was vital in negating power fluctuations. The lack of very fine control and accurate, real-time feedback made the overall control of the five machine system in [3] extremely difficult. Two separate control and measurements circuits were designed to overcome these problems along with the use of real time data acquisition cards. The control circuit was designed with components able to react to very fine control as well as withstand the high voltage and current requirements of the experiment. The IR IC proved to be a very powerful component in terms of control and high-side/low-side isolation. However, the IC was designed for three phase motor applications and brought with it certain limitations. Un-anticipated capacitive coupling between phases proved difficult to overcome but did not pose a problem once the cosinusoidal modulation component was converted to a DC signal. The measurement circuit utilized PTs and CTs that were able to step down the high voltages and currents to levels acceptable as inputs into a DAQ.

The LabView software component proved to be the most useful experimental tool used in this thesis. Control, data acquisition and measurements were all done through the use of LabView. The developed software and LabView's natural easy user graphic interface provided a robust tool which integrated fine control capabilities with experimental data displayed visual in real time. This allowed for the implementation of both manual and automated power negation algorithms.

LabView was also instrumental in achieving a correct set of modulation parameters. The modulation parameters suggested by [5] were ideal for a single machine system but did not suit the five machine system used in this thesis. The experiment in this thesis utilized a five machine system and as such required a different set of modulation parameters. The ideal parameters for a five machine system proved to be a modulation frequency of 5Hz and a modulation depth of 10Hz.

The combination of hardware and software designed for the sinusoidal modulation technique was able to achieve experimental power oscillations in the driver motor D0 which were less than 2% or an equivalent of 4W at half rated load. These power fluctuations were improved upon when compared with the New Phase Modulation technique which exhibited best case scenario power fluctuations of 10%. The optimal experimental results for the sinusoidal modulation were achieved through the use of magnitude and phase adjustment which proved that fluctuations on the driver motor D0 of unbalanced machines could be negated with the appropriate control algorithm. This was the ideal case scenario when taking into account the DC modulated component and measurement error. It was deducted that since the cosinusoidal modulation varied so little, it did not make a sufficient impact on the power fluctuations with respect to measurement error.

6-2 Recommendations for Future Work

As with any research topic, new areas of improvement are found during the course of a project. There are four noteworthy recommendations for further work that can serve to potentially better results and achieve rated loads experimentally:

1. An accurate way to measure speed is required and highly advised to be able to fully measure power fluctuations on the driver motor. The tachometers available for use in the laboratory provided inconclusive data. An accurate speed reading on the driver motor can be used to measure power fluctuations and as an accurate reading for a

feedback control loop. This completely changes the dynamic of the feedback loop and directly impacts the way automatic control can be handled by an algorithm.

2. The design and construction of a synchronous generator with a two phase rotor having a 90 degree special shift. Having a low impedance and low reactance rotor which is able to react to the 5Hz frequency modulations and able to be controlled in the direct and quadrature axes will allow for increased currents to be provided to the load. Sizing the generator appropriately for the largest load under test will ensure the manufacture will be able to test all future motors with minimum equipment alterations.

3. Although results proved to be extremely positive with the use of the sinusoidal modulation technique described in this thesis, they can still be improved upon. The IR IC proved useful in many ways but had the drawback of capacitive coupling between phases and thus could not be used as intended to power the direct and quadrature axes separately. Although it is widely know as well as proven in [3] that IGBTs can be hard to work with they can operate properly if handled and designed with care. It is my recommendation that a completely isolated full H-bridge is used for the sinusoidal component of modulation and a fully isolated half bridge is used for cosinusoidal modulations as they are never negative in polarity. This will provide the capability to implement the full sinusoidal modulation technique.

4. Although this point was communicated in [3] and this thesis, it is important enough to re-iterate here: Ensure that there is proper power supply isolation as it is instrumental to the proper workings of the experiment. Care must also be taken to isolate any measurement equipment and DACs. The use of only one DAC with a greater number of analog input/output channels simplifies this matter greatly although it adds cost to the experiment.

REFERENCES

[1] C. I. Hubert, "Electric Machines Theory, Operation, Applications, Adjustment, and Control," 2nd ed., New Jersey: Prentice Hall, 2002.

[2] J. C. Andreas, "Efficient Electric Motors," New York: Marcel Decker Inc., 1982.

[3] M. Peung, "Stabilizing Power Oscillation With the New Phase Modulation Method for Synthetic Loading of Induction Motors," McMaster Master's thesis, December 2006.

[4] A. E. Fitzerald, C. Kingsley Jr. and S. D. Umans, "Electric Machinery," 5th ed., McGraw-Hill Book Company, 1983.

[5] A. Mihalcea, "Equivalent Loading Methods for Determining Total Power Loss in Induction Motors," McMaster Master's thesis, September 1999.

[6] J. Hoolboom, J. Soltani and B. Szabados, "A New Synthetic Loading for Large Induction Machines With No Feedback Into the Power System," Institute of Electrical and Electronics Engineers Transactions on Energy Conversion, Vol. 17, Issue 3, pp. 319-324, Sept. 2002.

[7] G. Kron, "Equivalent Circuits of Electric Machinery," John Wiley & Sons, Inc., New York, N. Y., 1951.

[8] C. Grantahm and N. Sheng, "The Synthetic Loading of Three-Phase Induction Motors Using Microprocessor controlled Power Electronics," Record Institute of Electrical and Electronics Engineers Catalogue No. 95TH8025/1995, pp. 471-476.

[9] J. Soltani, B. Szabados, G. Hoolboom, "A New Equivalent Loading Test for Measuring Total Losses in Induction Machines," LESCOPE'00, Conference Proceedings pg 86-90, Halifax, July 2000.

[10] M. P. Romeira, "The Superimposed Frequency for Induction Motors," Proceedings Institute of Electrical and Electronics Engineers, Vol. 36, pp. 952–953, 1948.

[11] W. Fong, "New Temperature Test for Polyphase Induction Motors by Phantom Loading," Proceedings Institute of Electrical and Electronics Engineers Vol. 119, Issue 7, pp.883-887, July 1972.

[12] H. W. Lorenzen and A. Meyer, "Two-Frequency Heat Run – A Method of Examination for Three-Phase Induction Motors", Institute of Electrical and Electronics Engineers Transactions on Power App. Syst., Vol. PAS-98, Issue 6, pp. 2338-2347, Nov./Dec. 1979.

[13] P. C. Krause, "Analysis of Electric Machinery," New York: McGraw-Hill, 1986.

[14] R. H. Park, "Two-Reaction Theory of Synchronous Machines – Generalized Method of Analysis – Part I," American Institute of Electrical Engineers Trans., Vol. 48, July 1929, pp. 716-727.

[15] H. C. Stanley, "An Analysis of the Induction Motor," American Institute of Electrical Engineers Trans., Vol. 57 (Supplement), 1938, pp. 751-755.

[16] F. Ye, "Parameter Identification of Induction Motor Model With Variable Frequency Voltage Supply," McMaster Master's Thesis, 2003.

[17] G. Rizzoni, "Principles and Applications of Electrical Engineering," 4th ed., Boston: McGraw-Hill, 2004.

[18] Datasheet PD-96956 Rev F. "International Rectifier Integrated Power Hybrid IC for Appliance Motor Drive Applications," International Rectifier. Retrieved December 5, 2009 from http://www.irf.com/product-info/datasheets/data/iramx20up60a.pdf.

[19] Application Note AN-1044. "Integrated Power Module for Application Motor Drive," International Rectifier. Retrieved December 5, 2009 from http://www.irf.com/technical-info/appnotes/an-1044.pdf.